University of Stavanger

FACULTY OF SCIENCE AND TECHNOLOGY

MASTER'S THESIS

Study program/specialization: Petroleum Engineering Petroleum Engineering/Drilling Technology	Spring semester, 2019 Confidential
Author: Øystein Kristiansen	Øystein Kristiansen (Signature of author)
Faculty supervisor: Mesfin Belayneh External Supervisor(s): Bjørnar Kalsvik	
Title of Master thesis: *Optimization of perforation design at Oseberg South with regards to perforation clean-up and productivity*	
Credits (ECTS): 30	
Keywords: Dynamic underbalance Crushed zone Wireline perforating Productivity Core Flow Efficiency Section IV Test	Number of pages: 96 + supplemental material/other:7 Stavanger, 27.07.2019

ACKNOWLEDGMENT.

Firstly, I would like to thank Bjørnar Kalsvik, my supervisor at Halliburton for his dedication and tireless work to realize this project. The discussions and feedback have been most valuable. I would also like to thank Cato Prestegård at Halliburton for sharing his knowledge on perforating and dynamic underbalance.

Very much appreciate that Halliburton funded a trip to Jet Research Center in Texas to attend the experimental tests, and for providing me with coursing and necessary software to do this thesis.

Special thanks to my supervisor at the University of Stavanger, Mesfin Belayneh Agonafir, for his utmost effort, guidance, and inspiration.

My thanks also go to my family for their continuous support throughout this work.

Stavanger 27.07.2019

Øystein Kristiansen

ABSTRACT.

The Oseberg South field, originally estimated to contain 93.4 Sm3 oil equivalent of recoverable reserves, has been producing since 1985. Recent reports estimate remaining reserves to be approximately 25.1 Sm3 oil equivalents. Despite the reservoir being highly depleted, some uncertain still exists about the presence of isolated high-pressure pockets in the reservoir.

Traditionally Oseberg South has been perforated on pipe with highly overbalanced well pressure with a kill pill along the reservoir.

The main research task described by this report has been to evaluate the best perforation techniques for the depleted Oseberg South field with specific emphasis on perforation clean-up and cost.

Experimental work and simulations have been conducted to quantify expected perforation characteristics and predict associated productivity. The experimental work was performed at the Jet Research Center in Texas at downhole conditions, with simulation studies carried out with industry software.

Results from the study indicating:

- Significantly higher perforation performance when perforating on pipe in high overbalance with the 4-5/8” gun system compared to in balance with the 3-1/8” gun system on wireline
- Peak dynamic under balance was higher for the 4-5/8” gun system
- Improved perforation clean-up for the 3-1/8” gun system when perforating in balance
- Better well performance for the 3-1/8” gun system, perforated in balance

Based on these results, the conclusion of this thesis is that the wells at Oseberg South perforated in balance with the 3-1/8” gun system is expected to result in lower costs and most likely improved production.

Table of Content

LIST OF FIGURES.

LIST OF TABLES.

LIST OF SYMBOLS.

h	height of perforation interval
k	Permeability of formation
k_c	permeability of crushed zone
k_d	permeability of damaged zone due to invasion of mud
k_{dp}	permeability of damaged zone around the perforation
k_R	permeability of reservoir
L	flow length
L_p	length of perforation
n	number of perforation

r_{dp}	radius of damaged zone around the perforation
r_p	radius of perforation
S_{sp}	single-shot perforation skin
U	fluid velocity
β	inertial coefficient
μ	viscosity
ρ	fluid density
ΔP	pressure drop

LIST OF ABBREVIATIONS.

API	American Petroleum Institute
CFE	Core Flow Efficiency
CT	Computed Tomography
DUB	Dynamic Underbalance
FGV	Free Gun Volume
HPTK	Halliburton Perforating Tool Kit
WEM	Wellbore Evaluation Model

1 INTRODUCTION.

This thesis presents the experimental and numerical simulation analysis of two different perforating techniques to be considered in the depleted Oseberg South oil field. To maintain productivity and recovery rate, the right choice of cost-effective and efficient perforating technique is a key factor and needs to be evaluated prior to operation. This study investigates the productivity comparison of current high overbalance perforating with 4-5/8" guns on pipe and balanced perforating on wireline with smaller 3-1/8in guns.

1.1 Background

The Oseberg South field was discovered in 1979 and has been in production since 1985. As shown in Figure 1, it is located 140 km west of Bergen, at a water depth of 100 meters.

Figure 1- Map of Norwegian Continental Shelf showing the location of Oseberg South, [Norwegian Petroleum Directorate, 2019]

The main reservoirs are in the Tarbert and Heather formations and are of moderate reservoir quality. Several reservoir zones are separated by faults. Reservoir rock is a Middle Jurassic Brent group.

Figure 2 shows the well pressure prognosis used to drill Oseberg South. The zone to be investigated is at approximately 2700 mTVD.

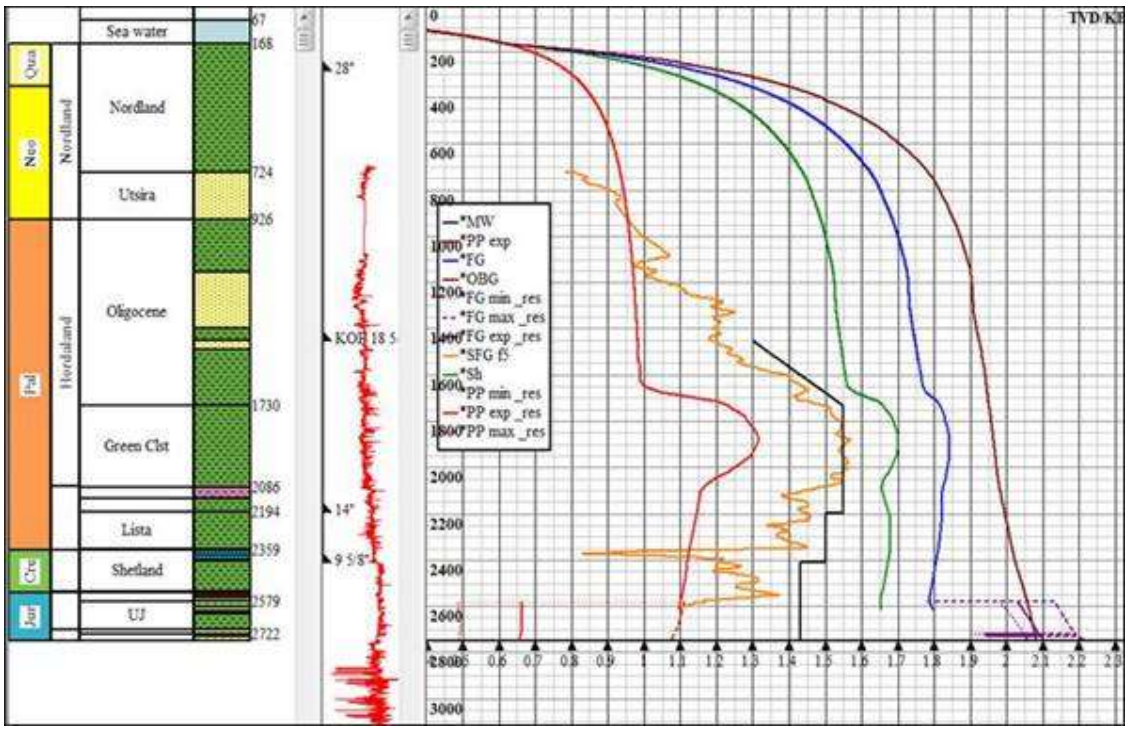

Figure 2- Pore pressure plot and formation geology, F-17 Oseberg South [Equinor, 2019]

The reservoir contains originally 93,4 Sm^3 oil equivalent recoverable reserves. Figure 3 shows annual production in Sm^3 oil equivalents. Table 1 provides an overview of the originally recoverable reserves and the remaining 25.1 Sm^3 reserves at the Oseberg South. Figure 3 shows production history for Oseberg South in standard cubic meter oil equivalents. As can be seen, most of the production is oil with a small amount of gas.

Table 1- Recoverable and remaining reserves at Oseberg South [Norwegian Petroleum Directorate, 2019]

	Oil	Gas	NGL	Condensate	Sum
Recoverable reserves originally	**66.7**	**22.2**	**4.4**	**0.0**	**93.4**
Remaining reserves	**12.00**	**11.2**	**1.9**	**0.0**	**25.1**

Figure 3- Oseberg South production history in million standard cubic meter [Norwegian Petroleum Directorate, 2019]

To increase recovery rate, Oseberg uses water and gas injection, with water alternating gas (WAG) injectors in parts of the field. The oil is transported through pipelines to Oseberg field center.

The motivation for this study is to recover the remaining hydrocarbon resources at Oseberg South in a cost-effective and efficient manner as possible. As provided in Table 1, most of the recoverable oil reserves are produced, and hence the reservoir is heavily depleted with pore pressure of 0,74 sg. New production wells in possibly pressure isolated reservoir pockets are being drilled before it is expected that the field will be converted to a gas field in 4-5 years. There is uncertainty whether these pockets are connected with the main reservoir or not and hence may contain high reservoir pressure.

Due to an internal focus on well control issues and avoiding kicks, Oseberg South has been perforated with high overbalance and a kill pill along the reservoir. Successful exploitation of the reserves has been done so far. However, Equinor still believes that the field is still not

producing at its full capacity. In lack of perforating techniques to increase productivity, Equinor considers perforating on wireline, which is a more cost-effective solution.

Hence they are looking to reduce cost without compromising productivity. Since the reservoir is heavily depleted, there are uncertainties whether the transient dynamic underbalance is sufficient to achieve clean and productive perforation tunnels, when perforating in high overbalance, with a kill pill along the reservoir.

Perforating on wireline in balance, with dynamic underbalance could be the way to reduce costs while maintaining or increasing current production. Dynamic underbalance (DUB) perforating in low-pressure reservoir has been investigated before. However, the combination of low reservoir pressure and high hydrostatic overbalance in the well has not been given enough emphasis. Enough time in dynamic underbalance is critical, and investigating the productivity potential of perforating on wireline compared to pipe is the main focus of this thesis work.

1.2 Problem formulation

As discussed, due to the low reservoir pressure, an appropriate perforation design is a key for efficient well performance in terms of better flow dynamics in the perforation tunnels immediately after perforating, and the possibility to reduce cost. The cost-effective part of changing current perforating strategy is directly reflected through: operational rig time, kill pill cost and no middle completion. Well F-17 at Oseberg South will be used for field data and well trajectory for simulations.

However, the main research issues to be addressed in this thesis is:

- Investigate the well performance when perforating in balance with wireline versus overbalanced pipe perforating with a kill pill along the reservoir.

1.3 Objective

The main objective of this thesis is to answer and describe the research questions addressed in section § 1.2. The work activities include:

- Literature studies on perforating with emphasis on dynamic underbalance and perforation clean-up.
- Simulate the balanced wireline, and overbalanced pipe perforating in HPTK and SurgePro, to determine gun charge performance and dynamic underbalance.
- Perform Section IV tests at Halliburton Advanced Perforating Flow Laboratory to investigate perforation clean-up and core flow efficiencies for both cases.
- Simulate both cases in WEM to quantify well performance.

Figure 4 outlines the research program designed to achieve the objectives.

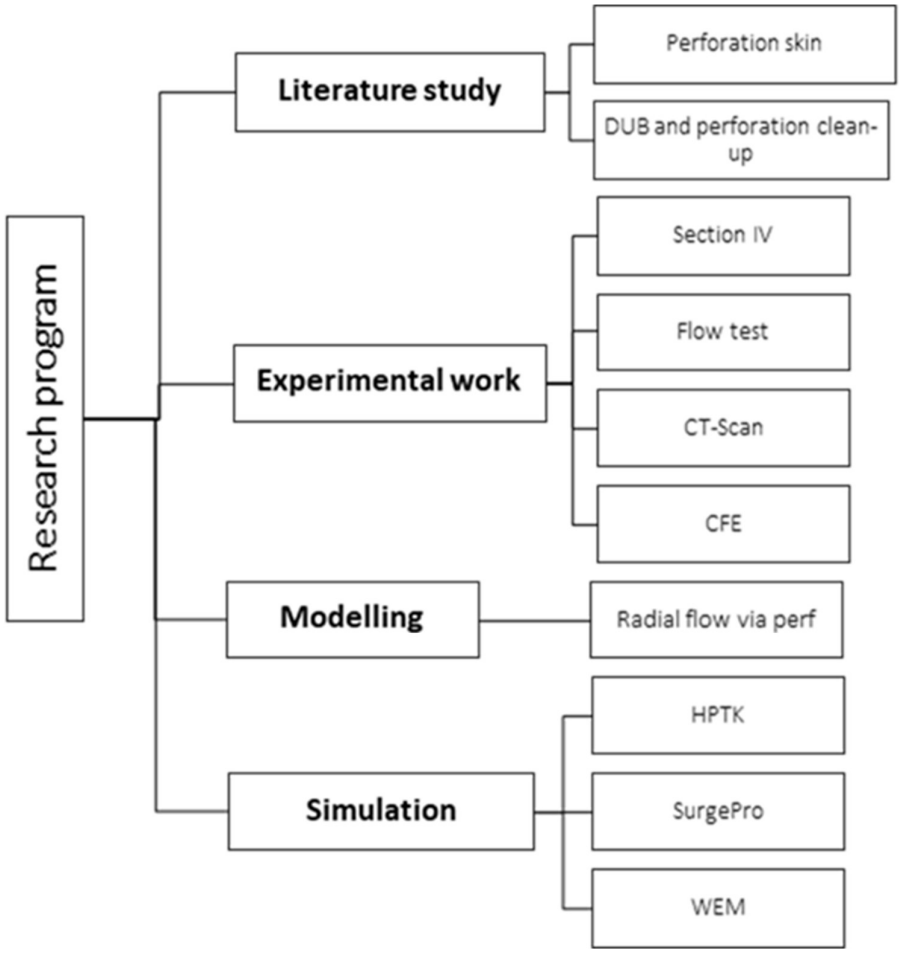

Figure 4- Research program implemented in this thesis work

2 LITERATURE REVIEW

This chapter will give a brief review of the perforation process and the criticality of obtaining a clean, highly productive perforation tunnel. Previous research work on dynamic underbalance perforation and its critical factors will particularly be investigated.

2.1 Perforating

Perforations allow effective flow communication between a cased wellbore and the reservoir (Tariq et al. 1995). The perforating technique has developed from the first commercial used bullet guns in the 1930s to shaped charges, which was developed during WW2 as an armor-piercing weapon. The steel bullet had low penetration in hard steel casing and hard formation. The shaped charges, when used properly, can create a relatively deep penetrating tunnel into the formation. According to Tariq et al. (1995), shaped charge perforations accounts for 95% of all perforating jobs today. Figure 5 shows a perforated well and damaged zones around the wellbore and the perforation tunnels.

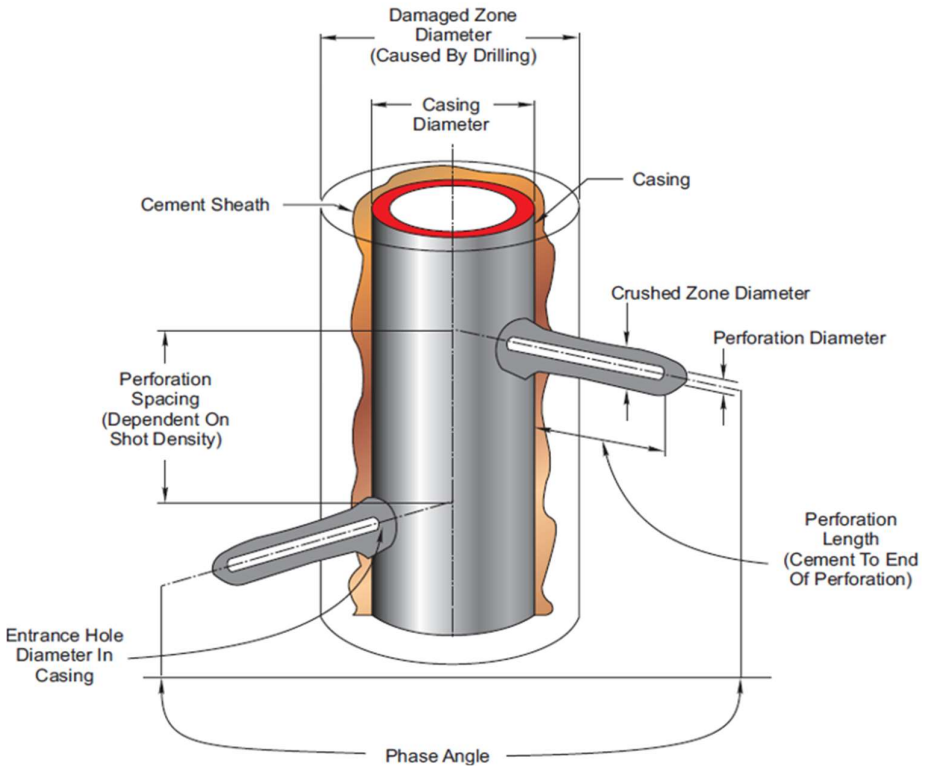

Figure 5- Perforated Wellbore Geometry (Halliburton Perforating Solutions, 2019)

Figure 6 shows a shaped charge with its components. The shaped charge consists of three components: case, explosives, and liner, with the latter being either parabolic or conical, depending on the desired shape and depth of the perforation. Perforating with conical liner is called deep-penetrating sequence and creates a relatively deep perforation with small hole geometry. If a parabolic liner is used, a much more massive, but slower-moving jet will be formed, creating a shallow penetration with a relatively large hole diameter (Halliburton Wireline and Perforating).

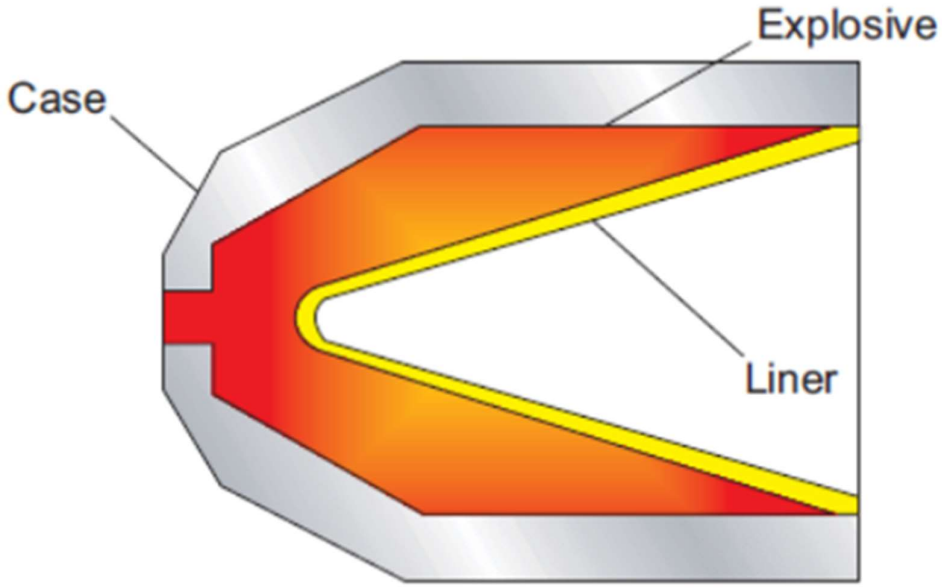

Figure 6- Shaped Charge Perforator (Halliburton Perforating Solutions, 2019)

2.2 Performance affecting factors

Charge design is critical to create the desired perforation geometry and will depend on the properties of the three components (Tariq et al., 1995):

- Liner
- Explosive
- Case

Liner and explosive are the most critical components. Liner size and angle will affect geometry and penetration length. Explosive type, density, and distribution will affect the pressure and

velocity of the jet. A strong case is critical to properly confine the explosive event, forcing the jet into the formation.

Figure 7 illustrates the development of liner collapse and forming of a deep penetrating jet. A wider liner angle would decrease penetration but increase hole diameter. The difference in explosive amount for the two charges to be tested will affect the performance significantly.

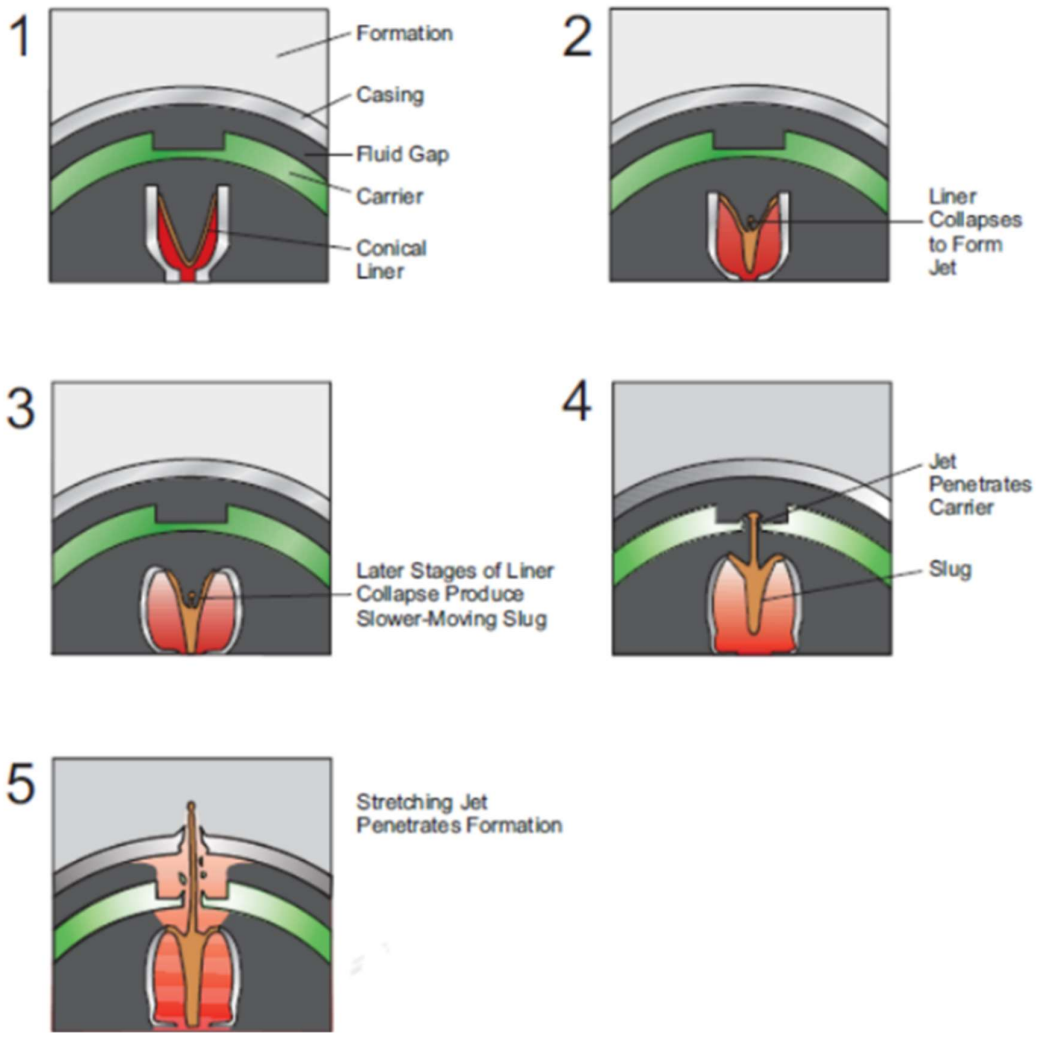

Figure 7- Deep penetrating shaped charge sequence (Halliburton Perforating Solutions, 2019)

In addition to perforator performance, shot density and phase angle of the perforations will also affect the overall well productivity. In horizontal wells Halliburton uses a 350/10 degree phasing, meaning perforation tunnels point upwards with 20 degrees between neighboring perforations. For upward-pointing perforations, gravity will help to pull debris and loose particles out of the tunnel. Pointing towards maximum vertical stress, the collapse of the perforation tunnel is less likely compared to horizontal perforations. Simulations performed by Divyankar et al. (2015) shows 350/10 degree phasing has a lower skin value than simple vertical perforations.

2.3 Perforating kill pill

In order to prevent fluid loss once connectivity between wellbore and reservoir is obtained, a fluid with properties to prevent losses into the formation is critical. Usually, a kill pill (certain volume of fluid) with specific properties is circulated into the well, covering all intervals to be perforated. Bridging particles is used to seal the perforation wall. However, plugging of the pores should be avoided to avoid permanent perforation skin.

Formation damage caused by kill fluid invasion results from the following processes (Han et al. 1996):

- Invasion of filtrate into the formation reducing relative permeability
- Invasion of solids into the formation possibly plugging pores
- Deposition of filter cake in the perforation tunnel

Back-flushing invaded filtrate and solids is critical to avoid permanent perforation skin but washing away a deposited filter-cake on the perforation wall, has proven to be difficult. The amount of drawdown necessary to wash out filter cake will depend on permeability, viscosity, and composition of the kill pill. The kill pill will be a critical difference between the two perforating techniques which will be investigated. Losses after perforating are usually about 1/3 of a gallon per perforation. If the bridging particles from the kill pill plugs of pores, significant skin can arise.

2.4 Skin and its consequence

Skin is a dimensionless number illustrating the increased or reduced pressure drop due to near-wellbore conditions, where a positive number represents an additional pressure drop, and a negative number illustrates less pressure drop or a stimulated well. Van Everdingen et al. (1953) defines it as: "Skin can be defined as the additional pressure drop in the near-wellbore area that results from the drilling, completion and production practices used."

2.4.1 Formation damage skin

Figure 8 illustrates the near-well skin damage and pressure decline across the skin. According to Hawkins et al. (1959), the skin factor due to wellbore altered permeability is given as:

$$S = \left(\frac{k}{k_d} - 1\right) \ln\left(\frac{r_d}{r_w}\right) \qquad (1)$$

Where, k = permeability of virgin formation, $k_d =$ permeability of damaged formation, $r_d =$ radius of the damaged formation and $r_w =$ radius of the wellbore

The pressure loss due to skin is given as:

$$\Delta P_s = \frac{141{,}2 * q_o * B_o * \mu_o}{kh} S \qquad (2)$$

Where, $q_o =$ oil flow rate, $\mu_o =$ viscosity, $B_o =$ formation volume factor, $h =$ reservoir thickness, $k =$ formation permeability, and S = skin factor

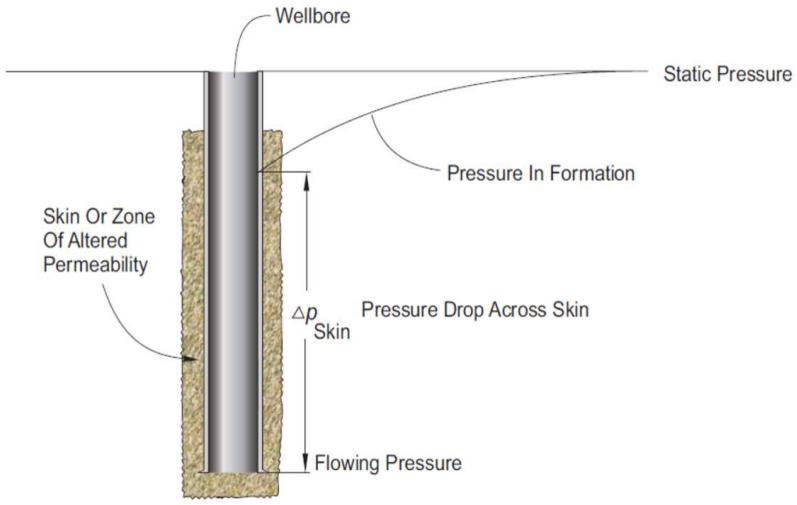

Figure 8- Illustration of pressure drop due to skin in near wellbore area (Halliburton Perforating Solutions, 2019)

2.4.2 Perforation skin

Perforation skin is the additional wellbore pressure drop caused by the permeability reduction around the perforations due to compacted or crushed rock material. According to Asadi et al. (1994), the shaped charge creates a pressure pulse of up to 4 million psi and velocity of 30 000ft/sec, pushing all rock material aside, leaving a compacted zone around the perforation tunnel. Experiments performed showed that permeability was reduced by 55% within the first ¼ inch and 20% within the second ¼ inch. As seen in Figure 9, the open perforation tunnel is surrounded by pulverization zone, grain fracturing zone, and crushed zone, all with reduced permeability. Outside the crushed zone, there is a non-damaged or virgin zone with original reservoir permeability. Density measurements have been done in cores in order to quantify the degree of compaction. "Obviously, the higher density means the pore spaces are proportionally smaller" (Sahimi et al. 1994). Experiments show that for sandstone, a high spike can be seen in density in the first centimeter of the perforated core.

Tariq et al. (1990) divide damage in perforation tunnels into two sub-categories:

1. Damage that is initially present but disappears as the formation is flowed back after perforating.
2. Damage that is so firmly lodged that it requires extremely large pressure gradients and velocities for its removal.

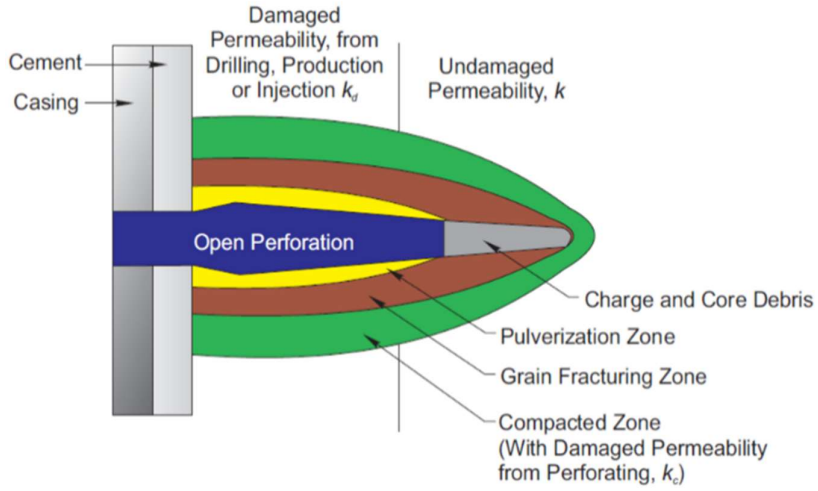

Figure 9- Illustration of perforation geometry and damaged zones (Halliburton Perforating Solutions, 2019)

2.4.2.1 McLeod et al.'s perforation skin model

Figure 10 illustrates the single perforation geometry penetrated through the casing, cement, and mud invaded zone. Around the perforation tunnel, the formation has been compacted and has a damaged permeability, kd. Using the radial flow equation, McLeod et al. (1983) derived a skin factor due to the compacted zone around the perforation tunnel:

$$S_{dp} = \left(\frac{h}{L_p n}\right) * \left(ln\frac{r_{dp}}{r_p}\right) * \left(\frac{k_R}{k_{dp}} - \frac{k_R}{k_d}\right) \qquad (3)$$

Where:

$h =$ height of perforation interval, $L_p =$ length of perforation, $n =$ number of perforations

$r_{dp} =$ radius of the damaged zone around perforation, $r_p =$ radius of perforation

$k_R =$ permeability of the reservoir,

$k_{dp} =$ permeability of damaged zone around the perforation

k_d is permeability of damaged zone due to invasion of mud, and usually $k_R > k_d > k_{dp}$

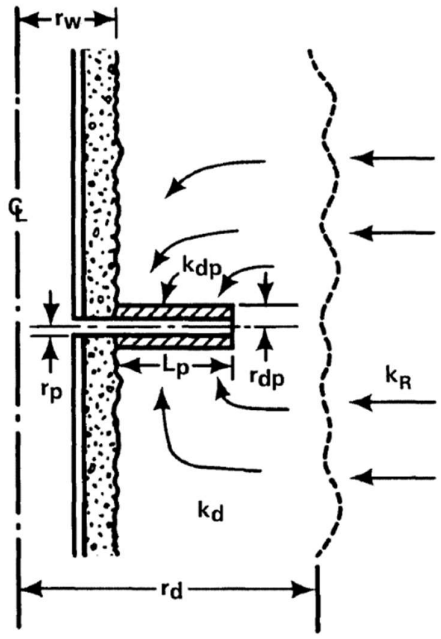

Figure 10- McLeod et al.'s perforation skin model (McLeod et al. 1983)

2.4.2.2 Jacques Hagoort perforation skin model

Unlike McLeod, Hagoort's model takes into account the flow towards the tip. As can be seen, perforation radius, damaged zone radius, and drainage radius are all hyperbolic functions. For slender perforations and large drainage area, Jacques' model becomes equal to McLeod's model. Figure 11 shows a two-dimensional ellipsoidal shaped perforation tunnel, assuming convergent flow. For this geometry, Hagoort et al. 2007 developed a model for estimating flow Impairment by perforation damage given as:

$$S_{dp} = \frac{h}{cn} * S_d = \frac{h}{cn} * \left(\frac{k_R}{k_d} - 1\right) * ln \frac{\tanh\left(\frac{\gamma_d}{2}\right)}{\tanh\left(\frac{\gamma_p}{2}\right)} \qquad (4)$$

Where: $\sinh(\gamma_p) = r_p/c, \quad \sinh(\gamma_d) = r_d/c\ , \quad c^2 = {L_p}^2 - {r_p}^2$

$L_p =$ length of perforation, $r_p =$ radius of perforation,

$r_d =$ radius of damaged zone around the perforation

$k_R =$ virgin reservoir permeability, $k_d =$ damaged perforation permeability

$n =$ number of perforations, $h =$ formation thickness/pay interval

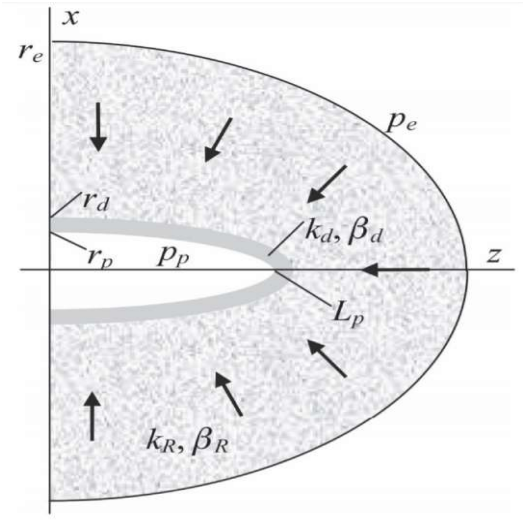

Figure 11- Jacques Hagoort perforation skin model (Hagoort et al. 2007)

To compare the McLeod and Hagoort perforation skin models, a sensitivity study was performed. Table 2 provides the input parameters used. The crushed zone and the tunnel geometry parameters were considered for the sensitivity analysis.

As can be seen for Figure 12 and 13, McLeod and Hagoort's models are equal (coinciding graphs) for relatively long, slender perforations. Figure 12 shows the reduction in perforation skin as a function of crushed zone permeability. Figure 13 shows how the thickness of the crushed zone increases perforation skin.

Table 2- Input parameters for McLeod and Hagoort models

PARAMETER	VALUE
RESERVOIR PERMEABILITY (MD)	200
HEIGHT (FT)	100
SPF	4
LENGTH OF PERFORATION (IN)	10
RADIUS OF PERFORATION (IN)	0.2
CRUSHED ZONE THICKNESS (IN)	0.5
CRUSHED ZONE PERMEABILITY (MD)	20

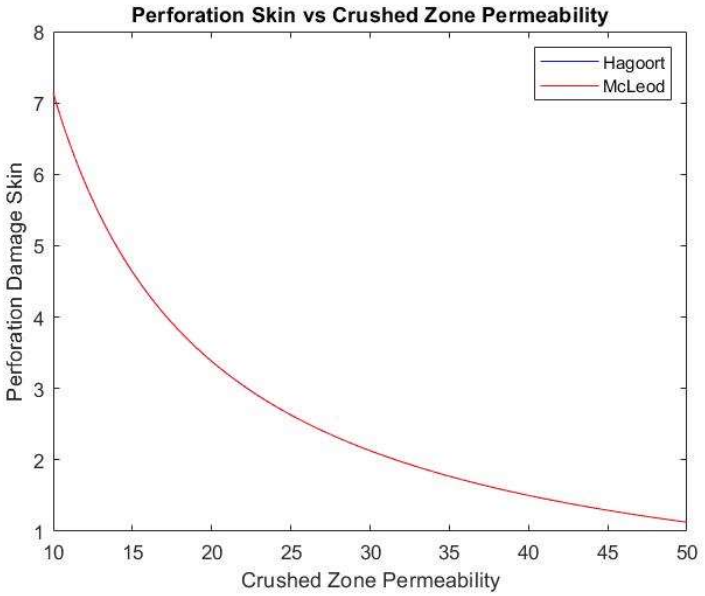

Figure 12- Perforation skin versus crushed zone permeability

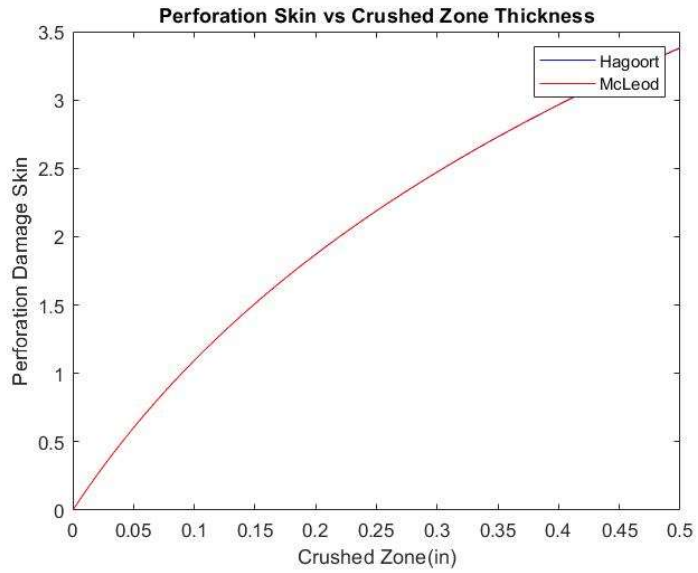

Figure 13- Perforation skin versus crushed zone thickness

Figure 14 shows how short perforation length increases perforation skin. For such short perforations, a small difference can also be seen between McLeod and Hagoort. Figure 15 shows perforation skin versus radius of perforation. Although the scale is smaller for Figure 15, the deviation between the two models is more clear when plotting perforation skin versus radius of perforation.

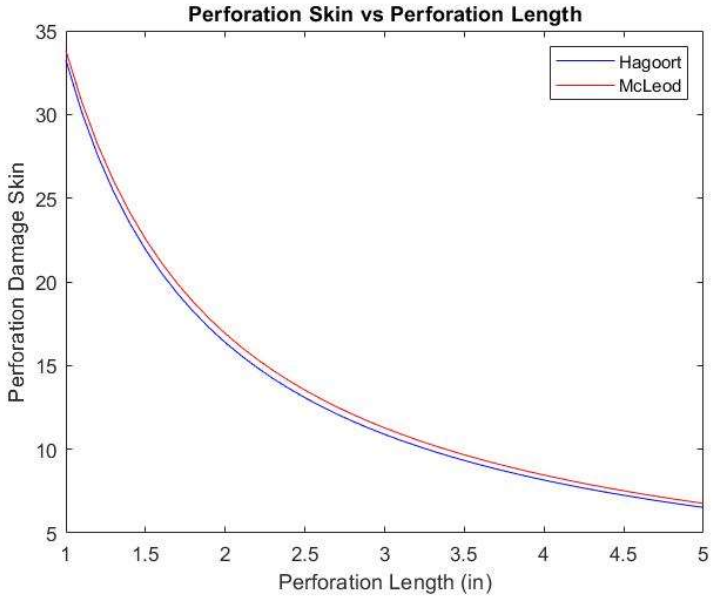

Figure 14- Perforation skin versus perforation length

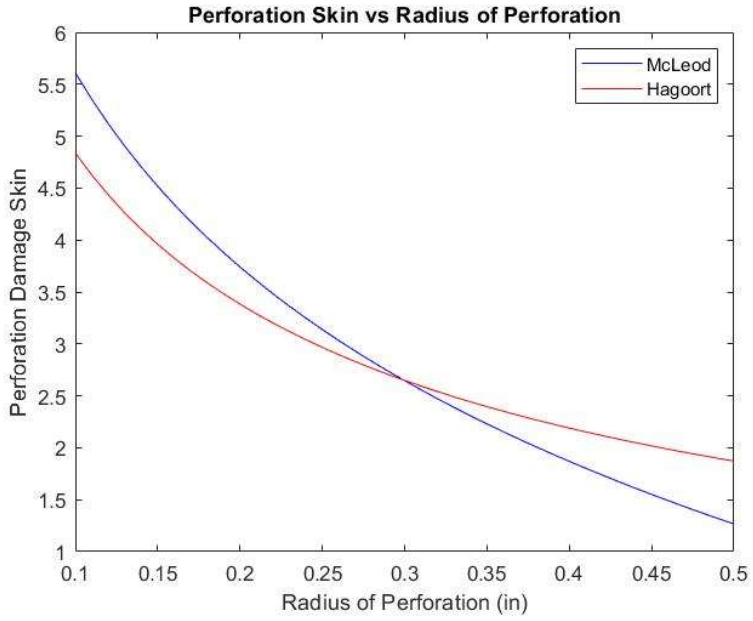

Figure 15- Perforation skin versus perforation length

2.4.3 Effect of total skin on productivity

In the productivity equation for radial flow, we find skin as a dimensionless number, which can be quantified as a pressure drop when multiplied with reservoir properties and production rate.

$$P_e - P_{wf} = \frac{q_o * \mu_o * B_o}{7.08 * 10^{-3} * k * h} * \left(\ln\left(\frac{r_e}{r_w}\right) + S\right) \qquad (5)$$

Where: q_o = oil flow rate in STB/D, μ_o = oil viscosity in cp , B_o = oil formation volume factor reservoir in bbl/STB, k = formation permeability in mD, h = pay zone thickness in feet, $P_e - P_{wf}$ = reservoir pressure and wellbore pressure respectively, in psia, r_e = reservoir radius in feet, r_w = wellbore radius in feet

S = total skin factor and is described by several skin parameters

$$S_t = S_c + S_p + S_d + \sum S_i \qquad (6)$$

- S_c represents the effects of partial penetration
- S_p represents perforation skin

- S_d represents the effects of formation damage mainly due to mud-filtrate invasion in the near-wellbore area
- $\sum S_i$ represents includes pseudo-skin factors, such as phase and rate-dependent effects

2.5 Perforation vs. clean-up methods

When perforating a well, the bottom hole pressure impacts perforation performance and clean-up instantly after the perforating event. The perforation can be done in different pressure modes: Overbalance/extreme overbalance, balance, and underbalance/dynamic underbalance. Choice of method will be decided by:

- Cost of each method
- Probability for failure
- Final productivity

According to Bundy et al. (1990), predicting productivity is the most difficult one, and will always contain a significant degree of uncertainty. Figure 16 shows improved perforation clean-up for underbalanced/dynamic underbalanced well pressure due to higher effective penetration and removal of the crushed zone.

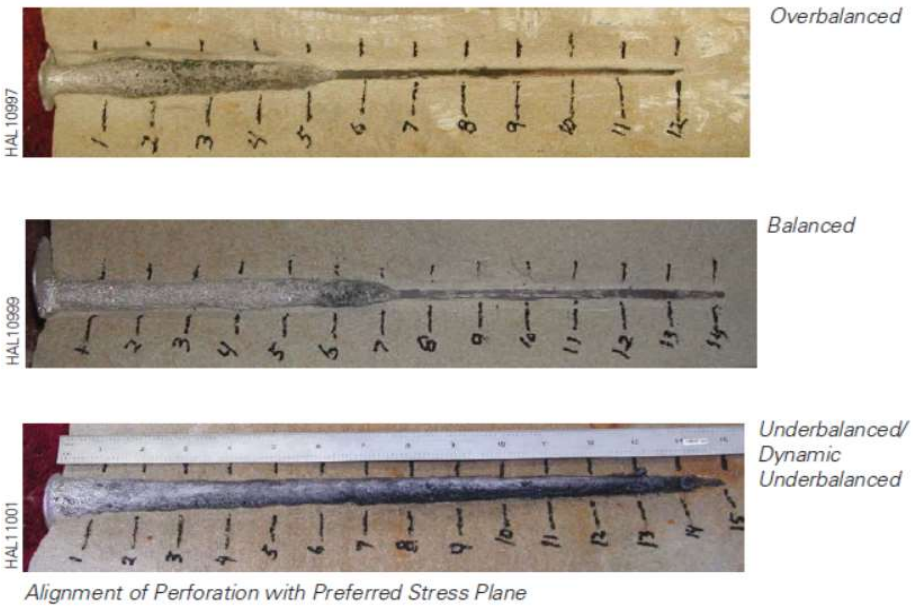

Figure 16- Visual perforating results from perforations at various pressures (Halliburton Perforating Solutions, 2019)

2.5.1 Overbalanced perforating

Overbalanced perforating means maintaining wellbore pressure above formation pressure before, under, and after the perforating:

$$P_{wellbore} > P_{formation} \qquad (7)$$

This usually leads to an un-cleaned perforation tunnel, due to wellbore pressure pushing the crushed formation into the perforation tunnel. This will naturally lead to a perforation tunnel with low flow efficiency.

Although conventional overbalanced perforating usually is seen as a non-productive solution, case study done by Bundy et al. (1990), shows that four high-pressure gas wells perforated in overbalance heavyweight mud had surprisingly good productivity. Predicted skin was 12,6, while pressure transient tests showed a skin of 2,6. He also believes that completion damage from perforating overbalanced decreases as reservoir pressure increases.

Extreme overbalanced perforating

Extreme overbalance (EOB) is a perforating technique which uses high well pressure well beyond formation breakdown pressure, creating several short fractures (Behrmann et al. 1996). Fractures can extend beyond the damage zone and create a highly conductive fluid path from virgin reservoir rock. Although EOB has proven to be successful in several cases, it does not improve perforation clean-up and will therefore not be further discussed.

2.5.2 Balanced perforating

In balanced perforating, the wellbore pressure is equal to the formation pressure:

$$P_{wellbore} = P_{formation} \qquad (8)$$

Balanced perforating does not have any unique effect on the perforation clean-up, but is regarded as a better solution than overbalanced. Balanced perforating is commonly used when doing assisted perforating (perforating a well with already existing perforations).

2.5.3 Static underbalanced perforating

During underbalanced perforating wellbore pressure is maintained below formation pressure:

$$P_{wellbore} < P_{formation} \qquad (9)$$

To prevent kick and well control incidents, hydrostatic underbalance in the well will require well control equipment on surface, which can be achieved with the use of wireline, coiled tubing, or pipe using a packer to displace a part of the well to lighter fluid. Experimental tests on underbalanced perforating evaluated by Hsia et al. (1991), indicates that there is a close relationship between underbalance and perforation clean-up. Cores in the permeability range of 96-115mD were used showing that analytic skin and skin derived from finite element method were reduced from 2,91 and 3,00 respectively, to -0,37 and -0,36 by increasing underbalance stepwise from 0-3000 psi.

However, increasing underbalance further did not indicate an even higher reduction in skin from the perforation. Halleck et al. (1989) concludes that the surging effects, removing debris and perforation damage, obtained from underbalanced perforating is a result of a short high transient fluid pressure gradient for a short period of time and by steady-state pressure gradients over an extended period of time.

2.5.4 Dynamic underbalanced perforating

Dynamic underbalance is a short transient period of time, where underbalance is achieved in the well at the time of perforating. Dynamic underbalance is obtained from the opening of atmospheric pressure gun volumes, and possibly additional chambers. As the guns are fired, wellbore fluids start to flow into the guns, reducing hydrostatic well pressure. If additional surge chambers are used, surge valves will open a short time after detonation, improving the duration and magnitude of dynamic underbalance. It has been proven that the negative pressure differential which appears along the perforation tunnel can be enough to surge out crushed debris. Well pressure will quickly be equalized by formation pressure, turning the well into a balanced state. As the fluid column stabilizes, the well goes back to the initial state.

“Perforation Cleanup via Dynamic Underbalance: New Understandings” written by Grove et al. (2011) have posited that the flow initiated by the pressure differential between the

reservoir and the wellbore has significant clean-up effects. According to Grove et al. (2011), increased effective tunnel length, increased tunnel diameter, and reduced thickness of the remaining crushed zone can also be achieved.

Although DUB has been used as a technique to achieve conductive perforation tunnel in overbalanced wells, it has been shown that the effect also accounts for hydrostatically balanced or underbalanced wells as well. A large-scale study from Tunu gas field in Indonesia shows production improvement in wells perforated in DUB compared to the conventional method, which in this case was static underbalance. Hence, both cases had static underbalance, but the additional drawdown due to DUB had an estimated increase in productivity between 10 and 33 percent and statistical confidence of 90 percent. Research work done on DUB at the Norwegian Continental Shelf by Tovar et al. (2010) also concludes that DUB pressure is critical to maximize perforation clean-up and obtain high productivity.

Fast gauges have well proven that well pressure can be reduced significantly, improving perforation tunnel clean-up. However, it's important to keep in mind that the valves for the surge chambers might not be located directly in front of the perforation tunnel. Thus, gauges by the valve can indicate a very optimistic pressure transient in the well, which may not reflect the pressure transient occurring at the perforation (Baumann et al. 2014). Another important uncertainty is the fact that once some of the perforation tunnels are cleaned and starting to produce, well pressure will be equalized quickly, limiting effect of dynamic underbalance on the other perforations (Baumann et al. 2014).

Figure 17 shows a comparison of static and dynamic underbalance wellbore pressure profiles. For dynamic underbalance we start above reservoir pressure, a high spike is seen in wellbore pressure, which is due to gunshots and gun powder burning, creating gas and increasing pressure. The pressure is then drastically reduced due to the free volume of guns and surge chambers before it equalizes with reservoir pressure. In static underbalance, the reservoir pressure is initially below wellbore pressure. Wellbore pressure increases as the guns are fired and then drops approximately down to initial hydrostatic wellbore pressure. Reservoir starts to flow because of underbalance and communication with wellbore. After some time, wellbore and reservoir pressure equalizes.

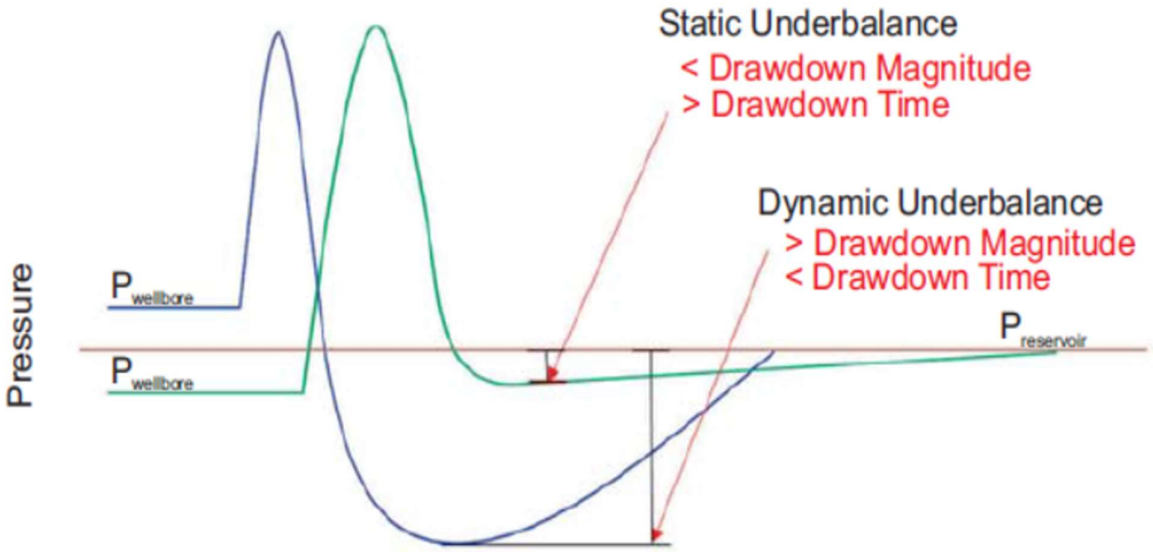

Figure 17- Static and dynamic underbalance wellbore pressure as function of time (Halliburton Perforating Solutions, 2019)

2.6 Process of perforation tunnel creation

The creation of a perforation tunnel is a multistage process including several parameters. The first stage in creating a perforation tunnel from a shaped charge occurs as the jet punches a hole in the formation rock (with possibly existing casing and cement) (Pucknell et al. 1991). As the jet travels through the rock, multiple microfractures are created, extending several inches into the formation creating a damaged/crushed zone, and the radial displacement of the rock creates elastic stress in the undamaged porous medium (Bolchover et al. 2006). This crushed zone can have significantly reduced permeability, causing flow impairment.

Decompression of the rock can cause failure of the crushed and damaged rock surrounding the perforation tunnel. Failed rock can fall into the perforation tunnel and be washed away by the surge flow together with other perforation debris (Bolchover et al. 2006).

McGregor et al. (2018) explains that for a dynamic underbalanced perforation, the rapid drop in wellbore pressure, which is transmitted to the pore-pressure is the cause for the additional failure in the rock matrix. As illustrated in Figure 18, local reduction in pore pressure increases effective stress in the rock matrix, causing failure (dynamic effective stress effect). Perforation cavity size and rock strength are properties affecting the magnitude of the failure, where large diameter tunnel reduces failure, and low rock strength increases failure.

Effective stress is given as (Aadnøy et al. 2011):

$$\sigma' = \sigma - P_o \qquad (10)$$

Where

- σ'=effective stress, σ=in-situ stress, P_o=pore pressure

Devinder et al. (2000) postulates that the failure of crushed rock can result from the erosional drag force exerted onto the crushed particles during the surge backflow.

Hence, the underbalance or the dynamic underbalance surge flow has two effects on the perforation tunnel:

- Clean out loose rock and jet debris
- Failure of the crushed zone

According to Bolchover et al. (2006), the failure of the crushed zone appears from three possible mechanisms:

- Compressive shear failure
- Tensile failure
- Fluidization/erosion, as described by Devinder et al. (2000)

Bolchover et al. (2006) believes tensile failure is the most critical mechanism. Walten et al. (2000) and Subiaur et al. (2004), postulates that for production purposes, the effect from the mechanical failure of the perforation damaged zone is posited to have a higher increase in perforation productivity, compared to the effect of removing loose perforation debris. However, cleaning out the perforation and jetting debris is critical when it comes to an injection scenario, as the injection fluid will push and compact loose debris in the perforation, creating an additional skin effect.

Although high drawdown improves collapse of the crushed zone and the cleanout surge, careful consideration should be given to the formation strength to ensure that drawdown pressure does not collapse the perforation tunnel or compromises downhole equipment (Gasmi et al. 2015).

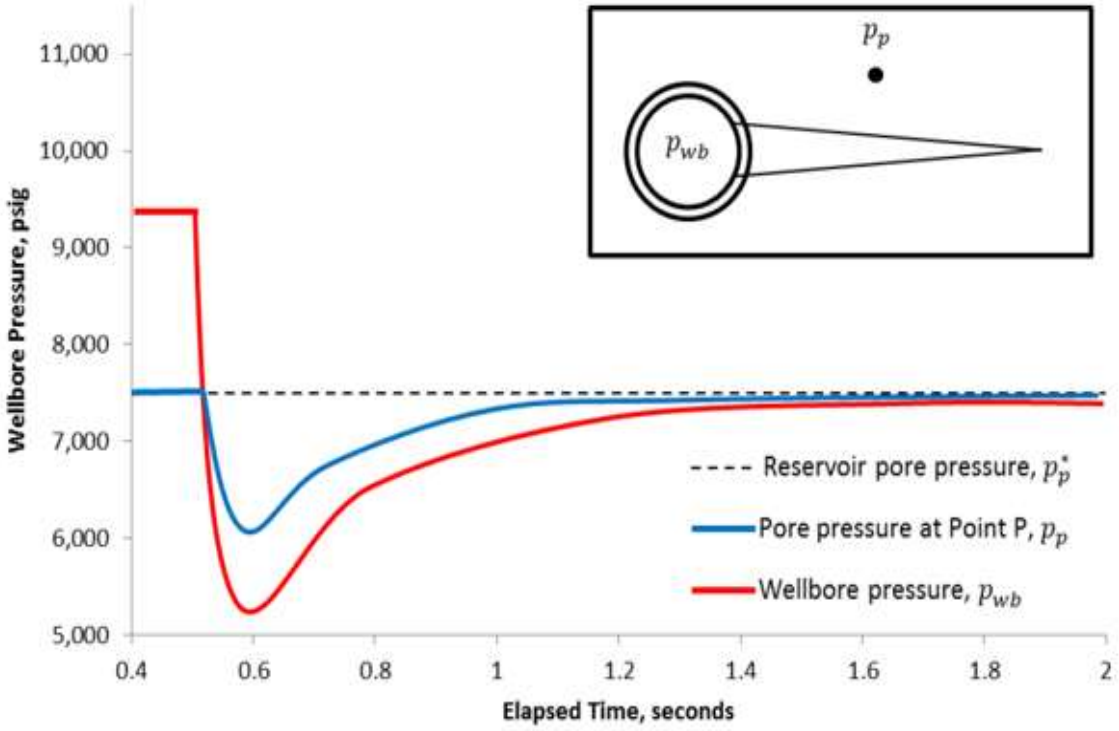

Figure 18- Dynamic underbalance and drop in local pore pressure (McGregor et al. 2018)

2.7 Factors affecting the effect of dynamic underbalance

Several of the physical parameters that affect the result of perforating in dynamic underbalance has been investigated before. The apparently most vital factors will here be described.

2.7.1 Permeability

In order to achieve high surging flow in the perforation tunnel, sufficient fluid needs to flow through the reservoir in near-wellbore area, through perforation tunnel, and into the wellbore. High permeability will lead to higher fluid flow from the reservoir to the perforation tunnel, and hence increasing surge effect. Hsia et al. (1991) tested Gold and Berea sandstones of respectively 100 and 200mD permeabilities for various underbalance, examining which underbalance required to obtain zero perforation skin in both cases. Results showed that the Gold sandstone required approximately twice the underbalance, compared to Berea sandstone, to achieve the same cleanout and skin values.

High permeability will also facilitate a rapid transmission of low well pressure to the pore pressure around the perforation tunnel which, according to McGregor et al. (2018), is critical in order to increase effective stresses in the damaged zone as quickly as possible.

Figure 19 illustrates the relationship between permeability and underbalance to obtain clean perforations. If acid wash did not improve production, it is considered that successful clean-out was achieved. Red "s" indicates successful clean-out, while blue "I" indicates unsuccessful clean-out. Oseberg South has a permeability of 200 mD.

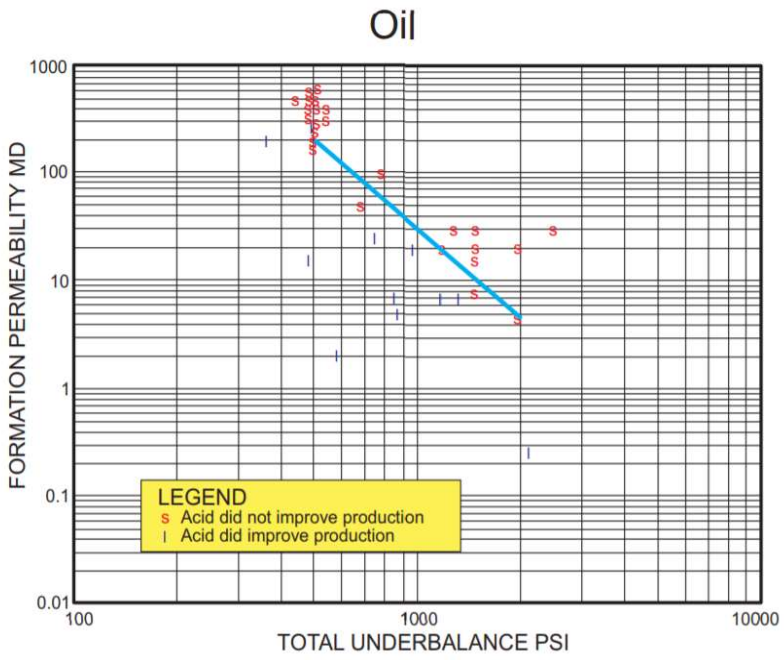

Figure 19-Perforating performed as a function of formation permeability and total underbalance (Halliburton Perforating Solutions, 2019)

2.7.2 Reservoir pressure

Reservoir pressure is also a limiting/amplifying factor when it comes to the effect of dynamic underbalance. "While the DUB technique itself is a step-change in enhancing productivity by cleaning out the perforation plugging and crushed zone, the fact that reservoirs are in a mid-pressure regime means that the DUB magnitude is limited, and the cleaning of perforations does not reach its full potential. In this case, the perforation tunnel is partially plugged, and the crushed zone is not fully removed" (Jumaat et al. 2013).

Although high reservoir pressure and high permeability appears to be the optimal environment for dynamic underbalance to work properly, work done by Stutz et al. (2014) shows significant productivity improvement could be achieved at low permeability, low-pressure Brady gas field. This is however a gas field and is not analogues to an oil field like Oseberg South.

Reservoir pressure will be a critical parameter when perforating at Oseberg South, because of the significant depletion of the field. Zone to be investigated will have a reservoir pressure of 2850 psi.

2.7.3 Wellbore pressure

Due to high focus on well control, previous wells at Oseberg South has been perforated in high overbalance (with dynamic underbalance), and the effect of reducing hydrostatic overbalance needs to be investigated. It is hypothesized that lower hydrostatic pressure will primarily extend the duration, and to less extent increase magnitude of the dynamic underbalance.

Wellbore pressure has additionally an effect on jet penetration performance. Behrmann et al. (1988) discovered a clear, consistent relationship between the penetration depth and wellbore pressure in a Berea Sandstone. Perforating at Oseberg South has traditionally been performed at high wellbore overbalance of approximately 2000 psi.

2.7.4 Free gun volume (FGV)

In a number of experiments performed at Jet Research Center by Haggerty et al. (2012), challenging the current perforation clean-up models, the sensitivity between FGV and perforation performance was thoroughly investigated. The conclusion was that higher FGV results in higher DUB, and higher fluid velocities through the perforation tunnel.

Figure 20 shows the effect of flow velocity by increasing the atmospheric volume in order to decrease wellbore pressure immediately after the guns are fired. Negative indicates fluid flow into the wellbore (clean-up).

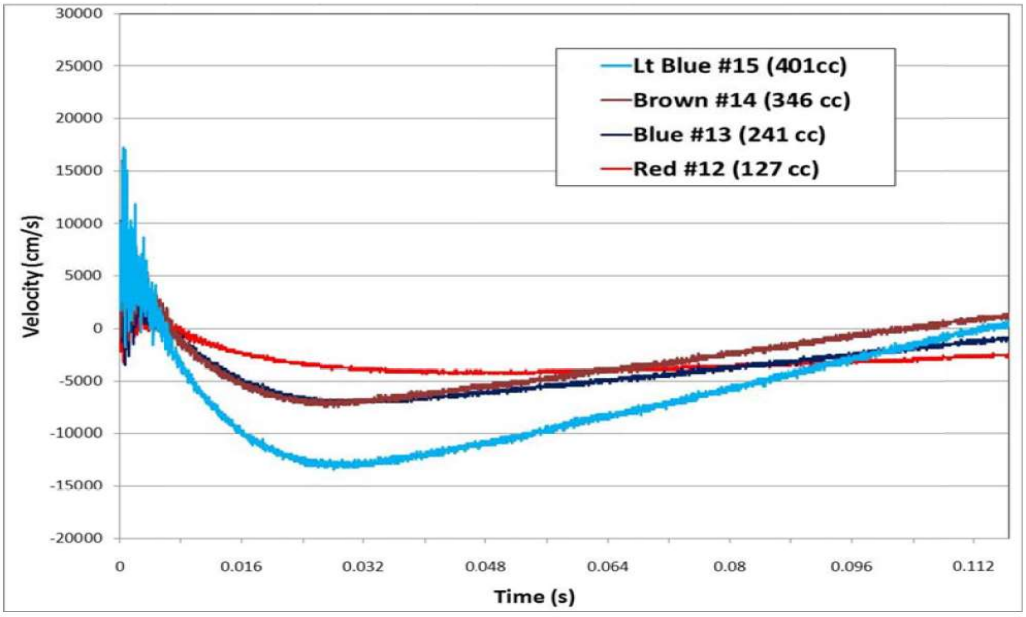

Figure 20- Fluid velocity through the perforation tunnel (Haggerty et al. 2012)

Table 3- FGV versus perforation performance properties (Haggerty et al. 2012)

TABLE 2—SUMMARY OF FGV TEST RESULTS AND PARAMETERS.						
Test ID	Entrance Hole Diameter, in.	Total Core Penetration, in.	Open Hole, in.	Percent Open Hole	Void Space in Gun, cc	Fluids Wellbore/Pore
12	0.35	8.7	1.2	13.80%	127	OMS/OMS
13	0.35	8.2	3	36.60%	241	OMS/OMS
14	0.32	8.35	6.95	83.20%	346	OMS/OMS
15	0,31	6.72	5.98	89.00%	401	OMS/OMS

2.7.5 Rock strength

Compressive rock strength is the most important formation property that determines the depth of penetration. Based on field observation, Smith et al. (1997) reported that the performance of the shaped charges depends on the compressive strength of the formation. When the compressive strength of the formation is sufficiently higher, the probability of the shaped charge's to bypass the drilling damaged formation is lower. However, they also pointed out that the possibility of increasing the penetrating depth by optimizing the perforator geometry design. Thompson et al. (1962) was the first to experimentally make a relationship between rock compressive strength and perforator performance by testing four

low permeability rocks. Table 4 shows penetration versus rock strength for one chalkstone, two limestones, and one sandstone.

Table 4- Rock strength versus penetration (Thompson et al. 1962)

Formation rock	Average compressive strength (psi)	Relative penetration (inches)
Austin Chalk	2300	17,2
Indiana Limestone	4900	7,6
Berea Sandstone	6500	5,2
Carthage Limestone	13000	2,4

However, laboratory study done by Saucier et al. (1978) shows not the same consistent relationship between rock compressive strength and penetration. The decrease in penetration as a function of rock compressive strength, in this case, flattened out after approximately 5000 psi. Formation penetration was not further reduced at strengths above this level. The majority of research done still concludes that there is a distinct relationship between rock compressive strength and formation penetration. It's worth mentioning that these tests were not performed to investigate rock strength impact on DUB specifically, but rather the overall impact rock strength has on perforating. Sandstone at Oseberg South has a compressive strength of approximately 2176 psi.

2.7.6 Perforation radius

Perforation radius also impacts the effect of surge flow in the perforation tunnel. According to Pearson et al. (1997), the flow velocity through the perforation tunnel decreases as the radius of the perforation increases. This will affect the transportation of particles along the tunnel. This is explained by Pearson et al. (1997) to be a result of the fact that the flow rate into the perforation from the formation will be linearly dependent on perforation radius. This is due to the fact that flow velocity v_o into the perforation is not too sensitive to the radius r_o.

$$q \approx 2\pi r_o * l * v_o \qquad (11)$$

On the other hand, fluid velocity inside the perforation will be a quadratic relationship of r_o. This gives us fluid velocity u inside the perforation tunnel.

$$u = \frac{q}{A} = \frac{2\pi r_o * l * v_o}{\pi {r_o}^2} = \frac{2 * l * v_o}{r_o} \qquad (12)$$

Hence, the increase in perforation radius will decrease fluid velocity, which reduces drag force on the particles to be cleaned out of the perforation tunnel, resulting in reduced clean-out. Figure 21 shows how the "permeability versus underbalance" trend shifts upwards as radius increases. For a 400 psi underbalance, perforation radius of 1 cm would require 1000 mD while 1,5 cm radius would require approximately 2000 mD. The effect is even more significant for 0,5 cm radius.

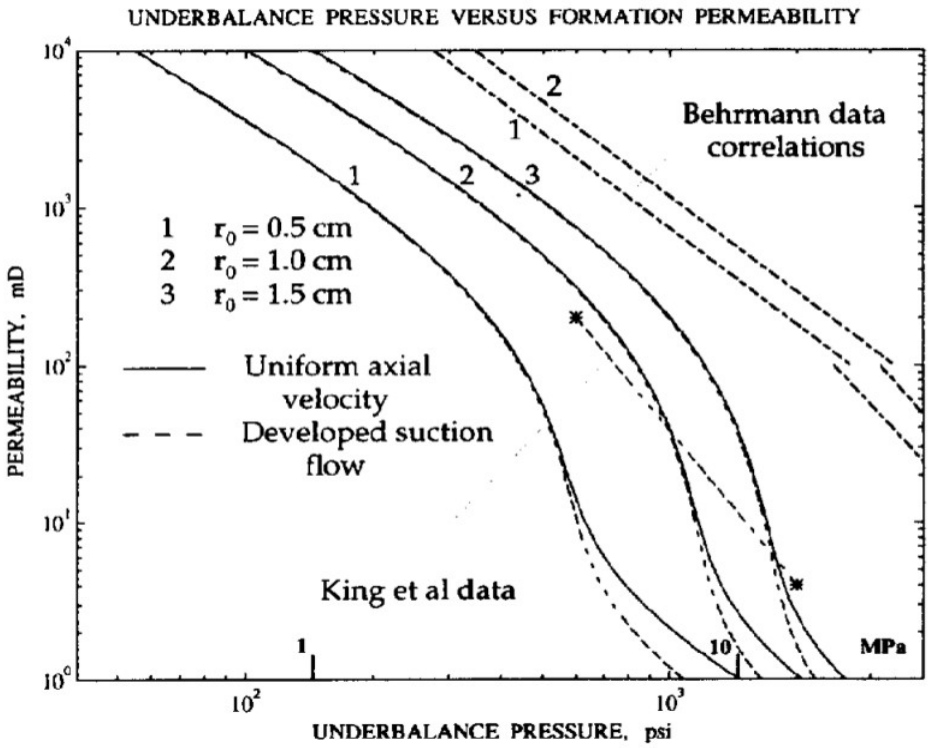

Figure 21- Underbalance pressure necessary for the perforation cleaning versus formation permeability for the radius of perforation (Pearson et al. 1997)

2.7.7 Time in dynamic underbalance

The time in which we will have dynamic underbalance across the perforation is an extremely critical factor to not only mobilize but completely flush particles out of the perforation tunnel.

If DUB time is insufficient, debris will be pushed back into the tunnel by wellbore overpressure, potentially plugging pores and leaving permanent debris behind. Figure 22 displays the dimensionless relationship between clean-up time and underbalance pressure.

Studies performed on a North Kuwait well also shows a significant positive impact on the clean-up process, if the duration of underbalance is extended (Al-Tahou et al. 2017).

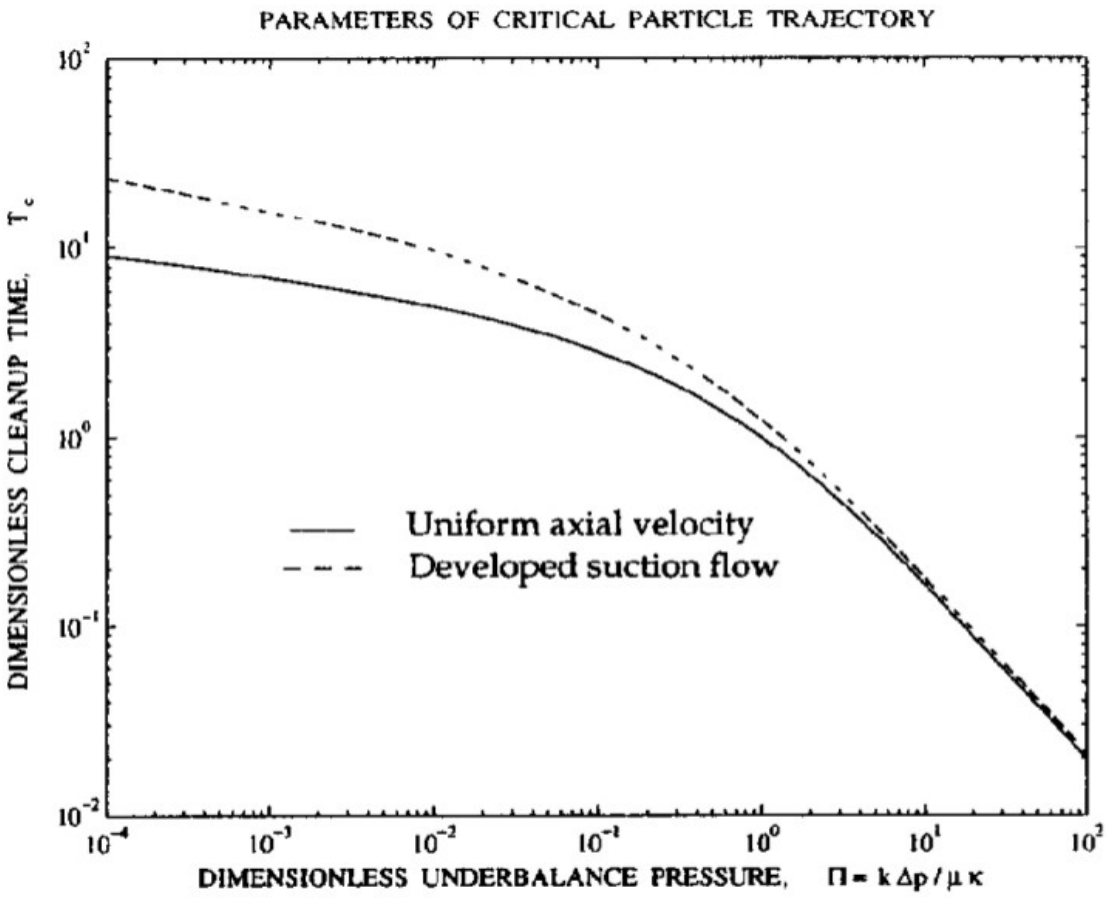

Figure 22- Dimensionless clean-up time versus underbalance pressure for critical particle trajectories (Pearson et al. 1997)

2.7.8 Fluid properties

As explained by Tariq et al. (1990), pressure drop and drag force onto particles during underbalanced perforating will be facilitated by the viscous and inertial term in Forchheimer equation. Quantification of these two terms for various flow rates can be performed to understand which fluid property will be dominant: density, or viscosity (see 3.1.2).

2.7.9 Fines in the perforation tunnel

In addition to the criticality of crushed and compacted rock around the perforation tunnel wall, is the amount of mobile fines present. According to Devinder et al. (2000), there are two sources of fines in the perforation:

1. Native fines (for example clay particles)
2. Fines generated as the rock was crushed during the perforating event

Fines can plug pore throats and decrease permeability around the perforation wall significantly. It is therefore critical to achieve a high fluid velocity of sufficient duration. If fines are flushed back and pushed towards the perforation wall with high force (due to high hydrostatic pressure in the well), a severe reduction in permeability could be seen.

Since a sufficient underbalance is required to clean out the perforation tunnel, it is worth noticing that at a critical amount of underbalance, native fines in virgin part of the formation will start to mobilize. Native fines moving from pore body to pore throats will reduce formation permeability. Hence, optimum underbalance should be sufficient to clean out debris and reduce crushed zone, but insufficient to mobilize the native fines.

$$\Delta P_{crit,clean\ up} \leq \Delta P < \Delta P_{mobilization\ of\ fines} \qquad (13)$$

3 Modeling, SIMULATION, AND EXPERIMENTAL DESIGNS

3.1 Modeling flow performance during dynamic underbalance

3.1.1 Flow facilitating clean-up

Flow in porous media is usually described using Darcy's law, where pressure drop is dominated by a viscous term. In 1901 however, Forchheimer found Darcy law to be non-valid as flow velocity increases, and therefore added another term, taking into account the inertial effects (Zeng et al. 2008):

$$\frac{\delta \mathrm{P}}{\delta L} = \underbrace{\frac{\mu}{K} U}_{viscous\ term} + \underbrace{\beta \rho U^2}_{inertial\ term} \qquad (14)$$

Where:

- $\Delta \mathrm{P}$ = pressure drop
- L = flow length
- μ = viscosity
- K = permeability, note this is not Darcy but Forchheimer permeability although it is very close to Darcy permeability
- β = inertial coefficient
- ρ = fluid density
- U = fluid velocity

According to Tariq et al. (1990), the low-velocity Darcy flow is insufficient to initiate clean-up of particles from the perforation tunnel. In this flow regime drag force onto particles is proportional to fluid velocity and is caused by shear stress due to viscous forces in the fluid. As fluid velocity increases, Darcy's law becomes invalid, and the inertial term in the Forchheimer equation starts to dominate. Tariq et al. (1990) uses field data and simulations to confirm that under such conditions, clean-up can initiate. Drag force will become a sum of the viscous force and the density-dependent inertial term, which is proportional to velocity squared.

To achieve completely turbulent flow, extremely high underbalance would be needed, which according to Tariq et al. (1990) would be both practically difficult and well beyond the critical underbalance in order to initiate clean-up.

3.1.2 Radial flow into to perforation

Based on Forchheimer, a simplified calculation can be done to investigate what amount of reservoir fluid which can be "produced" in the dynamic underbalance state. The impact of fluid properties can also be quantified. Figure 23 and Figure 24 show the model setup. For the modeling, the assumption considered were:

1. Pure radial flow into the perforations
2. Flow obeying Forchheimer law
3. Two zones of permeability, damaged/crushed, and virgin rock
4. Constant pore pressure at the periphery

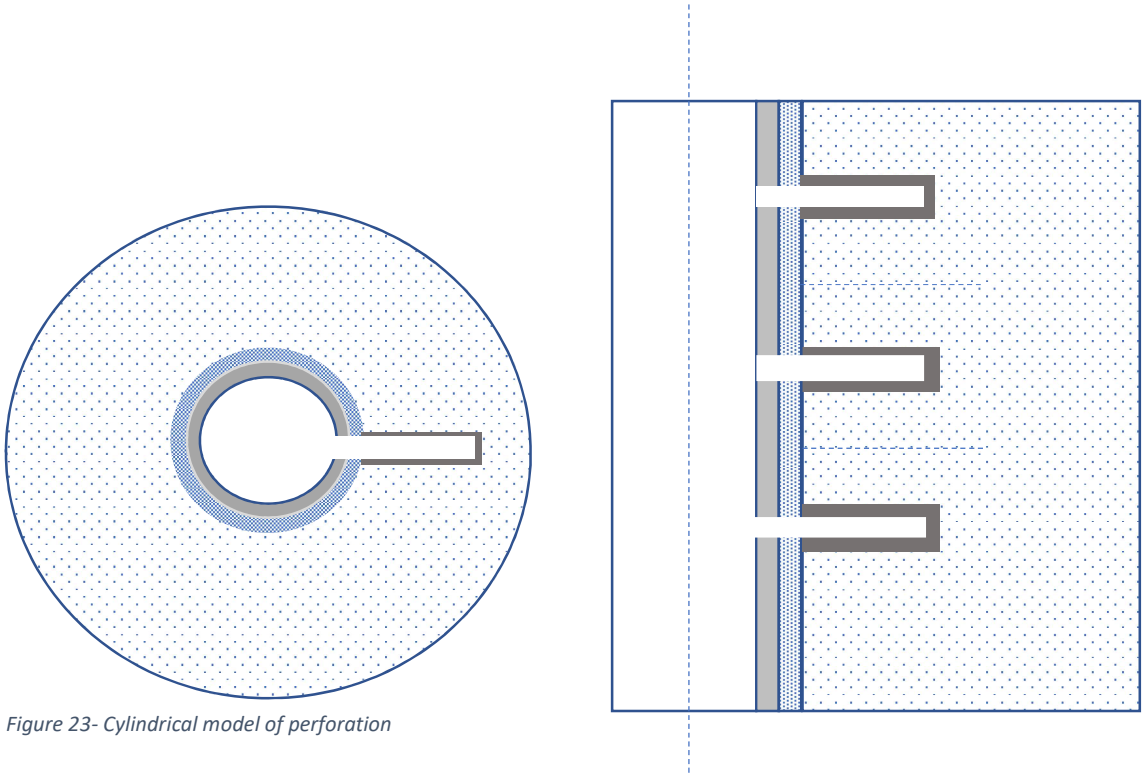

Figure 23- Cylindrical model of perforation

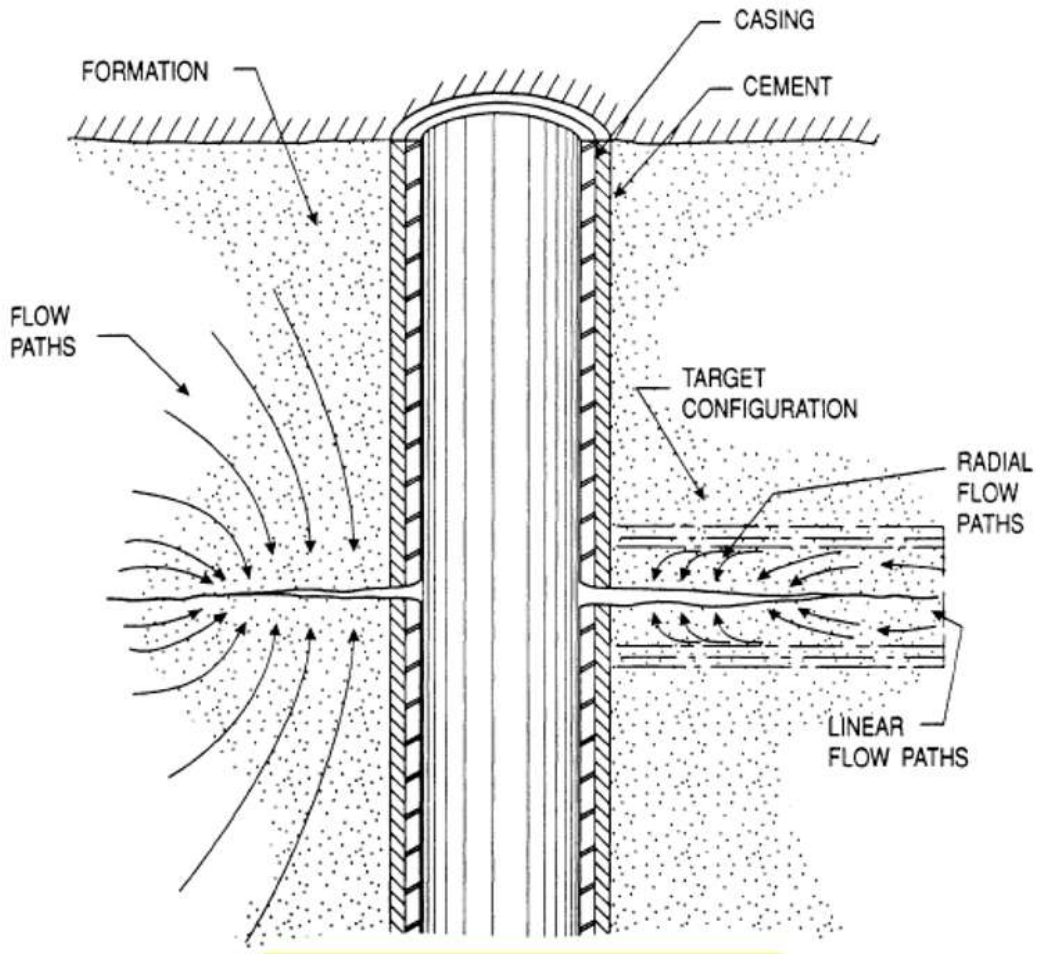

Figure 24- Flow into wellbore through perforations (Hsia et al. 1991)

$$\delta P = \frac{\mu}{K}\frac{q}{A} * \delta L + \beta\rho\frac{q^2}{A^2} * \delta L = \frac{\mu}{K} * q * \frac{\delta r}{2\pi L_p * r} + \beta\rho * q^2 * \frac{\delta r}{(2\pi L_p)^2 * r^2} \qquad (15)$$

$$\delta P = \frac{\mu}{K} * q * \frac{1}{2\pi L_p} * \int_{r_p}^{r_e}\frac{1}{r} * \delta r + \beta\rho * q^2 * \frac{1}{(2\pi L_p)^2} * \int_{r_p}^{r_e}\frac{1}{r^2} * \delta r$$

$$\Delta P = \frac{\mu}{K} * q * \frac{1}{2\pi L_p} * ln\left(\frac{r_e}{r_p}\right) + \beta\rho * q^2 * \frac{1}{(2\pi L_p)^2} * \left(-\frac{1}{r_{r_p}^{r_e}}\right)$$

$$\Delta P = \frac{\mu}{K} * q * \frac{1}{2\pi L_p} * ln\left(\frac{r_e}{r_p}\right) + \beta\rho * q^2 * \frac{1}{(2\pi L_p)^2} * (-1)\left(\frac{1}{r_e} - \frac{1}{r_p}\right)$$

$$\Delta P = \frac{\mu}{K} * q * \frac{1}{2\pi L_p} * ln\left(\frac{r_e}{r_p}\right) + \beta\rho * q^2 * \frac{1}{(2\pi L_p)^2} * \left(\frac{1}{r_p} - \frac{1}{r_e}\right)$$

This equation is only valid for one zone of permeability around the perforation. For a more realistic scenario, we will have a low permeability crushed zone. Total pressure drop can be calculated as the sum of pressure drop from exterior to crushed zone and pressure drop across the crushed zone, which will be in accordance with McLeod equation for perforation skin:

$$\Delta P = \frac{\mu}{K_d} * q * \frac{1}{2\pi L_p} * ln\left(\frac{r_e}{r_c}\right) + \beta\rho * q^2 * \frac{1}{(2\pi L_p)^2} * \left(\frac{1}{r_c} - \frac{1}{r_e}\right) + \frac{\mu}{K_c} * q * \frac{1}{2\pi L_p} * ln\left(\frac{r_c}{r_p}\right) + \beta\rho * q^2 * \frac{1}{(2\pi L_p)^2} * \left(\frac{1}{r_p} - \frac{1}{r_c}\right) \qquad (16)$$

Where we choose β to be:

$$\beta_1 = \frac{11500}{k * \varphi} \ (Li\ et\ al. 2001) \qquad (17)$$

Or

$$\beta_2 = 1{,}82 * 10^8 * k^{-\frac{5}{4}} * \varphi^{-\frac{3}{4}} \ (\text{Janicek et al. } 1953) \qquad (18)$$

Or

$$\beta_3 = \frac{2{,}6 * 10^{10}}{k^{1{,}2}} \ (\text{McLeod et al. } 1983) \qquad (19)$$

We can then flow rate through one perforation as a function of pressure drop:

Figure 25 shows the total flow rate for different beta factors. Figure 26 shows us the contribution of the viscous and inertial term to the pressure drop through one perforation. As can be seen, the uncertainty related to the inertial pressure drop is significant. Tortuosity and pore size distribution will affect this and needs to be investigated further in a laboratory.

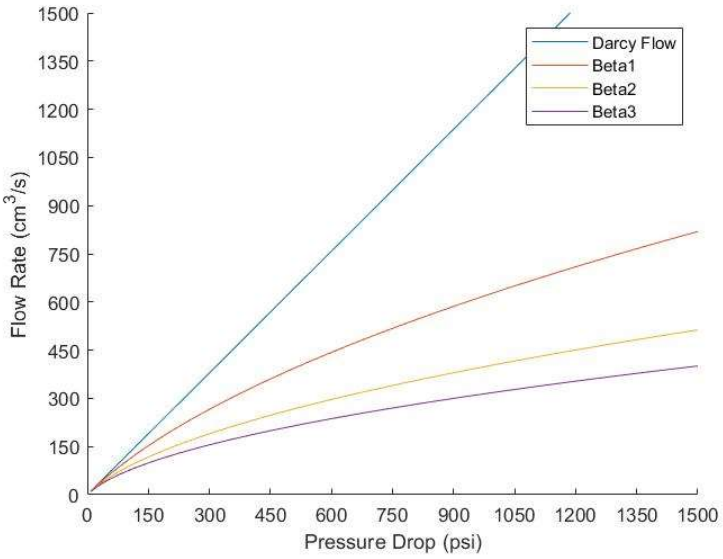

Figure 25-Pressure drop for Darcy Flow and three Beta factors

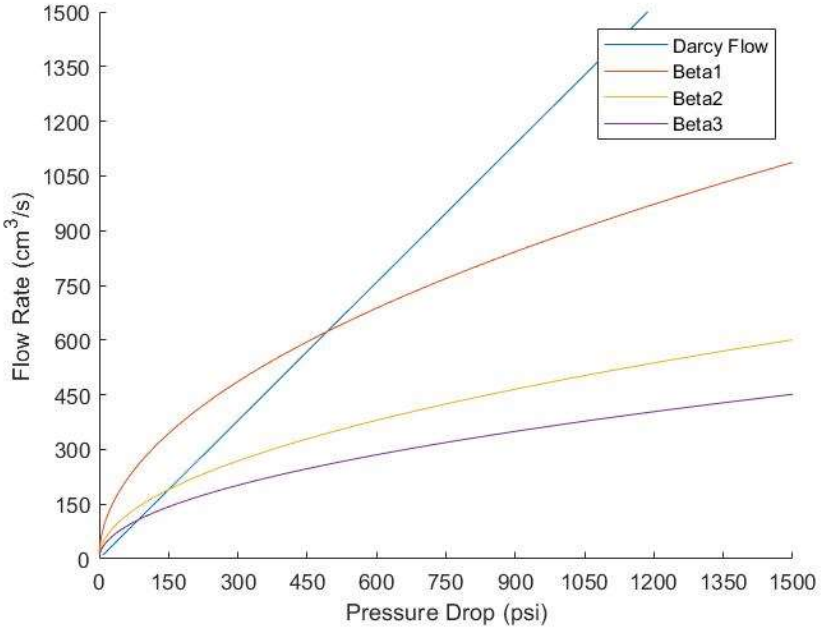

Figure 26-Comparison of the viscous and non-viscous term for three Beta factors

3.2 Dynamic underbalance Simulations design

The two perforating techniques will be evaluated through several simulations and Section IV tests.

3.2.1 Perforating on pipe with 4-5/8" gun system- overbalanced with kill pill

Oseberg South has been perforated on pipe with high overbalance (due to uncertainty in reservoir pressure) and dynamic underbalance achieved from free gun volume (surge chambers and volume from guns). 4-5/8" gun system with 39g HMX MaxForce has been used, which has proven to have long penetration. Even though this system has high charge performance, it is uncertain whether the flow dynamics due to low reservoir pressure and high overbalance is optimal to create clean perforation tunnels.

3.2.2 Perforating on wireline with 3-1/8" gun system- balanced with brine

The second option is to perforate with wireline on balance with dynamic underbalance. First shot will be in underbalance, but after the first shot, communication between reservoir and wellbore will result in a balanced state. Because of limited wire strength, 10-15 meters of perforations has traditionally been perforated on each run. In long horizontal wells at Oseberg South, 1000-1500 meters of perforations are planned, meaning 100 wireline runs would be necessary. However, Archer's new ComTrac wireline cable can carry up to 100 meters of perforating cannons. If perforating with wireline, a 17.5g HMX MaxForce charge would be used in a 3-1/8" gun system. This system has significantly lower charge performance compared to 39g HMX MaxForce. On the other hand, the advantage of perforating in balance can improve flow dynamics during the perforating, improving clean-up and productivity.

Figure 27 is an illustration of the perforating tool string for perforating on pipe (left) and wireline (right). These tool strings are not relevant for the perforating jobs at Oseberg South.

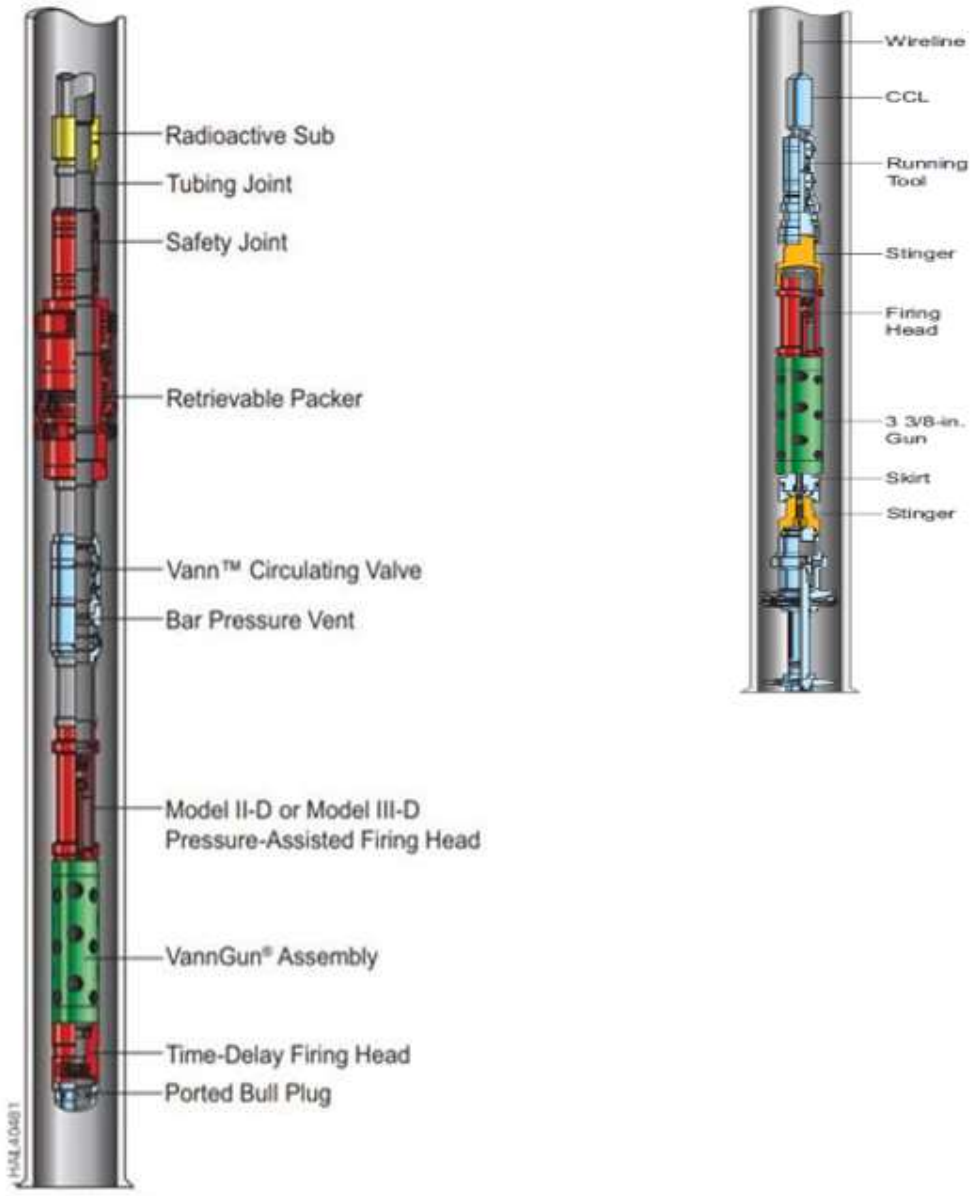

Figure 27- Tool string for perforating on pipe and wireline (Halliburton Perforating Solutions, 2019)

3.2.3 Halliburton Perforating Tool Kit (HPTK)

HPTK is a software designed to optimize perforating processes based on various input parameters. The primary objective is to reduce possible perforation skin and increase productivity by appropriate gun selection. By performing sensitivity studies and charge performance analysis, HPTK can improve perforation configuration and strategy. HPTK uses 3D finite element modeling from more than 500 perforating flow lab studies performed in API Section IV/API Section II, in order to simulate perforating performance (Wight et al. 2016). HPTK will for this project be used to estimate the charge performance:

- Formation penetration
- Effective penetration
- Casing exit hole diameter
- Perforation average diameter which is estimated to be casing exit hole diameter plus 0,05 inch

The outputs from HPTK will then be inputs for the SurgePro simulations.

3.2.4 SurgePro

SurgePro is a software developed by Schatz et al. (1999), and is used to simulate the perforating event, and to predict the dynamic behavior inside the perforation, wave propagations during production and injection, and pressurizations in the wellbore and the perforation. The model is physics-based and uses conservation laws for mass, momentum, and energy for each timestep. Navier-Stokes equations for wellbore, perforation and fracture flow, and solid rock mechanics describing formation breakdown inside the perforation. SurgePro takes into account, among others: the multiphase flow of compressible fluids, several energy sources such as perforating gun ignition, effects of multiple diameters in the well, return flow from perforations, and breakdown of perforation tunnels.

Based on the dynamic pressure behavior and fluid velocity in the perforation tunnel, SurgePro uses a modification of the Ergun equation to determine when the fluid has sufficient velocity to clean out crushed particles:

$$\frac{1.75}{a\phi^3}\left(\frac{d_p U_f \rho}{\eta}\right)^2 + 150\left(\frac{1-\phi}{a^2\phi^3}\right)\left(\frac{d_p U_f}{\eta}\right) = \frac{d_p^2 \rho C}{\eta^2} \quad (20)$$

Where

- U_f = fluid velocity
- ρ_f = fluid density
- n = fluid viscosity
- a = particle aspect ratio
- d_p = particle size
- C = particle cohesion
- φ = porosity

A case history from the El Furrial field in Venezuela showed production increase of approximately 59% and higher well-flowing pressure, following a DUB perforating job with SurgePro simulations in advance, optimizing damage zone removal. Productivity increase was estimated to be from 0,35bbl/psi to 0,91bbl/psi (Casas et al. 2009).

The perforation event is highly complex, and to model the pressure and flow behavior accurately is until now not possible. “Though the software can be configured to report a number of physical parameters of interest (e.g., pressure, force, temperature, etc.), caution must always be applied when using numerical solutions to such a tightly coupled system of equations containing disparate time and spatial scales” (Satti et al. 2018). SurgePro is, however, one of the most reliable software in perforation clean-up simulations and has a long and well-known history. Figure 28 shows how fast gauge data fit with the SurgePro predicted well pressure.

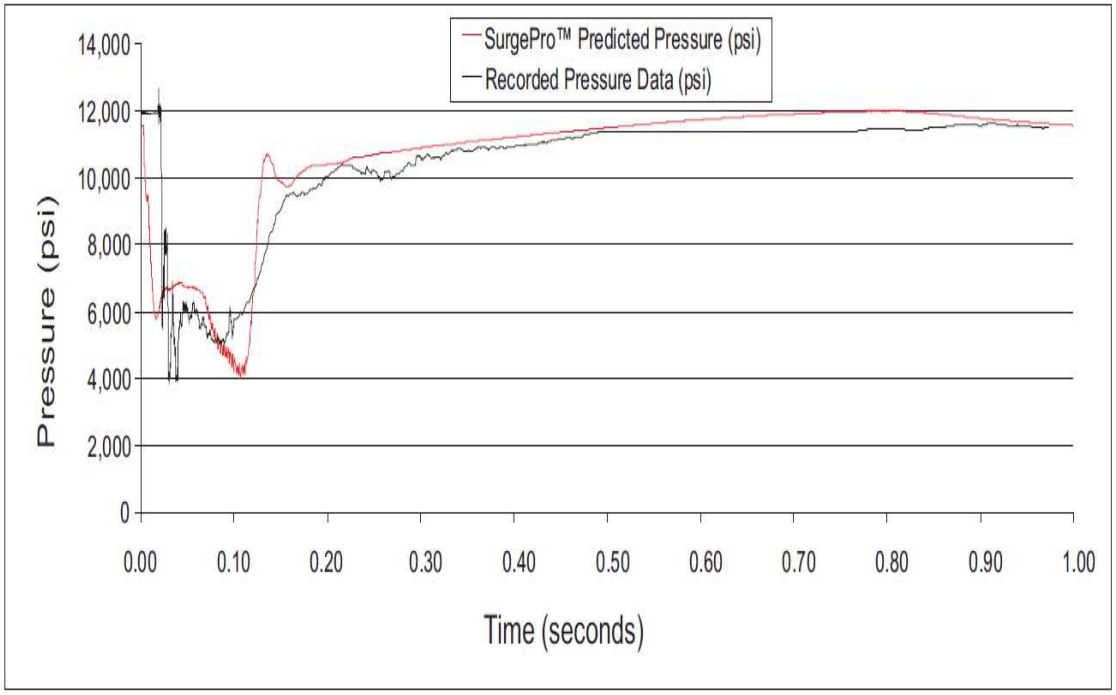

Figure 28- Surge Pro predicted pressure versus recorded data from Fast Gauge (Halliburton, 2019)

SurgePro will for this project be used to give an estimate of which dynamic underbalance we can expect downhole. Section IV tests will then be designed to fit the pressure response simulated.

3.2.5 WEM

Well Evaluation Model (WEM) is a nodal analysis software which simulates well performance. It includes PVT analysis, heat balance and can be used for multilateral wells and multilayer reservoirs. WEM will for this purpose be used to quantify well performance for the two cases to be tested. WEM uses a cylindrical model for the perforation tunnel with k_c/k, perforation length and diameter. After running simulations, WEM presents IPR curves to illustrate the inflow performance for the specific well.

3.3 Experimental work design

The Halliburton Jet Research Center (JRC) was founded in 1945 and was originally named Halliburton Well Services Company (Welex). JRC adapted bazooka technology from World War 2 to improve perforation efficiency compared to the previous bullet perforating technique. JRC is located in Alvarado, Texas, and is a fully integrated research, design, testing, and manufacturing facility.

3.3.1 Experimental test setup

Halliburton's Advanced Perforating Flow Laboratory (APFL) contains three pressure vessels for perforating tests:

- 50 000 psi vessel
- 25 000 psi vessel with the capability to rotate up to 180 degrees, to better understand sanding in horizontal wells
- 25 000 psi high-temperature vessel with flow temperatures up to 204 degrees Celsius

Data obtained from the tests can be used to develop perforating techniques in order to:

- Clean perforation tunnels more effectively
- Increase productivity
- Evaluate different perforating methods
- Assess new explosive compound and evaluate their performance
- Use metals with better performance

API Evaluation of Perforators

API Section I-IV provides means for evaluating perforating systems (API 19B):

- Performance under ambient temperature and atmospheric pressure test conditions.
- Performance in stressed Berea sandstone targets (simulated wellbore pressure test conditions).
- How performance may be changed after exposure to elevated temperature conditions.
- Flow performance of a perforation under specific stressed test conditions.

For this test program, 4 section IV tests will be conducted.

Section IV Evaluation of Perforators

"The purpose of Section IV is to provide a basis for the comparison, development, and evaluation of perforators and perforating performance in general through the use of tests looking at the flow performance of perforations shot into rock cores, shot under in situ conditions" (API 19B).

It contains the following instructions:

a. A basic target preparation and constructions technique specification;

b. A basic equipment and technique specification highlighting common test artifacts for consideration;

c. Standard qualification test description(s), including core saturation procedures; and

d. Minimum requirements for comparative tests.

Figure 29 shows a Section IV test apparatus.

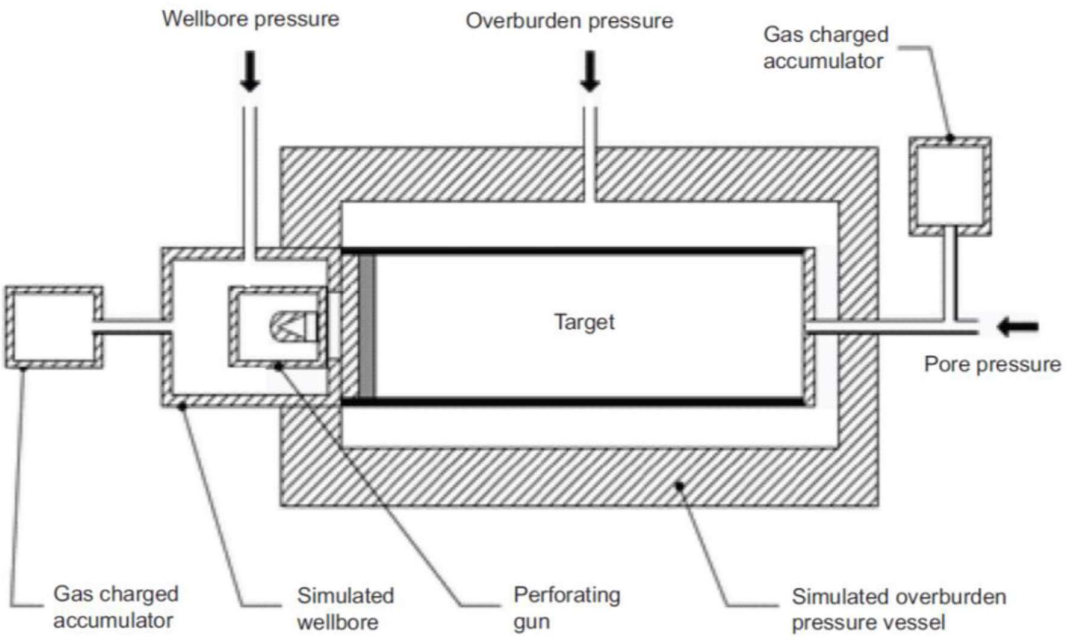

Figure 29- Schematic diagram of testing equipment, Jet Research Center (API RP 19B)

Figure 30 is a cutaway model of a wellbore assembly according to API RP 19B.

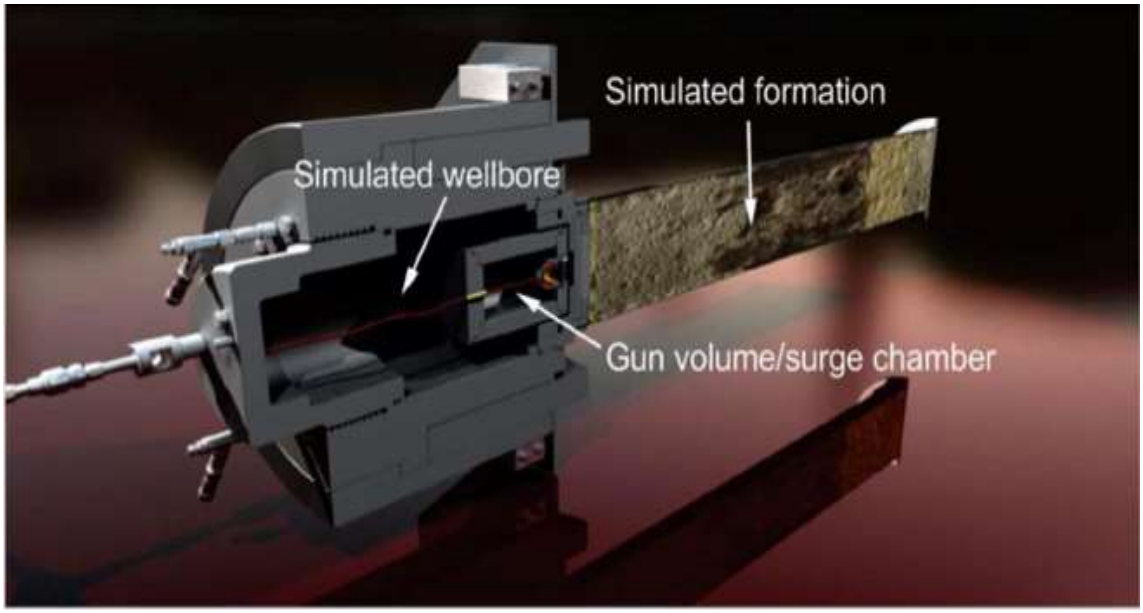

Figure 30- Cutaway model for testing equipment (Jet Research, 2019)

Figure 31 shows a schematic of the test vessel. The core is placed on a flow distribution disk. Confining the core is a bladder to which water applies overburden pressure. Steel rods between the core and the bladder allows for axi-radial flow. The core is then placed in the pressure vessel. Fluid loss pill fills the wellbore chamber surrounding the loaded gun. Pore and wellbore nitrogen accumulators can pressure up the core and wellbore respectively through inlets in the bottom and the top of the assembly. Pore and wellbore pressure transducers measure the far-field pore and wellbore pressure, while piezo-electric measurements within the wellbore chamber will give local wellbore pressure. The pressure accumulators and wellbore isolation valve are used to control the pressures before and after detonation. The bypass valve is used to let flow and pressure bypass the core if necessary.

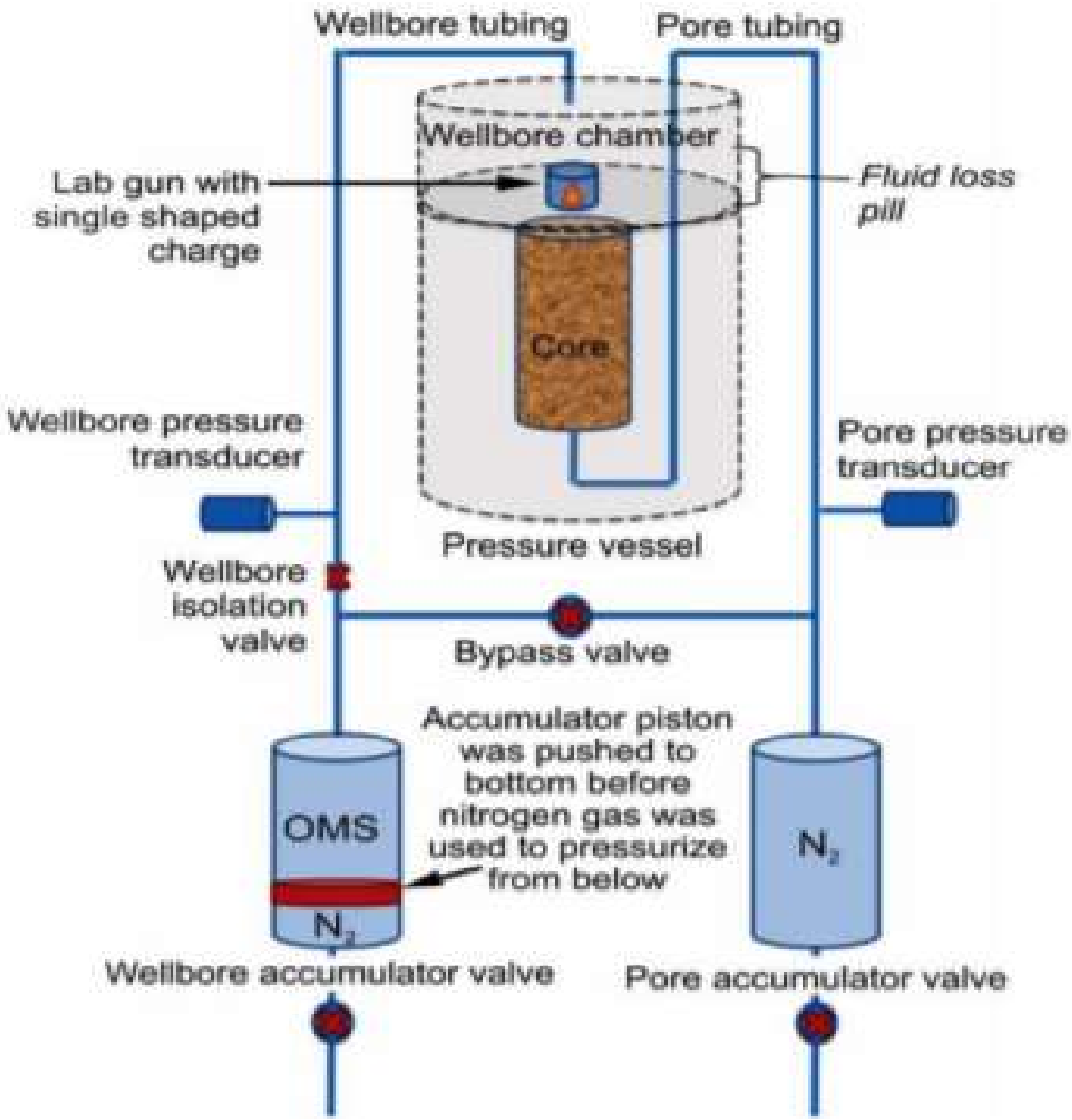

Figure 31- Schematic of the test cell and pressure lines (Jet Research Center, 2019)

3.3.2 Description of cores and fluids

Cores for perforating tests can be provided in three ways:

- Harvest cores from the field
- Make artificial cores, by cementing blocks with similar properties as the formation
- Order rock samples with similar properties as the formation

Cores for evaluating Oseberg South perforating techniques will be provided by producing artificial cores. Blocks are cemented with properties to match the formation to be perforated.

After solidification and drying, cores are drilled out of the block and then saturated with odorless mineral spirit (OMS).

Table 5- Test setup

	Test	1	2
Piece Parts	Charge	390 MaxForce	175 MaxForce
	Charge PN	102054947	101826652
	Casing PN	SK 10077	SK 10077
	Scallop PN	SK 10075	SK 10076
	Spacer PN	0.352 Spacer	1.892 Ring
	WB Fluid	Baroid Pill	3% NaCl
Shot-time Pressures (psi), Temp. (F), & Configuration	Confining	8294	8294
	Pore	2840	2840
	WB	5000	2840
	SOB(+)/SUB(-)	+2160	+0
	Eff. Stress	5454	5454
	Temp	230	230
	Configuration	Axi-Radial	Axi-Radial
	Target Core	Berea Buff SS	Berea Buff SS

Figure 32 shows various possibilities for flow distributions for a perforated core. For a 4 shots per foot completion, axi-radial is the most realistic and will be used during post-shot flow tests.

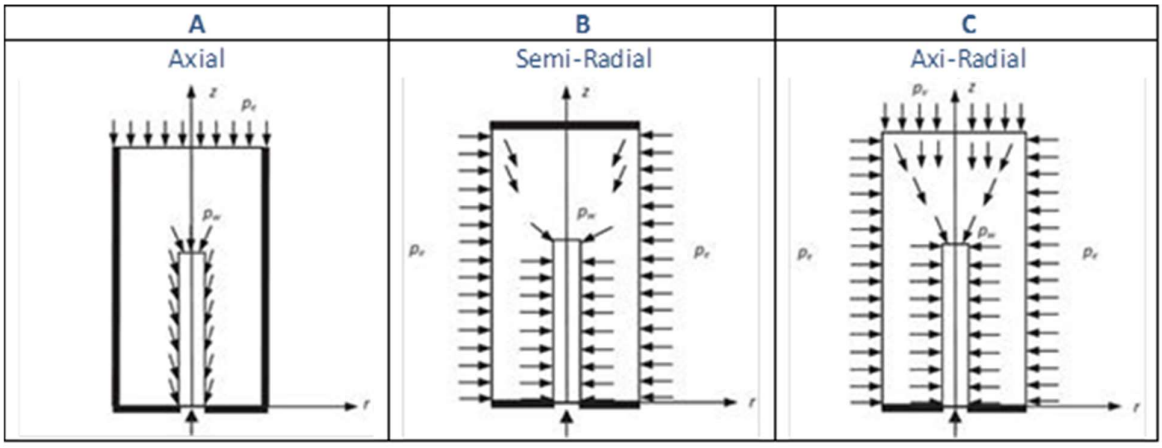

Figure 32- Flow distribution for perforated core (Jet Research Center, 2019)

Table 6 shows the chemical components and concentrations used in the kill pill system.

Table 6- Kill pill

PRODUCT	FUNCTION	CONCENTRATION
CLAIRSOL NS	Base Oil	0.4 m^3/m^3
EZ MUL NS	Emulsifier	15 kg/m^3
PERFOR MUL	Emulsifier	35 kg/m^3
DRILTREAT	Oil Wetting Agent	10 kg/m^3
GELTONE II	Viscosifier	20 kg/m^3
DURATONE E	OBM Filtration Control Agent	20 kg/m^3
LIME	Alkalinty Control Agent	8 kg/m^3
CACL2 BRINE (1.129 SG)	Salinity/Weight Agent	0.46 m^3/m^3
BARACARB 50	Bridging	90 kg/m^3
BARACARB 5	Bridging	50 kg/m^3

3.3.3 Perforation characterization methods

3.3.3.1 Perforation geometry

Figure 4 displays the terms used to characterize the perforation tunnel geometry. The perforation geometry can be quantified by measuring diameter and 3 different penetration properties, using CT images:

- Total core penetration (TCP)
- No-debris penetration (NDP)
- Lower-bulk-density penetration (LDP)

Effective perforation penetration can be evaluated using an equation for “clear tunnel%”:

$$clear\ tunnel\ \% = \frac{clear\ tunnel\ penetration}{total\ core\ penetration} \qquad (21)$$

To visualize which flow-path the fluid takes through the core, injection dye flow testing will be performed. This will leave a light blue color where the fluid has flown, and a darker purple color, where it has been little or no flow.

Figure 33 illustrates the characterization of a perforation tunnel and the terminology used.

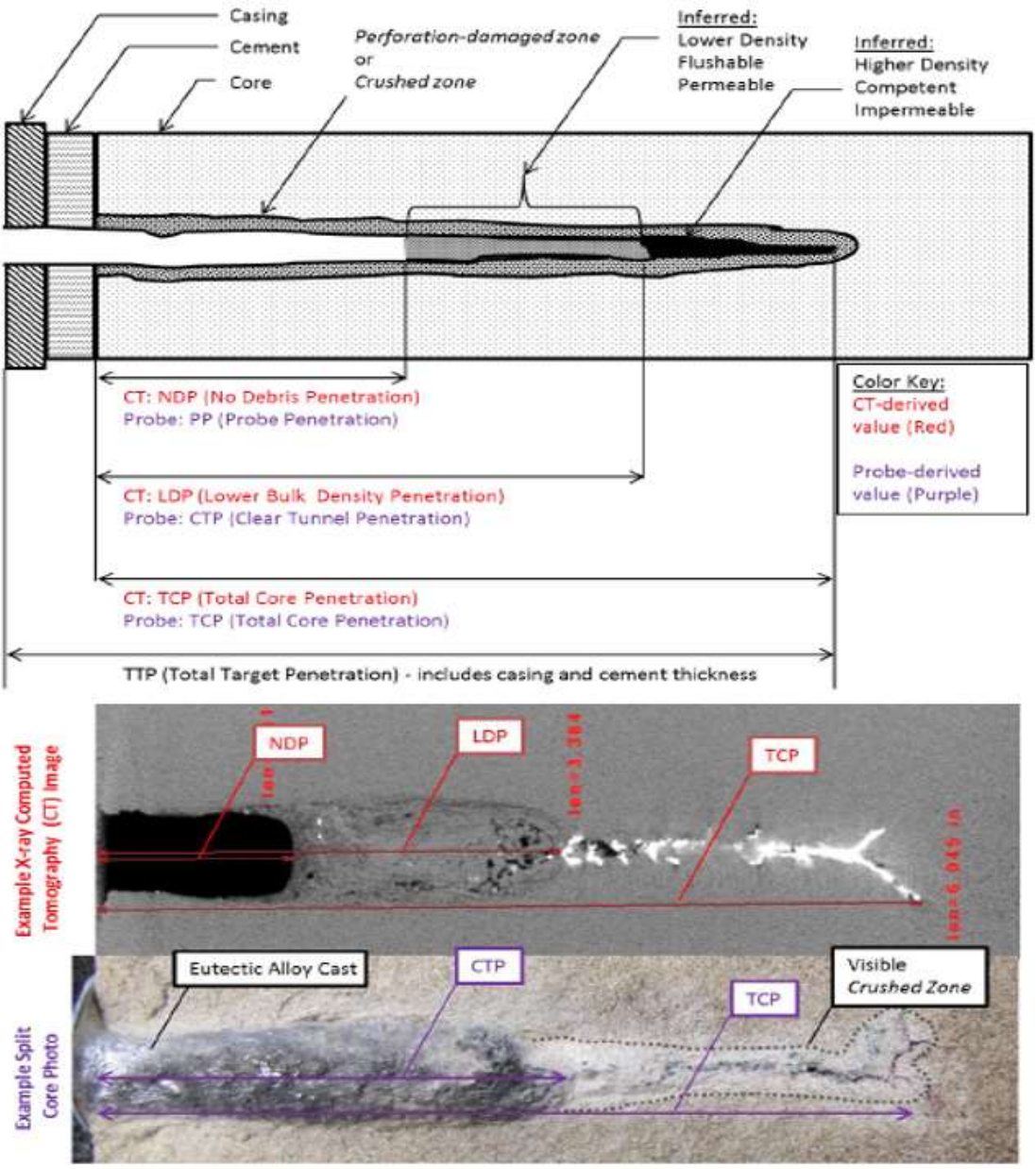

Figure 33- Perforation characterization sketch (Jet Research Center, 2019)

3.3.3.2 CT-Scanner

The CT-scanner is used to obtain a 3D high-resolution model of the perforation tunnel. It can identify “no-debris penetration”, “lower bulk density penetration”, and “total core penetration”, as well as perforation diameter. The model of the perforated core is developed using multiple X-ray images, taken from different angles. Advantage of CT-scanning before physically splitting the core is to discover anomalies, that would not be possible in 2D (split

core). Figure 34 shows a core sample placed between the X-ray tube on the right and the detector on the left.

Figure 34- CT scanner (Jet Research Center, 2019)

3.3.4 Core Flow Efficiency

The same principle of productivity ratio applies to the "Core Flow Efficiency" (CFE), which is simply the flow ratio between a simulated, perfectly clean perforation tunnel, and a perforated core. A clean perforated core will be simulated and represent a perfectly clean perforation tunnel. CFE=1 if the perforated core would have no perforation skin.

$$CFE = \frac{PI_{perf}}{PI_{th}} \qquad (22)$$

For the analytical approach an equivalent uniform (i.e. average) perforation radius is used. The average radius was determined by minimizing the difference in lateral surface areas between the variable tunnel geometry and the idealized tunnel geometry. Figure 35 shows the idealized representation of the perforation used for the analytical analysis superimposed onto the post-scrubbed tunnel geometry measured for each half of the split core.

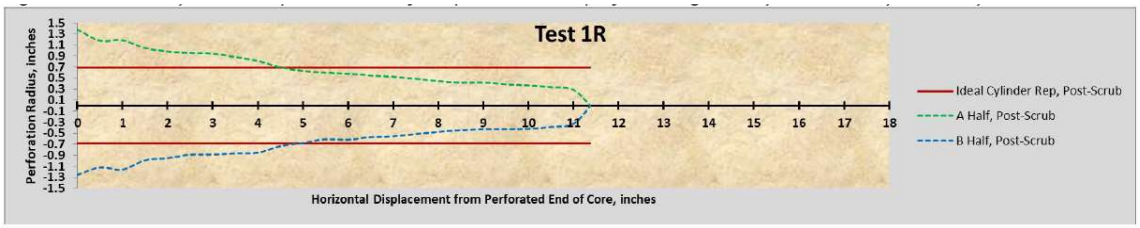

Figure 35- Idealized cylindrical representation of the post-scrubbed perforation geometry used in the analytical analysis (Jet Research Center, 2019)

Equation 23 is the simplest analytic expression for calculating the theoretical ideal viscosity-corrected rate index of the perforated target subjected to a purely radial pressure/flow boundary condition (see Figure 36 below for representation).

$$PI_{th} = \frac{q\mu}{\Delta p} = \frac{2\pi k_{dia} L}{ln\left(\frac{r_o}{r_c}\right)} \qquad (23)$$

k_{dia} is the core's virgin diametral permeability (measured from core-plugs after perforating), L is the perforation's "perfectly clean" tunnel length (excluding the casing and cement), r_o is the outer radius of the core, and r_c is the perforation's "perfectly clean" radius after scrubbing.

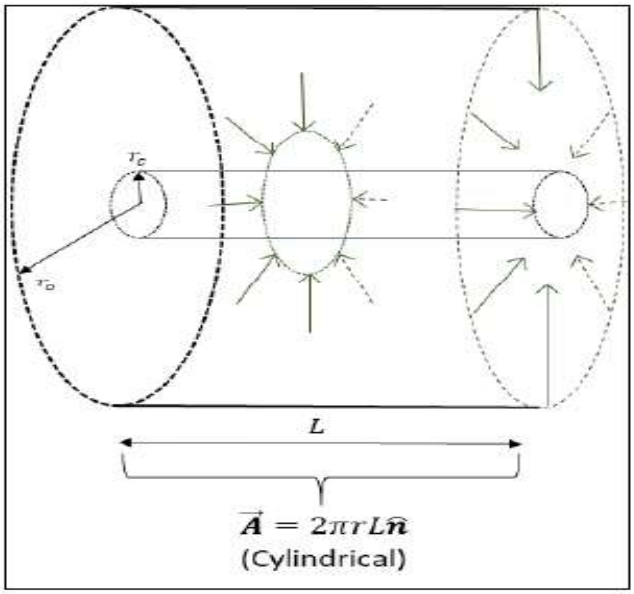

Figure 36- Illustration of pure radial flow into idealized perforation (Jet Research Center, 2019)

3.4 Summary- simulation and experimental design

To investigate the performance of the two perforating systems, pressure behavior, and clean-up, includes several stages. To obtain an expected dynamic pressure response, SurgePro simulations needs to be performed. However, in SurgePro, penetration characteristics such as penetration length, diameter of perforation, and casing exit hole diameter are inputs. These parameters can be simulated in HPTK.

Upon simulating pressure response for both cases, section IV tests can be performed. Through analysis, Section IV can give us the expected core flow efficiency, from which a crushed zone thickness and permeability can be derived.

Utilizing nodal analysis, such as WEM, a full wellbore simulation can be performed, to predict IPR for this particular well. Figure 37 below shows the workflow and outputs obtained from each step.

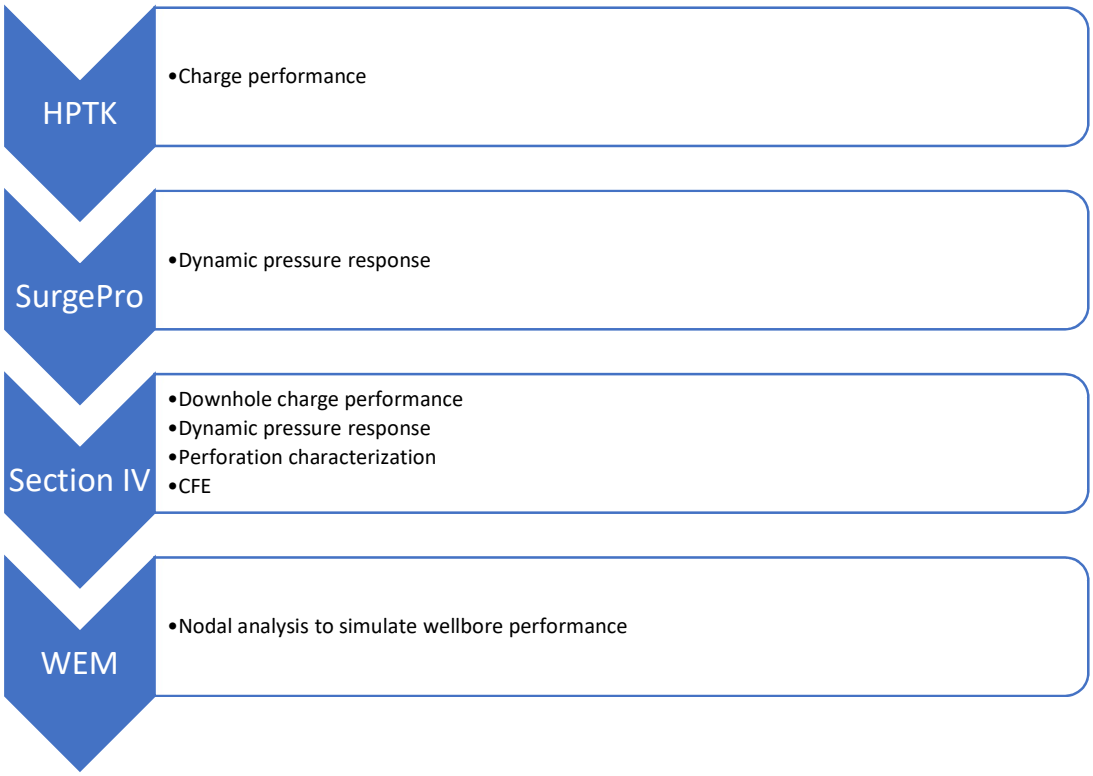

Figure 37- Workflow for simulations and testing

4 RESULTS AND DISCUSSION

This chapter presents the experimental and simulation results designed in chapter 3. The experimental results will first be represented, then the simulations necessary to perform the Section IV tests. At last, WEM simulations will be represented.

4.1 Experimental results

4.1.1 Absolute permeability of the cores

The pre-shot axial absolute permeabilities of the cores were evaluated assuming the traditional graphical solution to Darcy's equation for steady-state linear flow. Figure 38 contains plots of the tests' data, plotted according to Darcy's law. The slope of the line will give us the permeability in Darcies. As can be seen, the average 269 mD permeability measured, deviates some from the expected Oseberg average permeability of 200 mD. It is however, according to Equinor well within the range for Oseberg South. Both cores have similar permeabilities and a good correlation with Darcy's Law. The measured pressure and flow are presented in Appendix A.1.

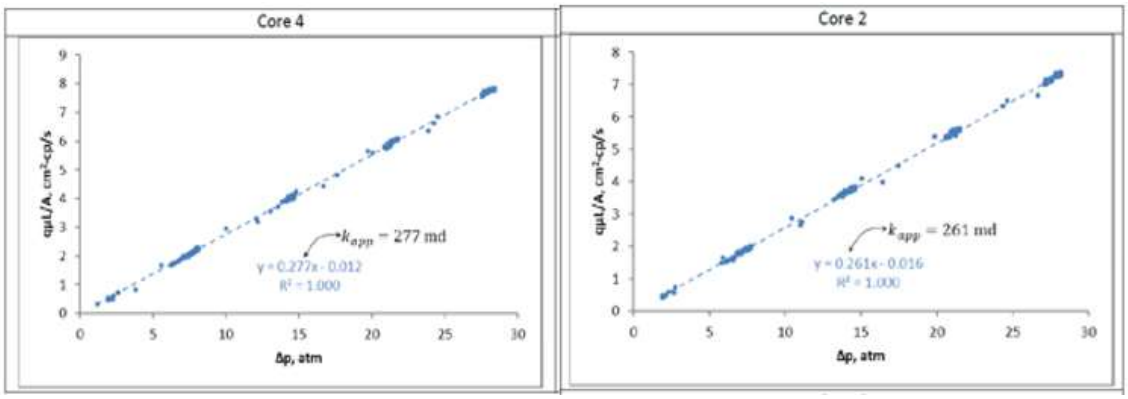

Figure 38- Core permeability measurements

4.1.2 CT- Images

4.1.2.1-4-5/8” gun system

Figure 39 shows the CT-scans from the 4-5/8” gun system. As can be seen a “no-debris” penetration of 2,965” was achieved. Total core penetration was measured to be 11,374”. The material between “no-debris” penetration and total core penetration is permeable and will is considered a part of the “clear tunnel penetration”, see Figure 40 of dye injection test. However, the light, higher density material at the tip of the perforation is assumed to be non-permeable (most likely liner debris).

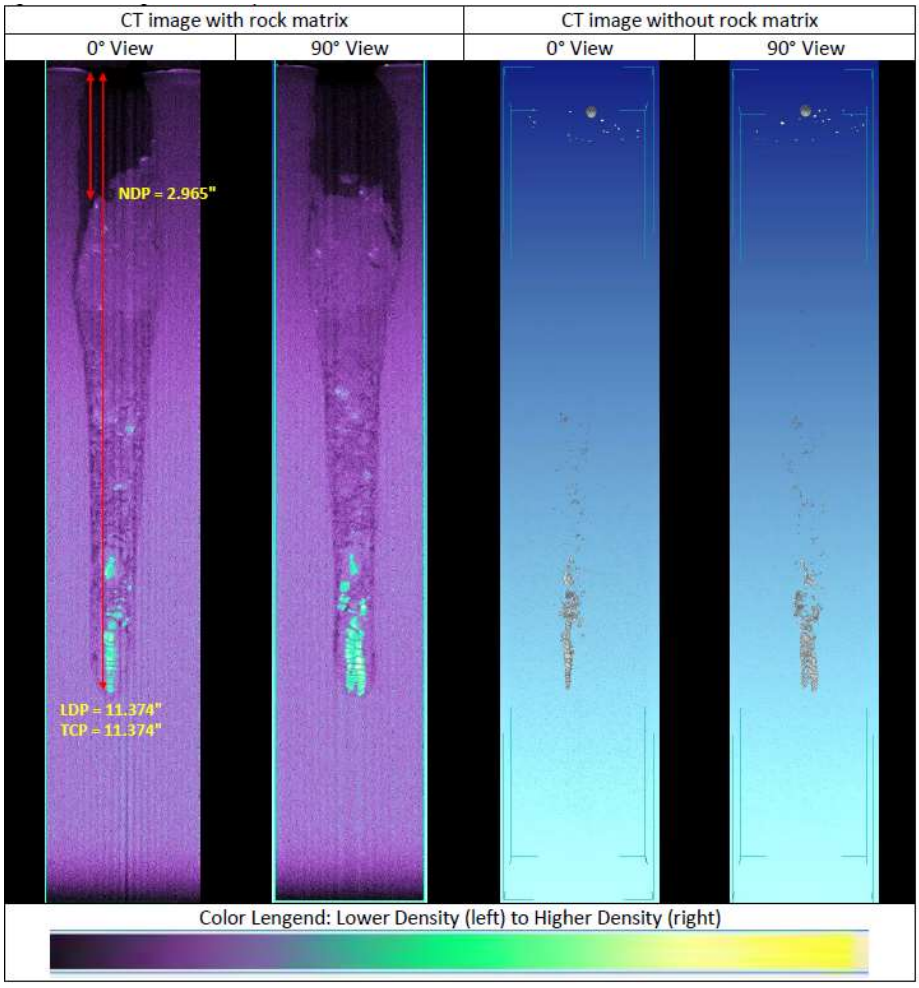

Figure 39- CT images for 4-5/8" gun system with 39g HMX MaxForce charge

Effective perforation penetration can be evaluated using an equation for “clear tunnel%”:

$$clear\ tunnel\ \% = \frac{clear\ tunnel\ penetration}{total\ core\ penetration} = \frac{11.374}{11.374} = 100\%$$

HPTK simulations showed effective penetration of 9,49”, slightly lower than the 11,374” from the Section IV test.

Figure 40 below shows the core after injection dye test. The light blue indicates where fluid flows and darker purple is the non-productive area of the core. It seems like the entry of the hole, and the tip has been the least productive areas around the perforation tunnel. Flow into the perforation seems to have been axi-radial and has occurred between 4 and 10 inches. The little flow around the tip is a common phenomenon, because here will the liner debris be compacted. However, the reason for the non-productive entry of the perforation tunnel is unknown. The kill pill can have plugged of the pores in this region.

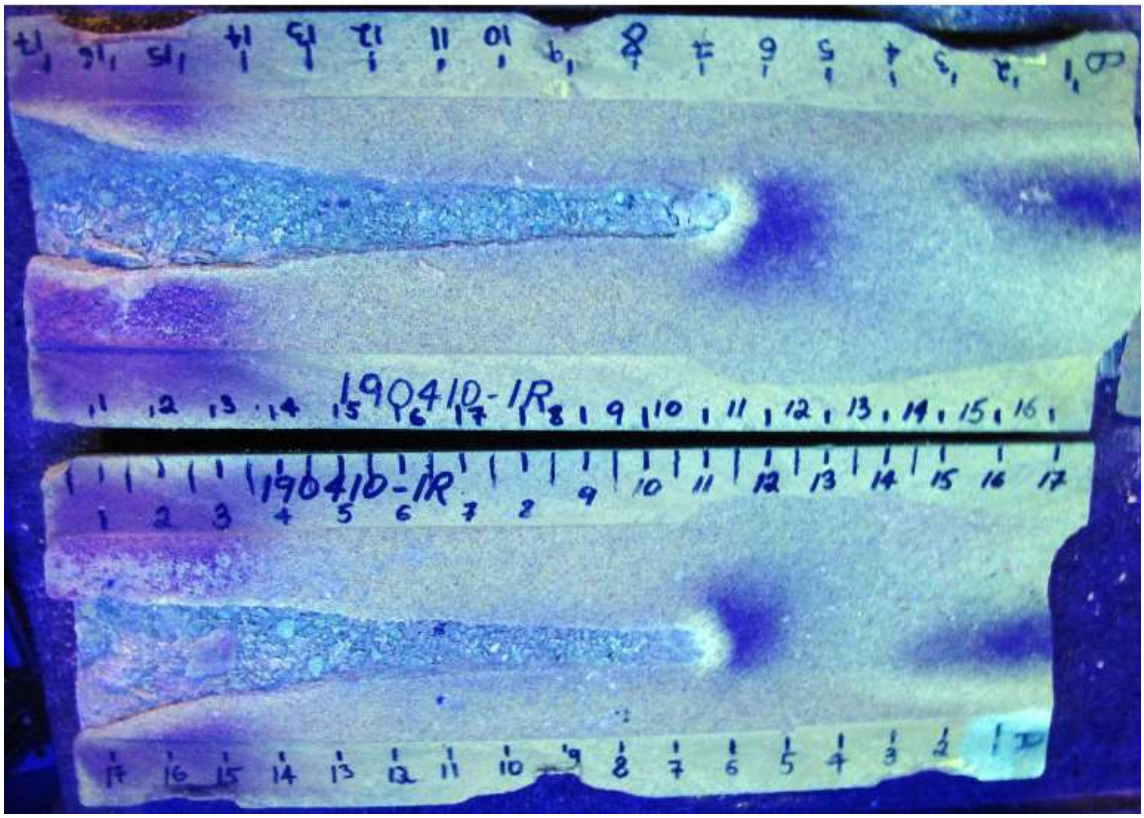

Figure 40- Split core showing results after dye injection test for the 4-5/8" gun system with 39g HMX MaxForce charge

Figure 41 shows the core after it has been split. From 3 inches and throughout the perforation we see loose, crushed debris, which according to Figure 40 is highly permeable.

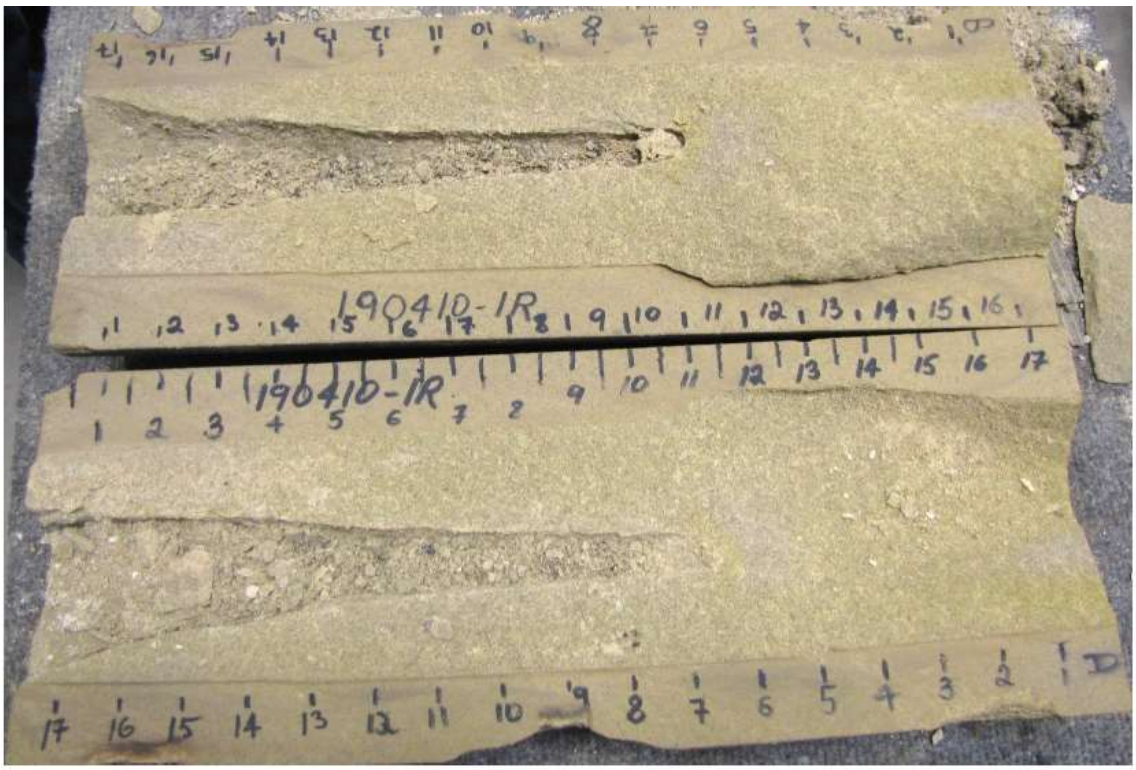

Figure 41- Split core for the 4-5/8" gun system with 39g HMX MaxForce charge

4.1.2.1-3-1/8" gun system

Figure 42 shows the CT-scans from the 3-1/8" gun system. "No-debris" penetration was 1,949". Lower bulk density penetration was 4,297", and total core penetration was 5,295". The tip with high-density material seems to be filled with non-permeable material (liner debris) and will not contribute to flow.

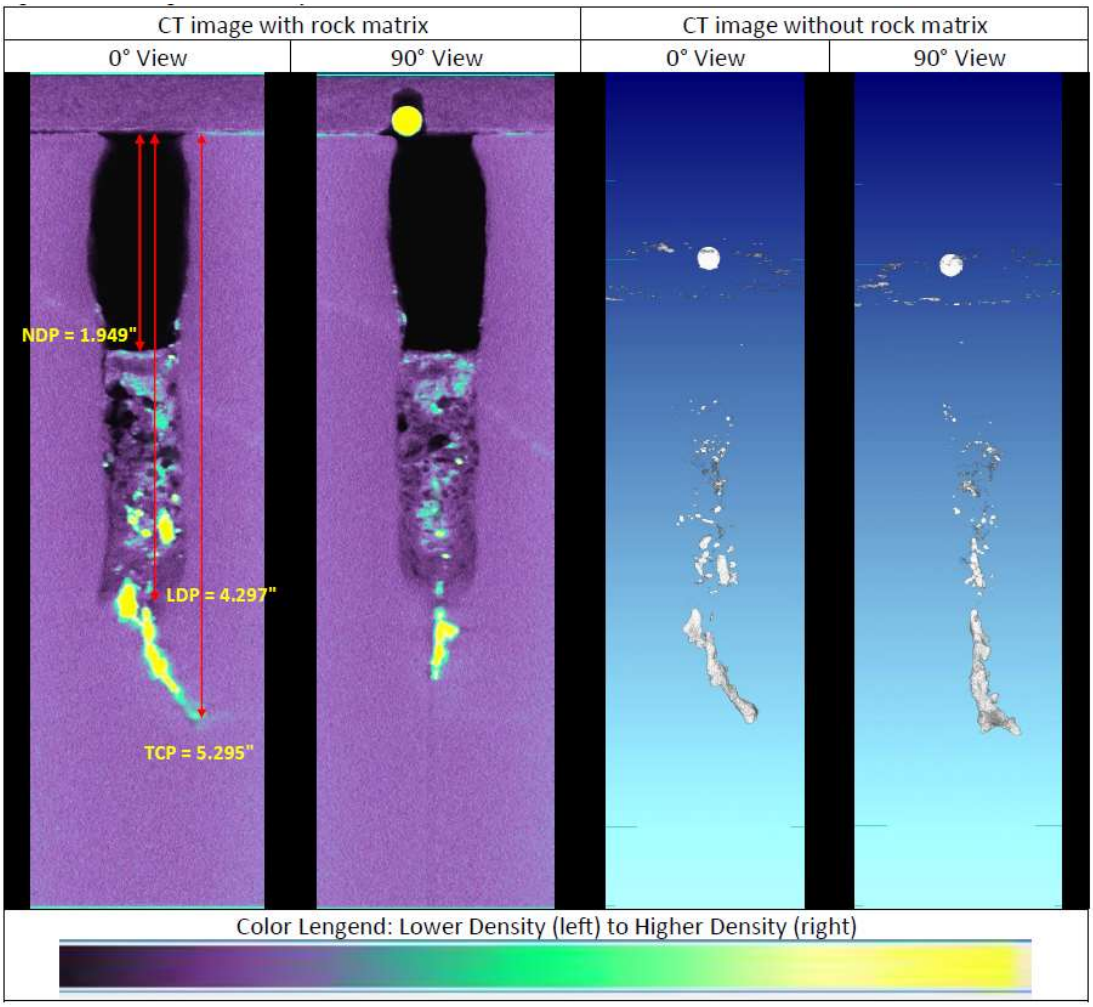

Figure 42- CT images for 4-5/8" gun system with 17.5g HMX MaxForce charge

$$clear\ tunnel\ \% = \frac{clear\ tunnel\ penetration}{total\ core\ penetratio} = \frac{4.297}{5.29} * 100 = 81.23\%$$

Figure 43 is the dye injection test for the 3-1/8" test. As can be seen, most of the flow has been radial, with little axial flow through the tip. The debris plug looks dark and should indicate low flow, but from Figure 44 we see the debris plug is initially black due to carbon black and

hence does not necessarily indicate low flow. The weakly dark area around the 3-inch mark still indicates that most of the flow has occurred in the no debris region up to 2 inches.

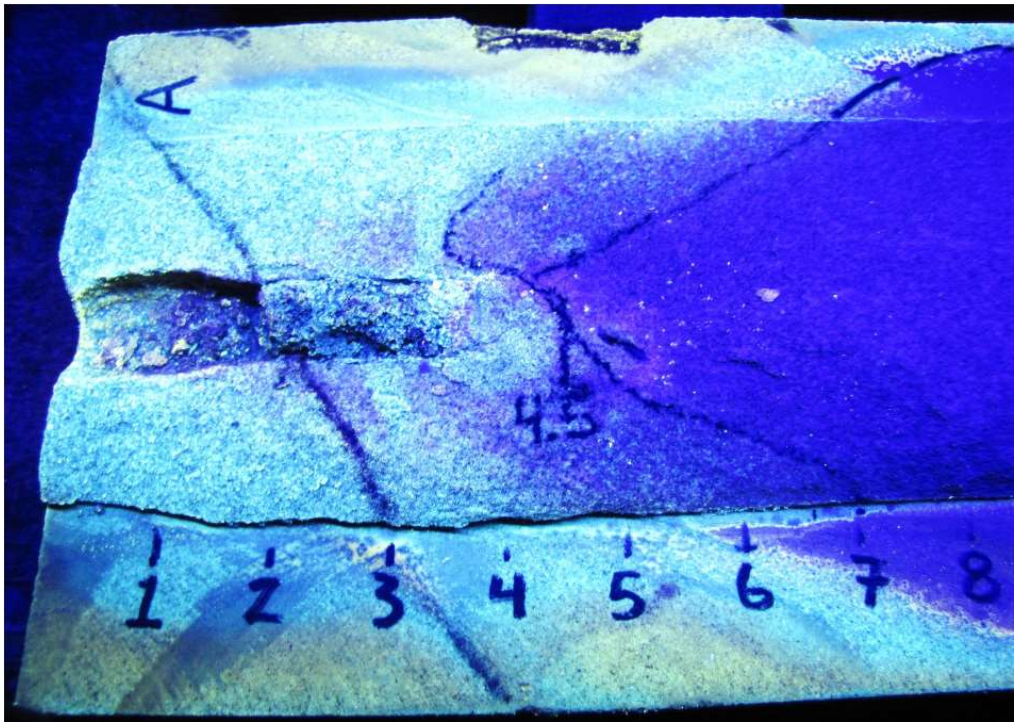

Figure 43- Split core showing results after dye injection test for the 4-5/8" gun system with 17.5g HMX MaxForce charge

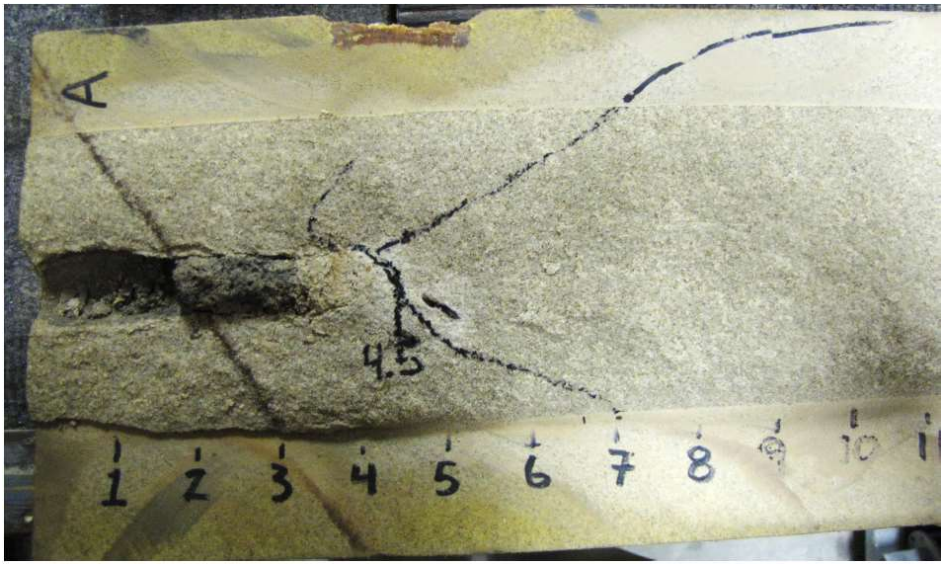

Figure 44- Split core for the 4-5/8" gun system with 17.5g HMX MaxForce charge

4.1.3 Dynamic Pressure Response

4.1.3.1 -4-5/8" gun system

This test was conducted with a 39g HMX MaxForce charge. Figure 45 shows wellbore chamber pressure at 2160 psi overbalance (5000 psi wellbore), pore pressure was 2840 psi, and DUB was recorded to be 1022 psi (lowest wellbore pressure recorded was 1818 psi). Confining pressure around the core was approximately 8250 psi. Total duration in DUB was approximately 1 second. Wellbore isolation valve and nitrogen feed were used to bring the wellbore back to initial pressure.

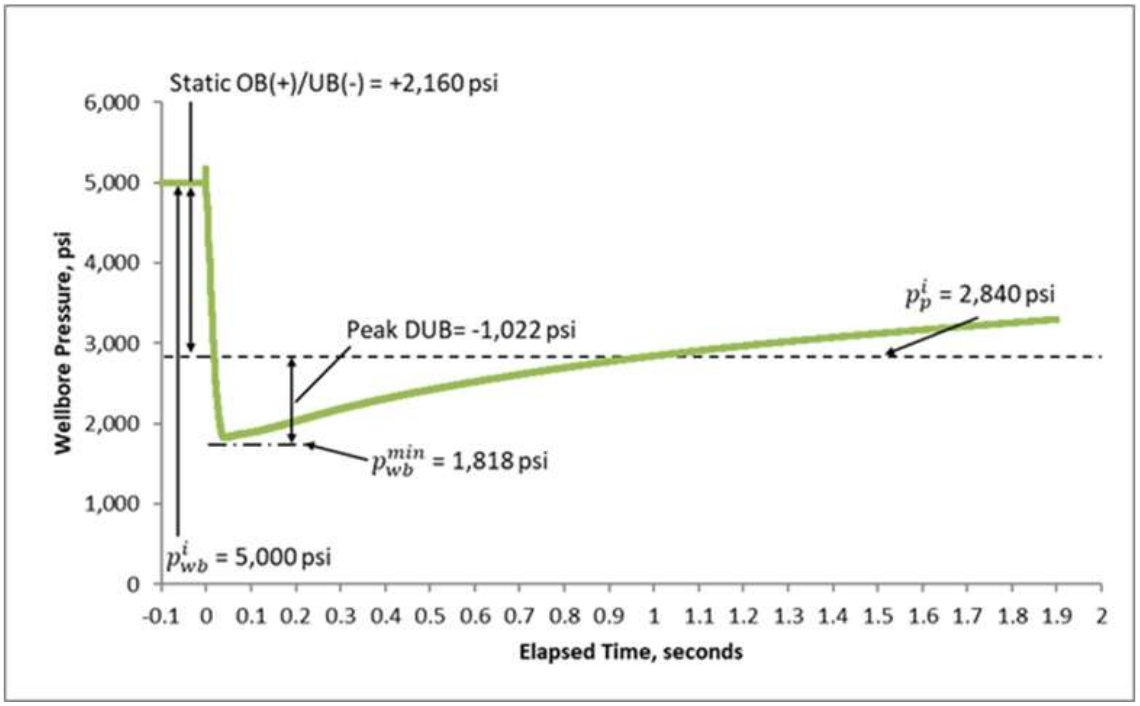

Figure 45- Dynamic pressure response for the 4-5/8" gun system with 39g HMX MaxForce charge

Figure 46 Shows pressures outside and inside the core, in addition to temperature measurements. Far-field wellbore and pore pressures are measured at the pore/wellbore pressure transducers in the flowline. The pore pressure transducers can indicate the local pore pressure drop and hence indicate dynamic effective stress (DES). The confining pressure is the fluid pressure around the bladder which adds overburden pressure to the core. DES is measured as a peak value of 6476 psi.

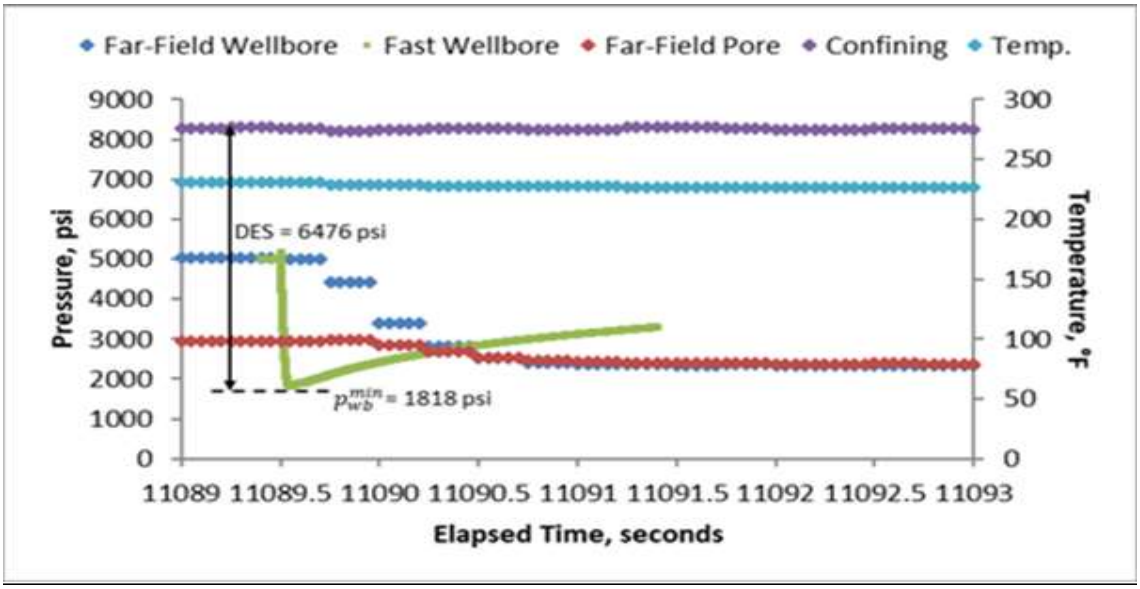

Figure 46- Pressures and temperature inside and outside the core for the 4-5/8" gun system with 39g HMX MaxForce charge

4.1.3.2- 3-1/8" gun system

This test was conducted with a 17.5g HMX MaxForce charge. Figure 47 shows wellbore chamber pressure on balance with pore pressure at 2840 psi. DUB was recorded to be 741 psi (lowest wellbore pressure recorded was 2099 psi). Confining pressure around the core was approximately 8250 psi.

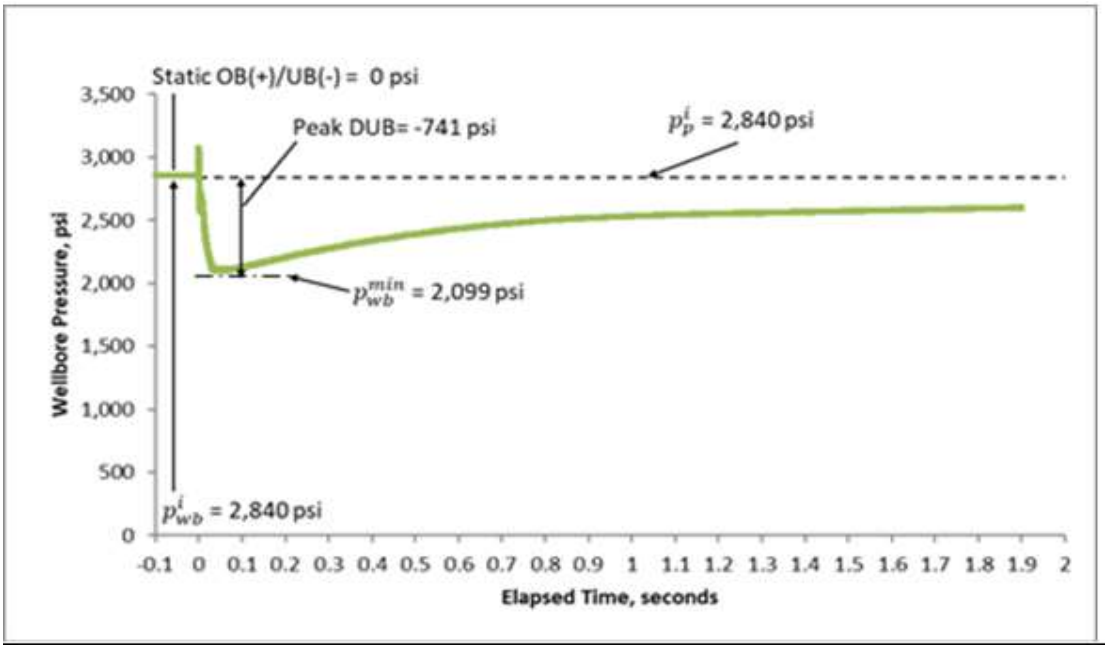

Figure 47- Dynamic pressure response for the 4-5/8" gun system with 17.5g HMX MaxForce charge

Figure 48 shows wellbore and pore pressure response for the 3-1/8" system. DES was estimated to be 6195 psi.

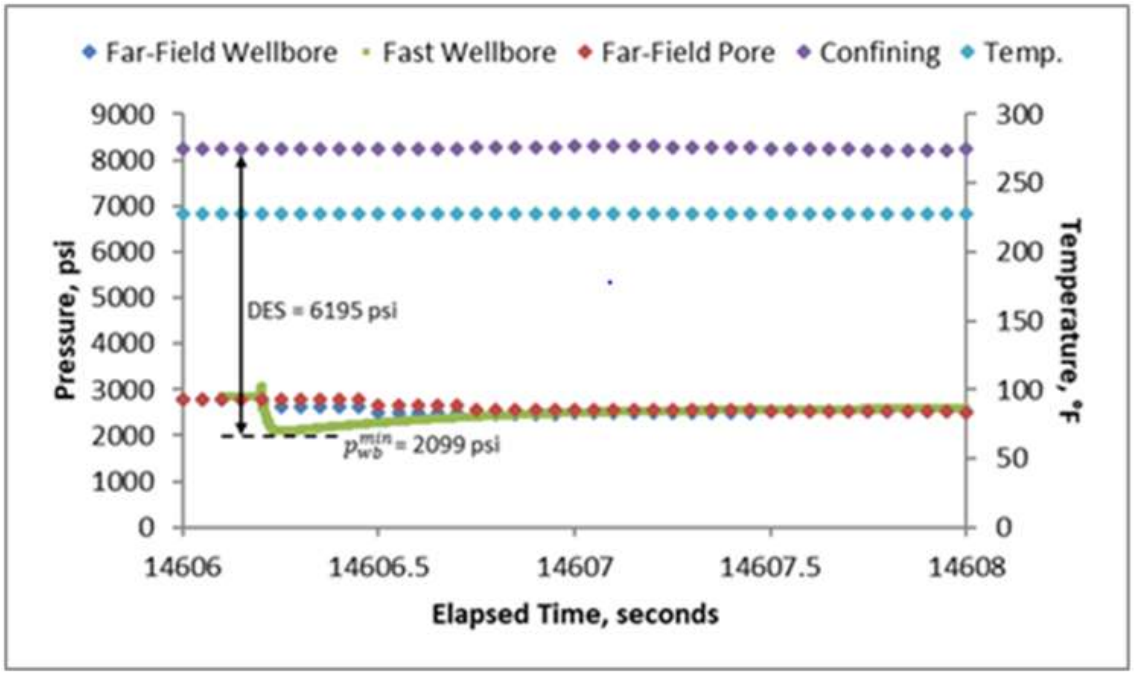

Figure 48- Pressures and temperature inside and outside the core for the 4-5/8" gun system with 17.5g HMX MaxForce charge

4.1.4 Flow tests

4.1.4.1 -4-5/8" gun system

Figure 49 shows the flow test from an ISCO pump. Stable rates were not achieved in the Section IV barrel. The ISCO pump uses zero wellbore pressure, and effective confining pressure, equal to the one in Section IV. Meaning if we had 8250 psi confining and 2850 pore pressure for Section IV flow test, we would have 5600 psi confining and 0 psi pore pressure for the ISCO pump.

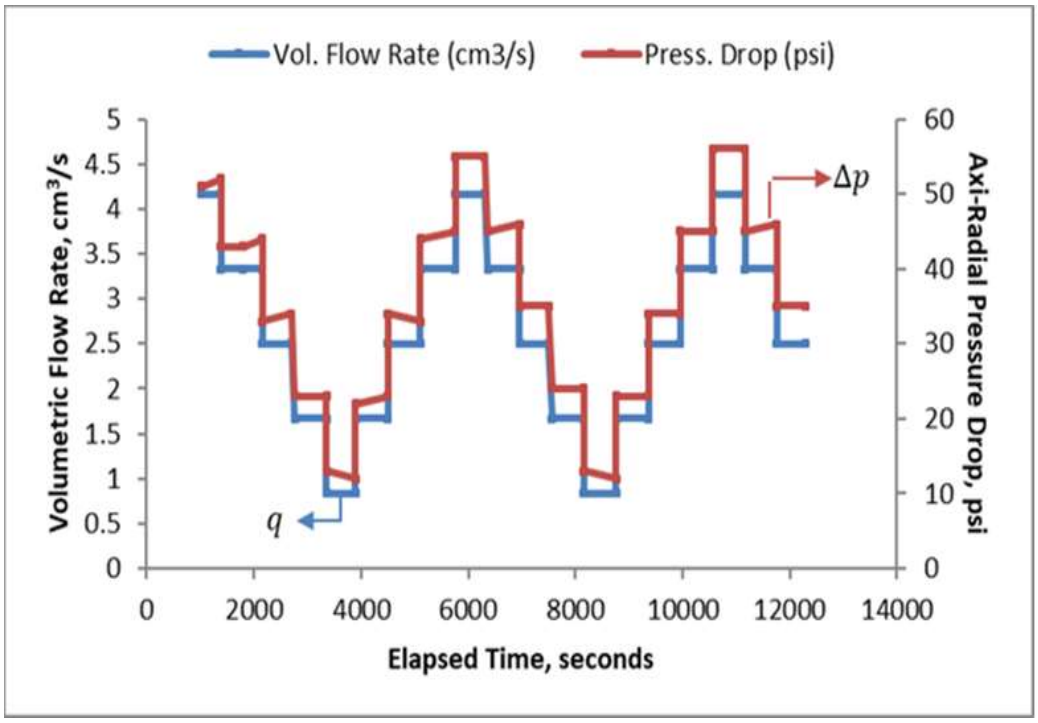

Figure 49- Flow test for core perforated with the 4-5/8" gun system with 39g HMX MaxForce charge

Figure 50 shows the viscosity corrected flow rate versus pressure drop across the perforated core. As can be seen, the different points correlate well with Darcy law (99% correlation).

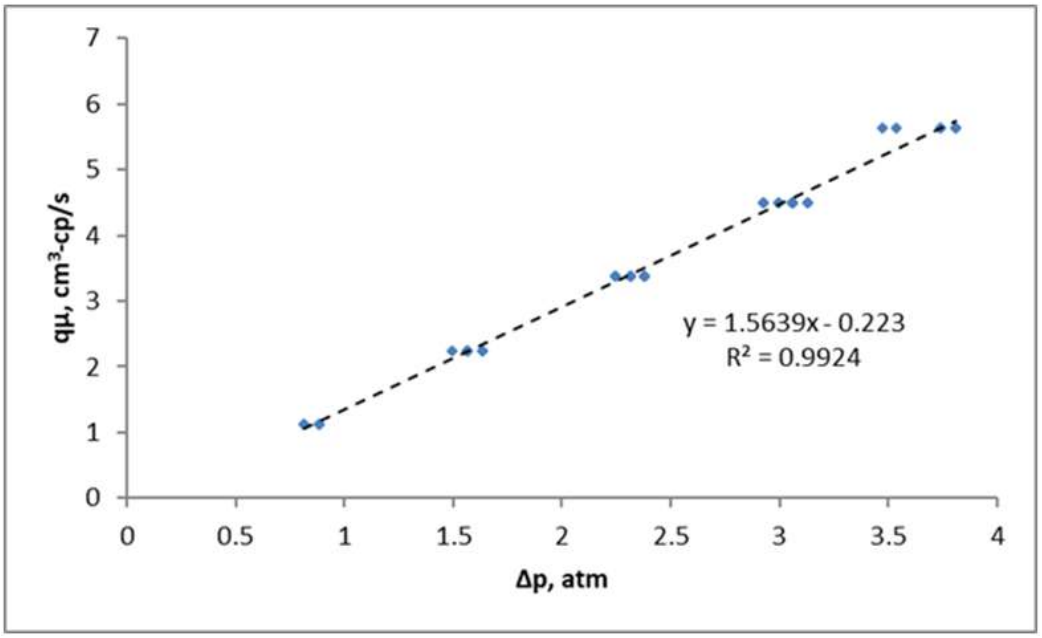

Figure 50- Viscosity corrected flow rate versus pressure drop through core perorated with the 4-5/8" gun system and 39g HMX MaxForce Charge

4.1.4.2-3-1/8” gun system

Figure 51 shows the flow test for 3-1/8” gun system core. Red (right axial scale) indicates pressure drop across the core. Blue (left axial scale) is the measured flow rate through the core. When stabilized flow rates are observed for different pressure drops, the flow performance can be calculated by plotting rates versus pressure drops, see Figure 53. The rates are viscosity corrected to account for the change in viscosity as pressure changes.

Figure 52 shows the inlet and outlet temperature, pore pressure, and wellbore pressure. Viscosity and density are also calculated for the respective pressure and temperature. Inlet temperature indicates pore- fluid temperature and outlet indicates wellbore temperature (this plot is not included for the 4-5/8” test since the flow test had to be done with an ISCO pump).

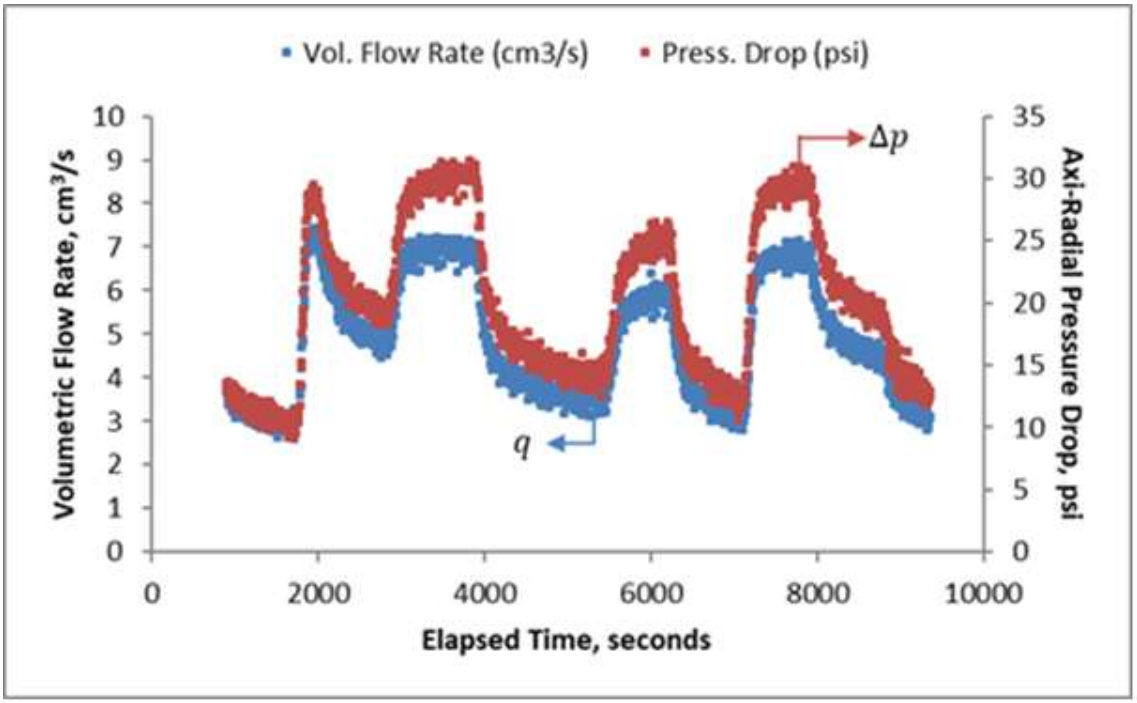

Figure 51- Flow test for core perforated with the 4-5/8" gun system with 17.5g HMX MaxForce charge

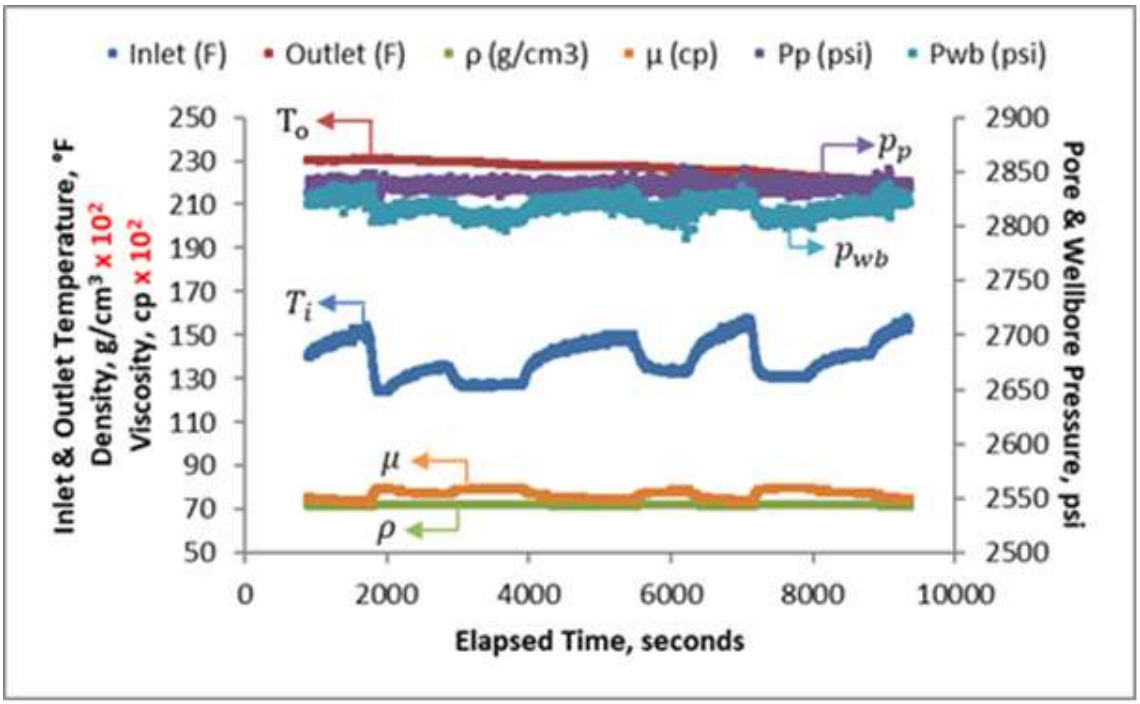

Figure 52- Temperatures and pressures in the test vessel

Figure 53 shows the viscosity corrected flow rate versus pressure drop across the perforated core. As can be seen, the different points correlate well with Darcy law (98% correlation).

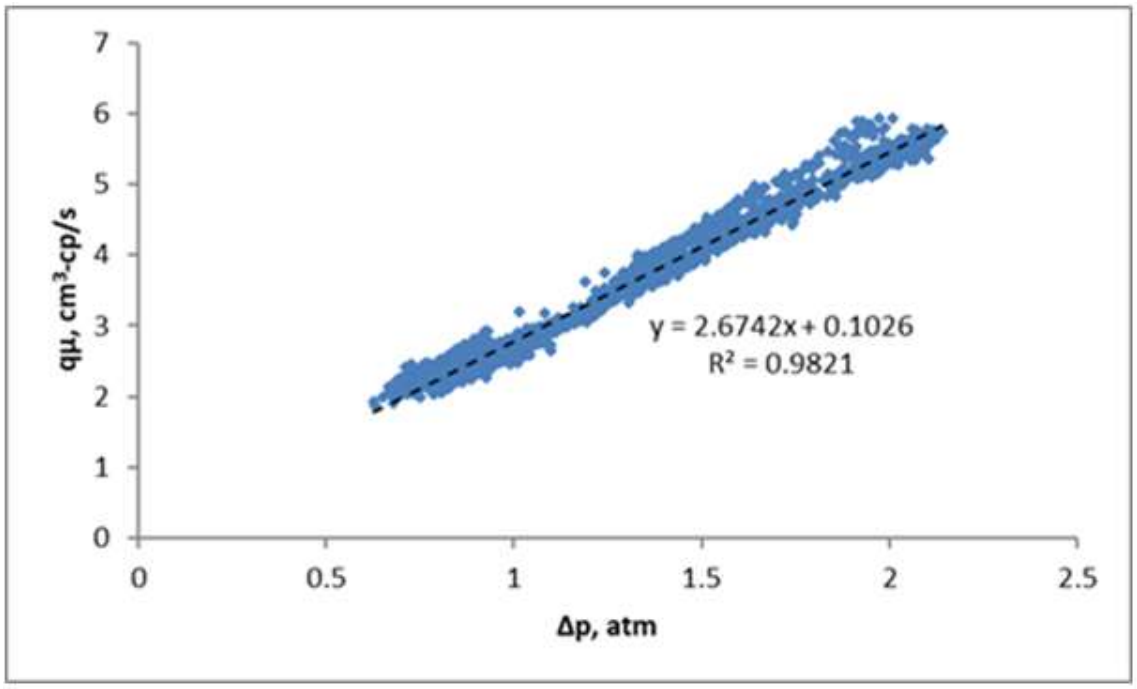

Figure 53- Viscosity corrected flow rate versus pressure drop through core perorated with the 3-1/8" gun system and 17.5 HMX MaxForce Charge

4.1.5 Core flow efficiency analysis

The first step in evaluating core flow efficiency is to determine the post-shot diametral permeability. This is important since the overall permeability of the core is altered during the perforating event (Behrmann et al. 1991). The diametral average permeability is calculated from two principal permeabilities k'_{dia1} and k'_{dia} . Principal permeabilities are measured from plugs cut out from the core. The perforation radius is measured before and after scrubbing to obtain r_p and r_c respectively. The contribution to flow through the tip of the perforation is typically negligible when the axi-radial pressure/flow boundary configuration is used. A pure radial flow will therefore be assumed.

4.1.5.1 Test 1: 4-5/8" Gun system with 39g HMX MaxForce charge, perforated on high overbalance

The following values were measured for Test 1:

- $L = 11.374$ in $= 28.89$ cm (total target penetration)
- $l = 11.374$ in $= 28.89$ cm (effective penetration)
- $r_o = 3.25$ in $= 8.26$ cm (outer radius of the core)
- $r_c = 0.688$ in $= 1.75$ cm (perfectly clean perforation radius)
- $r_p = 0.638$ in $= 1.62$ cm (average pre-scrubbed perforation radius)
- $k'_{di} = 231\ mD$
- $k'_{dia2} = 185\ mD$

$$k_{dia} = \sqrt{k'_{dia1} * k'_{dia2}} = 207\ mD \qquad (24)$$

The theoretical ideal viscosity-corrected rate index for a perfectly clean perforation tunnel is calculated as:

$$PI_{th} = \frac{q\mu}{\Delta p} = \frac{2\pi k_{dia} L}{ln\left(\frac{r_o}{r_c}\right)} = \frac{2\pi * 0.207D * 28.89cm}{ln\left(\frac{8.26cm}{1.75cm}\right)} = 24.21 \frac{cm^3 - cp}{atm - s}$$

The experimentally observed viscosity-corrected rate index of the perforated target was found to be 1.564 (cm3-cp)/(atm-s), Figure 50. Thus, the CFE is calculated as:

$$CFE = \frac{PI_{perf}}{PI_{th}} = \frac{1.564 \frac{cm^3 - cp}{atm - s}}{24.21 \frac{cm^3 - cp}{atm - s}} = 0.065 = 6.5\%$$

This result means the perforated tunnel will only produce 6,5% of its potential, which is extremely low.

Single-shot perforation skin becomes as derived in Grove et al. (2012):

$$S_{sp} = \left(\frac{l}{L} * \frac{1}{CFE} - 1\right) * ln\left(\frac{r_o}{r_c}\right) \qquad (25)$$

$$S_{sp} = \left(\frac{11.374in}{11.374in} * \frac{1}{0.065} - 1\right) * ln\left(\frac{8.26cm}{1.75cm}\right) = 22.47$$

Where l is the effective penetration length, equal to total target penetration. This is a high value for perforation skin, indicating severe damage.

From S_{sp} we can use the formula from Grove et al. (2012) to calculate crushed zone permeability:

$$\frac{k_c}{k_{dia}} = \frac{ln\left(r_c/r_p\right)}{S_{sp}} \qquad (26)$$

$$\frac{k_c}{k_{dia}} = \frac{ln\left(1.75cm/1.62cm\right)}{22.47} = \frac{0.00343mD}{mD}$$

$$k_c = 207mD * \frac{0.00343mD}{mD} = 0.71mD$$

Such low crushed zone permeability will impair flow significantly.

Crushed zone thickness will be:

$$t_c = r_c - r_p \qquad (27)$$

$$t_c = 1.75cm - 1.62cm = 0.13cm$$

Crushed zone permeability and thickness has been calculated to be 0.71mD and 0.13cm respectively. An important assumption for these calculations is that all damage is caused by a uniform permeability reduced crushed zone. However, kill pill can also severely damaged the tunnel, but to quantify the different mechanisms, that increase perforation skin is difficult. Perforation damage will therefore only be quantified through crushed zone permeability and thickness.

Since the first 3.5 inches of the perforation seems to be non-productive, a new CFE will be calculated, taking into account only the productive length of the perforation. If we assume absolutely no flow through the first 3.5 inches of the tunnel, this approach can give a more

realistic crushed zone characteristic. Figure 54 shows the new effective perforation tunnel length which will be considered.

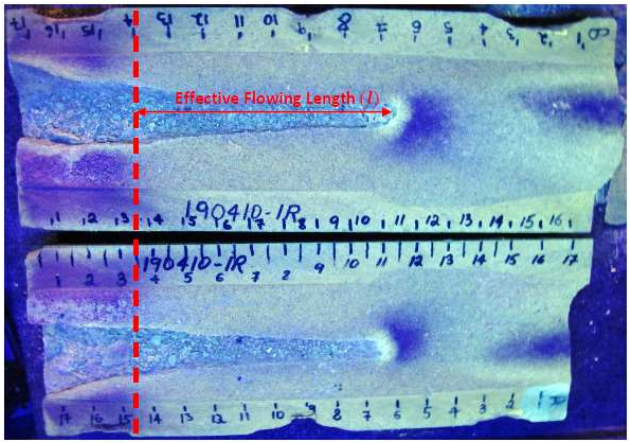

Figure 54- New effective length for CFE calculations

Considering the new effective length of the perforation tunnel, modified perforation geometry for this analysis will be:

- $L = 7.874$ in $= 19.99$ cm (total target penetration)
- $l = 7.874$ in $= 19.99$cm (effective penetration)
- $r_c = 0.480$ in $= 1.218$ cm (perfectly clean perforation radius)
- $r_p = 0.433$ in $= 1.099$ cm (average pre-scrubbed perforation radius)

The theoretical ideal viscosity-corrected rate index for a perfectly clean perforation tunnel is calculated as:

$$PI_{th} = \frac{q\mu}{\Delta p} = \frac{2\pi k_{dia} L}{ln\left(\frac{r_o}{r_c}\right)} = \frac{2\pi * 0.207D * 19.99cm}{ln\left(\frac{8.26cm}{1.218cm}\right)} = 13.6\frac{cm^3 - cp}{atm - s}$$

The experimentally observed viscosity-corrected rate index of the perforated target was found to be 1.564 (cm3-cp)/(atm-s), Figure 50. Thus, the CFE is calculated as:

$$CFE = \frac{PI_{perf}}{PI_{th}} = \frac{1.564\frac{cm^3 - cp}{atm - s}}{13.6\frac{cm^3 - cp}{atm - s}} = 0.0115 = 11.5\%$$

Single-shot perforation skin becomes as derived in Grove et al. (2012):

$$S_{sp} = \left(\frac{l}{L} * \frac{1}{CFE} - 1\right) * ln\left(\frac{r_o}{r_c}\right) = \left(\frac{19.99cm}{19.99cm} * \frac{1}{0.115} - 1\right) * ln\left(\frac{8.26cm}{1.218cm}\right) = 14.73$$

Where l is the effective penetration length, equal to total target penetration.

From S_{sp} we can use the formula from Grove et al. (2012) to calculate crushed zone permeability:

$$\frac{k_c}{k_{dia}} = \frac{ln\left({}^{r_c}/_{r_p}\right)}{S_{sp}} = \frac{ln\left({}^{1.218cm}/_{1.099cm}\right)}{14.73} = \frac{0.007mD}{mD}$$

$$k_c = 207mD * \frac{0.007mD}{mD} = 1.44mD$$

Crushed zone thickness will be:

$$t_c = r_c - r_p = 1.218cm - 1.099cm = 0.119cm$$

The new calculations show a higher crushed zone permeability and less perforation skin. CFE was almost increased by a factor of two. Based on this we could conclude that CFE for this perforation will be between 6.5% and 11.5%.

4.1.5.2 Test 2: 3-1/8" Gun system with 17.5g HMX MaxForce charge, perforated on balance

The following values were measured for Test 2:

- $L = 5.5$ in $= 13{,}97$ cm (total target penetration)
- $l = 4.5$ in $= 11.43$ cm (effective penetration)
- $r_o = 3.25$ in $= 8.26$ cm (outer radius of the core)
- $r_c = 0.395 = 1.004\ cm$ (perfectly clean perforation radius)
- $r_p = 0.354$ in $= 0.899$ cm(average pre-scrubbed perforation radius)
- $k'_{dia1} = 212\ mD$
- $k'_{di} = 272\ mD$

$$k_{dia} = \sqrt{k'_{dia1} * k'_{dia}} = 240\ mD$$

The theoretical ideal viscosity-corrected rate index for a perfectly clean perforation tunnel is calculated as:

$$PI_{th} = \frac{q\mu}{\Delta p} = \frac{2\pi k_{dia} L}{ln\left(\frac{r_o}{r_c}\right)} = \frac{2\pi * 0.240D * 13.97cm}{ln\left(\frac{8.26cm}{1cm}\right)} = 10\frac{cm^3 - cp}{atm - s}$$

The experimentally observed viscosity-corrected rate index of the perforated target was found to be 2.691 (cm3-cp)/(atm-s), Figure 53. Thus, the CFE is calculated as:

$$CFE = \frac{PI_{perf}}{PI_{th}} = \frac{2.691\frac{cm^3 - cp}{atm - s}}{10\frac{cm^3 - cp}{atm - s}} = 0.269 = 26.9\%$$

Single-shot perforation skin becomes as derived in Grove et al. (2012):

$$S_{sp} = \left(\frac{l}{L} * \frac{1}{CFE} - 1\right) * ln\left(\frac{r_o}{r_c}\right) = \left(\frac{11.43cm}{13.97cm} * \frac{1}{0.269} - 1\right) * ln\left(\frac{8.26cm}{1.004cm}\right) = 4.301$$

Where l is the effective penetration length, equal to total target penetration.

From S_{sp} we can use the formula from Grove et al. (2012) to calculate crushed zone permeability:

$$\frac{k_c}{k_{dia}} = \frac{ln\left(r_c/r_p\right)}{S_{sp}} = \frac{ln\left(1.004cm/0.899cm\right)}{4.301} = \frac{0.0256mD}{mD}$$

$$k_c = 240mD * \frac{0.0256mD}{mD} = 6.15mD$$

Crushed zone thickness will be:

$$t_c = r_c - r_p = 1.004 - 0.899 = 0.105cm$$

This perforation seems to be significantly cleaner compared to Test 1. CFE was approximately 27%, and perforation skin 4.301. This indicates a much cleaner perforation

tunnel compared to the first test. Crushed zone permeability of 6.15mD was much higher compared to the first test. Crushed zone thickness was also thinner compared to Test 1, but the most significant difference was in crushed zone permeability.

4.2 Simulation results

4.2.1 HPTK simulations

As described in section §3.2.3, HPTK software is used to optimize perforating processes aiming at increasing charge performance and reduce perforation skin. This is done by selecting an appropriate gun. This section presents the simulation sensitivity studies and charge performance analysis through HPTK, which can improve perforation configuration and strategy

4.2.1.1 Simulation set up

Table 7 provides the most critical parameters for determining penetration and hole diameter. The strength of the casing, which is determined by casing weight (thickness) and grade, rock strength (compressive), is the resistance which the charge needs to overcome to penetrate the formation. The explosive amount and charge design will affect the charge performance (see 2.2).

Table 7- Main parameters for HPTK simulations

PARAMETER	VALUE
BOREHOLE	8,5 in
CASING GRADE	N-80
CASING WEIGHT	29 lb/ft
CASING SIZE	7 in
PERMEABILITY	200mD
OVERBURDEN GRADIENT	0,9 PSI/ft
UCS	3000 PSI
CHARGE NAME	390 HMX MaxForce (39g), 175 HMX MaxForce (17.5g)
GUN POSITION	Eccentered*
SHOT PATTERN	350/10

*Eccentered means the gun will not be centralized in the wellbore, this will increase the fluid gap between gun and casing and could decrease performance.

4.2.1.2 Simulation results

Figure 55 illustrates the perforation terminology used in HPTK. EPT will correspond to LPD from the Section IV tests.

Where, TTP = Total Target Penetration , FP = Formation Penetration, EPD = Effective Perforation Tunnel, EHD = Entry Hole Diameter, DZ= Damage Zone

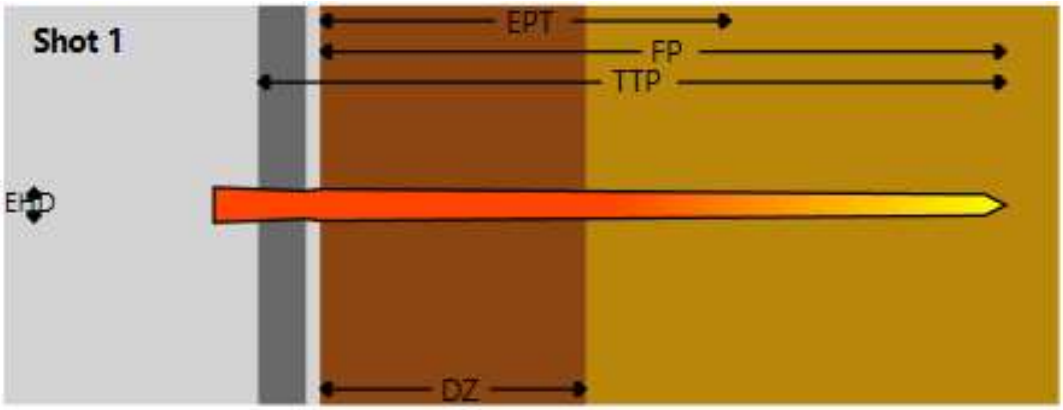

Figure 55- HPTK perforation characterization drawing

Figure 56 shows the shot orientation for these simulations.

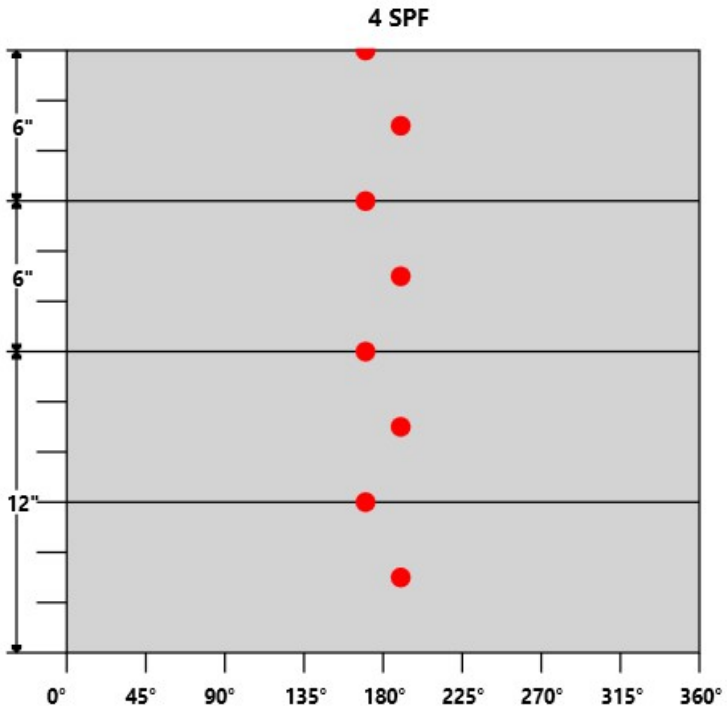

Figure 56- Shot pattern

Figure 57 shows HPTK calculated relationship of underbalance and permeability necessary to create clean perforation tunnel. It was estimated to be 510 psi for 200 mD

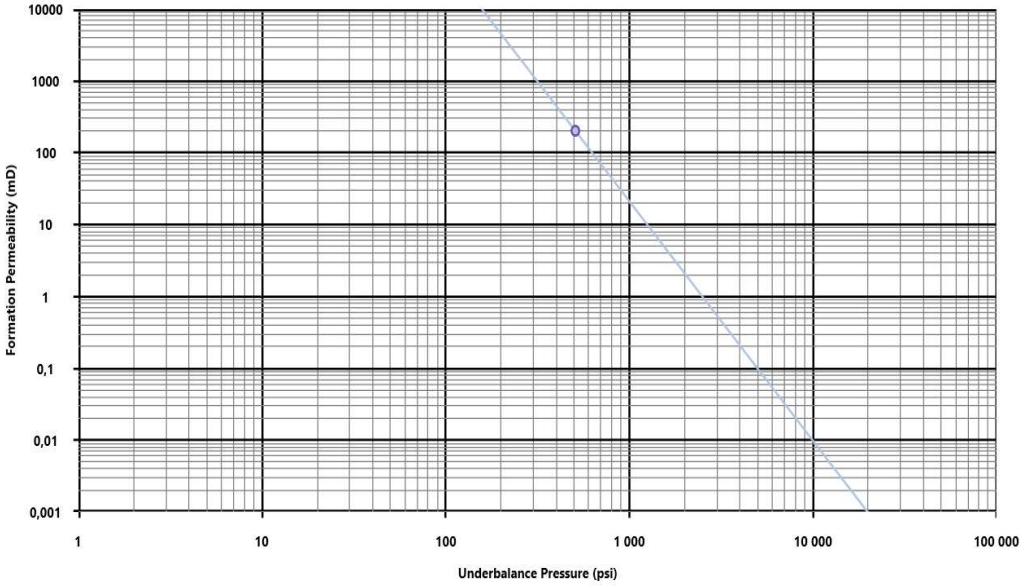

Figure 57- Permeability versus underbalance to achieve clean perforation tunnel, HPTK

4.2.1.2.1 -4-5/8" Gun System

The effective penetration (9.49 inches from Table 8, the average exit hole final casing (0.31 inches), and the perforation diameter (0.31in+0.05in) will be used as inputs in SurgePro for the pipe case.

Table 8- Charge performance 39g HMX MaxForce

Gun	Charge Name	Gun Size (in)	Total Target Penetration (in)	Effective Perforation Tunnel (in)	Formation Penetration (in)	Thompson Weeks Formation Penetration (in)	Average Exit Hole Final Casing (in)
1	MaxForce HMX	4 5/8	24.18	9.49	23.02	53.24	0.31

The effective penetration (6.42 inches from Table 9, the average exit hole final casing (0.29 inches), and the perforation diameter (0.29in+0.05in) will be used as inputs in SurgePro for the wireline case.

4.2.1.2.1 -3-1/8" Gun System

Table 9- Charge performance 17.5g HMX MaxForce

Gun	Charge Name	Gun Size (in)	Total Target Penetration (in)	Effective Perforation Tunnel (in)	Formation Penetration (in)	Thompson Weeks Formation Penetration (in)	Average Exit Hole Final Casing (in)
1	MaxForce HMX	3 1/8	11.88	6.42	10.72	24.79	0.29

4.2.2 SurgePro simulations

The theory and the working principle behind the SurgePro simulator are presented in section §3.2.4. SurgePro is designed to simulate the perforating event and to predict the dynamic pressure behavior inside the perforation, and pressurizations in the wellbore and the perforation are among others. The perforation phenomenon is highly complex. SurgePro is however one of the most reliable software in perforation clean-up simulations and has a long and well-known history.

4.2.2.1 SurgePro simulations set up

Zone of 100 meters with perforations will be investigated. The well has in total 9 zones which on pipe will be perforated simultaneously. For the wireline case, the same interval will be perforated with existing perforations below.

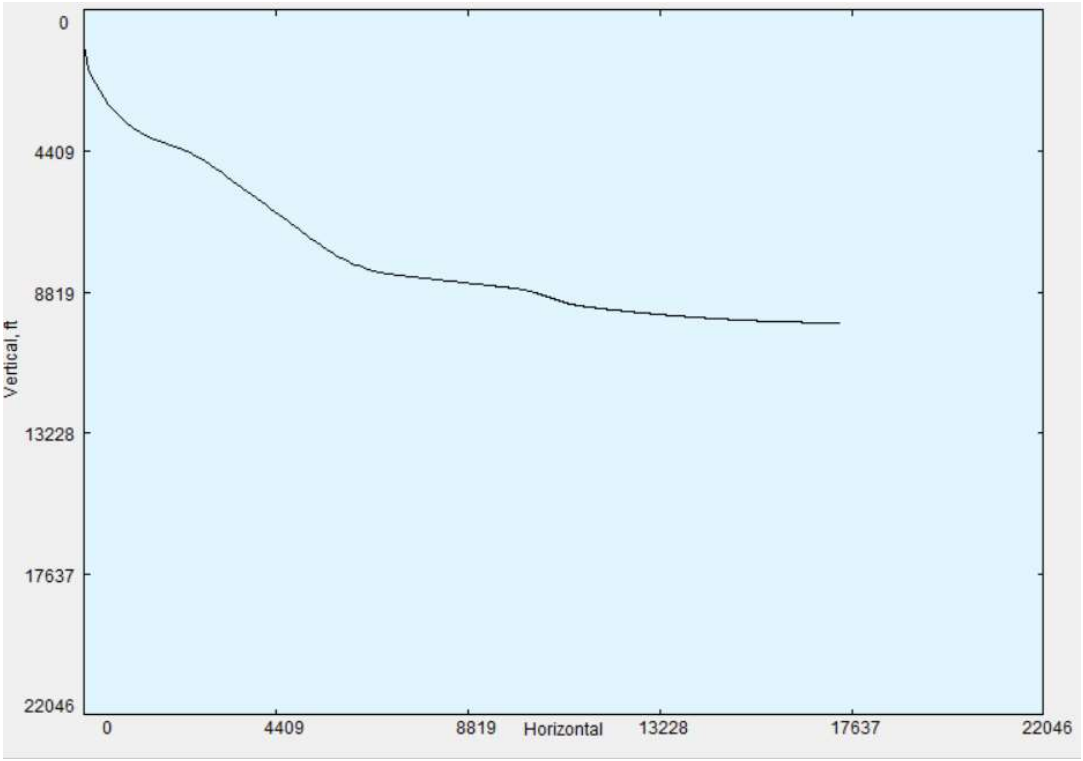

Figure 58- Well trajectory, F-17 Oseberg South

Figure 59 shows the tool string for perforating on pipe (left) and wireline (right). It is a horizontal part of the well shown in Figure 58. The well consists of 9 zones in total, as for pipe, they are perforated simultaneously. For wireline each zone is perforated in one or multiple runs, starting from the bottom of the well. In this case, the sixth zone from below is being

perforated. The importance of including existing perforations is that they will also surge reservoir fluid once the well experiences free gun volume. This effect will shorten dynamic underbalance if existing perforations are close to the zone being perforated.

Perforating on pipe

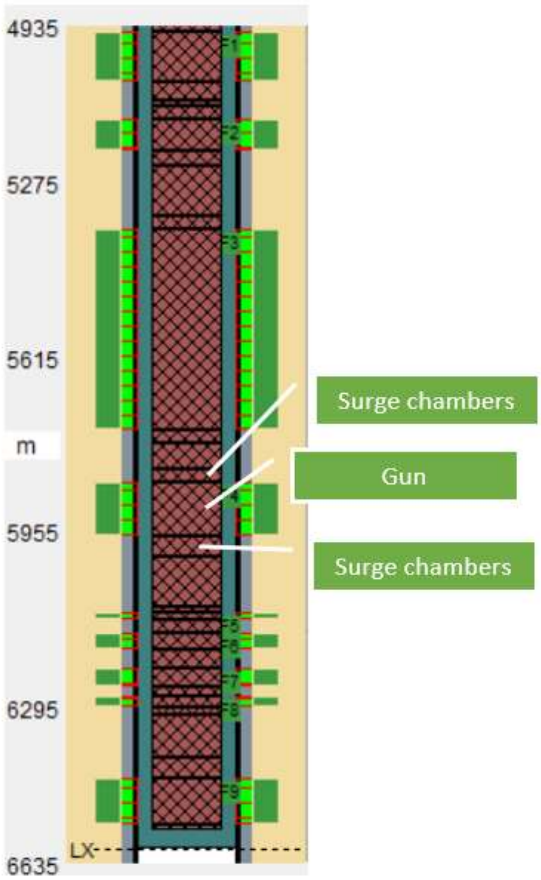

Perforating on wireline

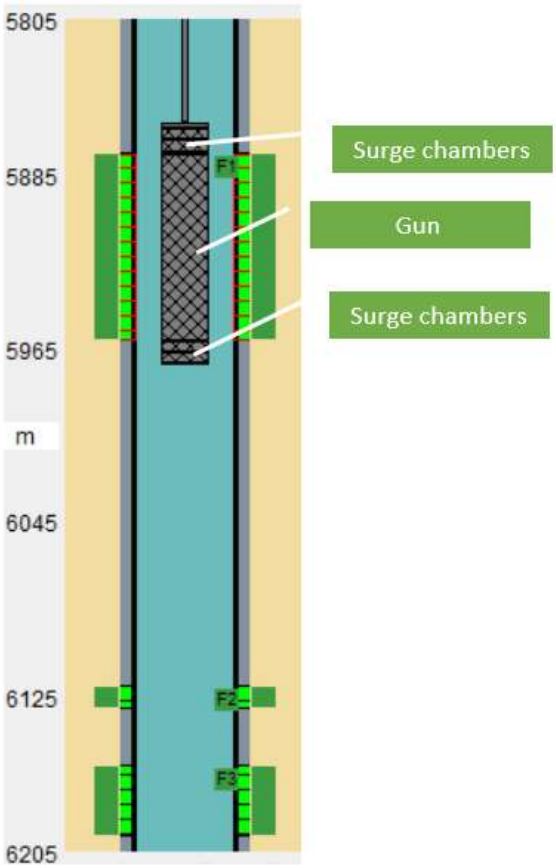

Figure 59- Perforating F-17 Oseberg South.

Table 10- Important difference in input parameters for the two gun systems. Full list of input parameters in Appendix

PARAMETER	3-1/8" WL	4-5/8" PIPE
STATIC WELL PRESSURE (PSI)	**Balanced**	**2150 overbalance**
CARRIER OD (IN)	3.125	4.625
FGV	0.74	0.79
PENETRATION (IN)	6.42	9.49
FORMATION HOLE (IN)	0.34	0.36
CASING EXIT HOLE (IN)	0.29	0.31
CHARGE WEIGHT (G)	17.5	39

Evaluating results from SurgePro simulations, it's important to distinguish between a long dynamic underbalance and a proper hole cleaning. Some parameters will both increase the duration of dynamic underbalance and increase clean-up from perforations, for example; free gun volume. Other parameters will reduce the duration of dynamic underbalance such as permeability, but still improving clean-up due to higher fluid velocity through the near-wellbore area and the perforations. Increasing viscosity would, on the other hand, prolong the duration of dynamic underbalance, but reduce fluid velocity through the near-wellbore area and the perforations. Because of this, a plot will also be made from the simulated amount of fluids produced during the perforating and clean-up event.

4.2.2.2 Simulation results- DUB

Simulated pressure response from the tool strings in Figure 60 and 61 have been made in order to aim for expected DUB at the Section IV tests.

4.2.2.2.1 Pipe

Figure 60 shows a DUB with an average peak of 696 psi, for the 4-5/8" gun system, perforating on pipe. The Green line represents a pressure sensor just below the surge chambers and has a peak DUB of 876 psi. This simulation does not fit perfectly with the Section IV test peak DUB of 1022 psi. The pressure point close to the top of the perforation interval is however close, and we could expect similar clean-up in the perforations close to the surge chambers. The simulations show longer duration in DUB compared to the Section IV test which had 1 second

in DUB. Longer duration of DUB is common for long TCP tool strings, because of the increased total atmospheric volume in the well.

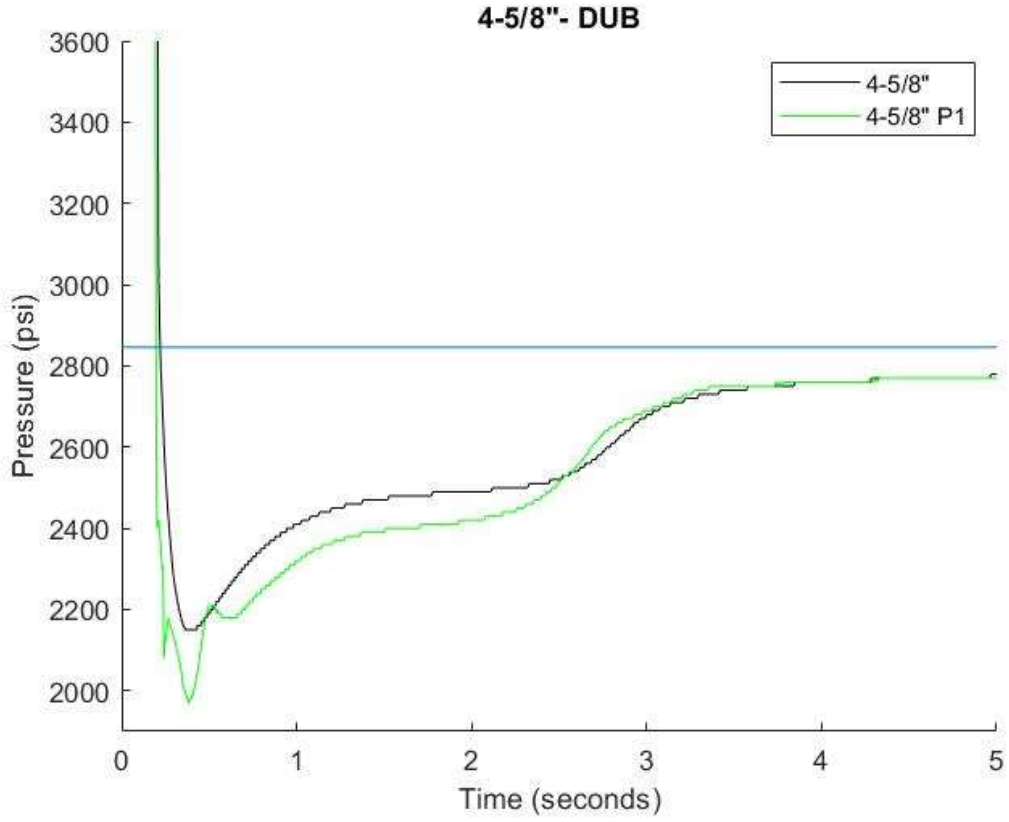

Figure 60- SurgePro pressure response for perforating on pipe

4.2.2.2.2 Wireline

Figure 61 shows a more rapid pressure response in the 3-1/8” gun system, perforating on wireline. Average peak DUB for the tool string was 636 psi, and 766 psi for the pressure sensor just below the surge chamber. Recorded peak DUB in the Section IV test cell was 741 psi, which is a good match with the simulations. Simulations had a more rapid increase in pressure after peak DUB compared to the Section IV test.

Figure 62 shows a comparison of the two perforating techniques. As can be seen, the detonation (indicated by a high peak pressure) of the 4-5/8” gun system is later than the 3-1/8” gun system. This can be due to the high displacement of fluid in the wellbore due to higher tool string OD on the 4-5/8” gun system. 4-5/8” gun system has a longer duration of DUB which is due to higher FGV.

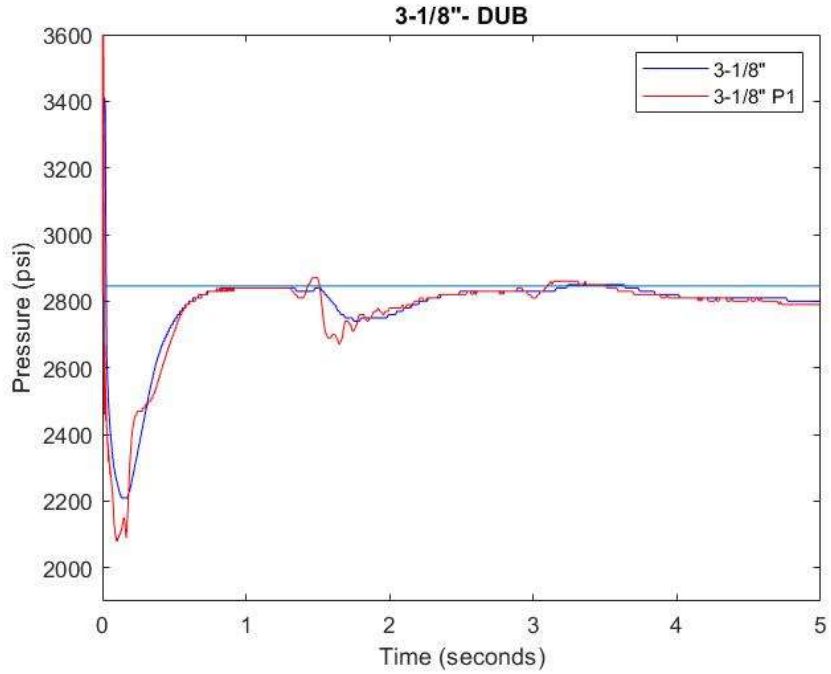

Figure 61- SurgePro pressure response for perforating on pipe

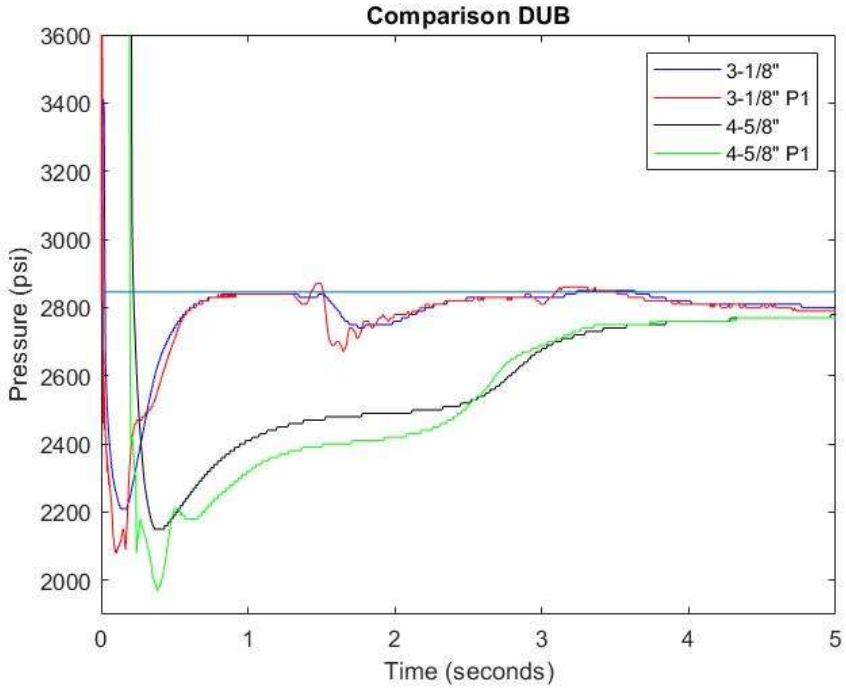

Figure 62- Comparison of pressure respons for pipe and wireline perforating

Simulations of the flow through each perforation during the DUB event can be seen in Figure 63. Negative indicates flow into the wellbore. For the 4-5/8” gun system a high rapid influx to the perforations followed by a rapid production from the perforation after detonation can be seen. This is most likely due to the high wellbore pressure, which injects fluids immediately after detonation. Influx is also seen for the 3-1/8” gun system. Although the well is in balance with the reservoir, the tool gas will increase the wellbore pressure locally, initiating an influx into the reservoir for a short period of time. Peak flow into the wellbore from 3-1/8” gun system was 328 cm^3/s and 482 cm^3/s for the 4-5/8” gun system.

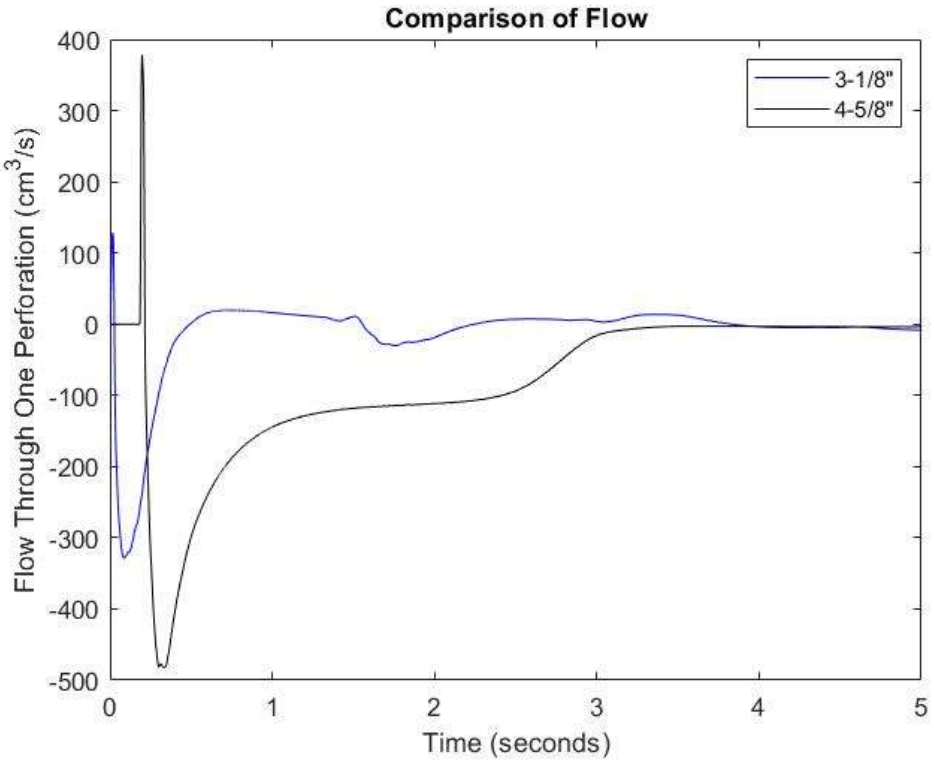

Figure 63- Comparison of flow through the perforations for perforating on pipe and wireline

4.2.3 WEM simulations

WEM uses a default 0.5 cm crushed zone thickness. Standardizing crushed zone permeability to this crushed zone thickness can be done through the equation for single-shot perforation skin.

$$\frac{k_c}{k_{dia}} = \frac{ln\left(r_c/r_p\right)}{S_{sp}} \rightarrow S_{sp} = \frac{k_{dia}}{k_c} * ln\left(r_c/r_p\right)$$

$$\left(S_{sp}\right)_{WEM} = \left(S_{sp}\right)_{CFE}$$

$$\left(\frac{k_{dia}}{k_c}\right)_{WEM} * ln\left(r_c/r_p\right)_{WEM} = \left(\frac{k_{dia}}{k_c}\right)_{CFE} * ln\left(r_c/r_p\right)_{CFE}$$

$$\left(\frac{k_{dia}}{k_c}\right)_{WEM} = \frac{\left(\frac{k_{dia}}{k_c}\right)_{CFE} * ln\left(r_c/r_p\right)_{CFE}}{ln\left(r_c/r_p\right)_{WEM}} = \frac{\left(\frac{k_{dia}}{k_c}\right)_{CFE} * ln\left(r_c/r_p\right)_{CFE}}{ln\left(\frac{r_c}{r_c - t_c}\right)_{WEM}}$$

For the perforation tunnel perforated with the 3-1/8" gun system we get:

$$\left(\frac{k_{dia}}{k_c}\right)_{WEM} = \frac{\left(\frac{240}{6.15}\right)_{CFE} * ln\left(1.004/0.899\right)_{CFE}}{ln\left(\frac{1.004}{1.004 - 0.5}\right)_{WEM}} = 6.25 \rightarrow \left(\frac{k_c}{k_{dia}}\right)_{WEM} = \frac{1}{6.25} = 0.16$$

For the perforation tunnel perforated with the 4-5/8" gun system we get:

$$\left(\frac{k_{dia}}{k_c}\right)_{WEM} = \frac{\left(\frac{207}{0.71}\right)_{CFE} * ln\left(1.75/1.62\right)_{CFE}}{ln\left(\frac{1.75}{1.75 - 0.5}\right)_{WEM}} = 66.89 \rightarrow \left(\frac{k_c}{k_{dia}}\right)_{WEM} = \frac{1}{66.89} = 0.01495$$

For the perforation tunnel perforated with the 4-5/8" gun system and only accounting for the productive length of the perforation we get:

$$\left(\frac{k_{dia}}{k_c}\right)_{WEM} = \frac{\left(\frac{207}{1.44}\right)_{CFE} * ln\left(1.218/1.099\right)_{CFE}}{ln\left(\frac{1.218}{1.218 - 0.5}\right)_{WEM}} = \rightarrow \left(\frac{k_c}{k_{dia}}\right)_{WEM} = \frac{1}{27.96} = 0.03576$$

WEM Simulations shown in Figure 64 shows the difference in expected inflow performance relationship (IPR) for the 3-1/8" gun system perforated in balance (blue line) and the 4-5/8"

gun system perforated in high overbalance with a kill pill along the reservoir (green and black line). The black line includes the entire length of the perforation tunnel while the green line only takes into account the apparently productive length of the perforation tunnel (see 4.1.5). Y-axis indicates the expected flowing well pressure for a certain flow rate on the X-axis.

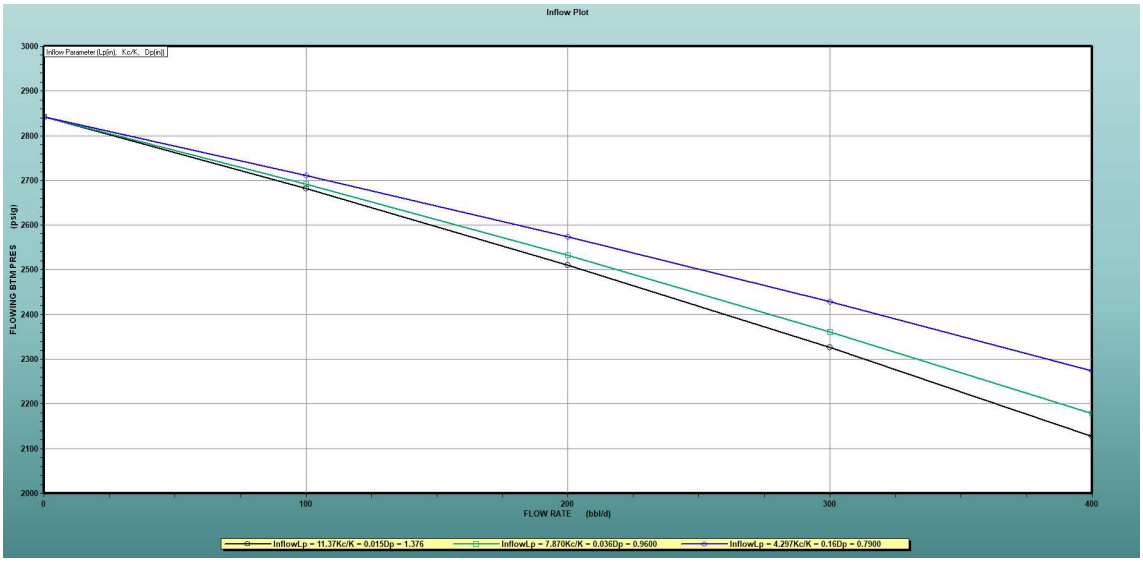

Figure 64- WEM simulations

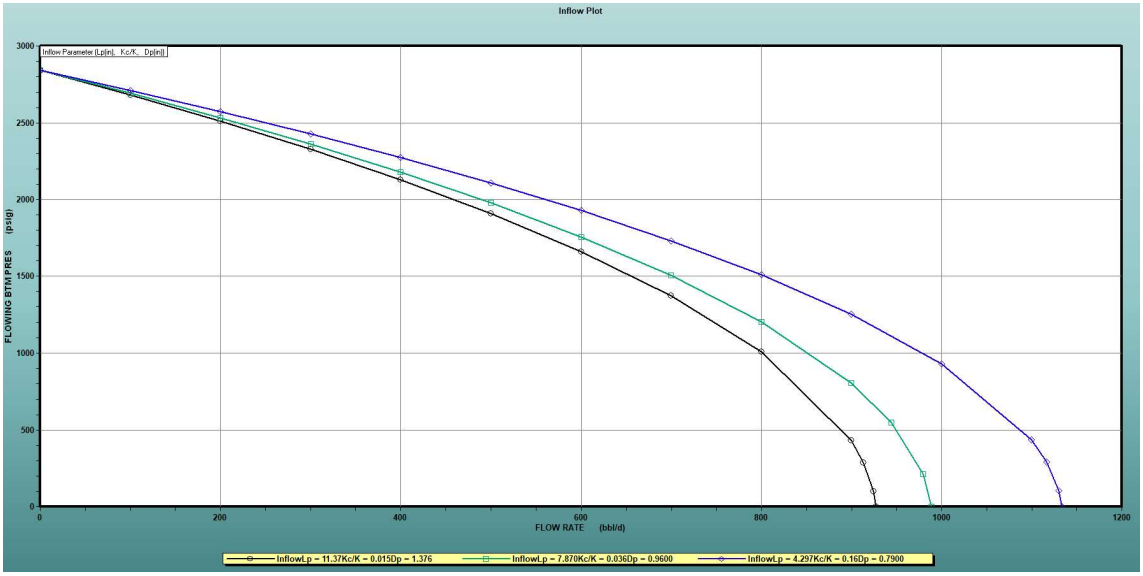

Figure 65- WEM Simulations

According to WEM simulations performed the 3-1/8” gun system will give the highest production. For a flowing well pressure of 2500 psi a well perforated with the 4-5/8” gun system will give a production (for the 100 meters perforated) of 200 bbl/d. The well perforated with 3-1/8” gun system will give a production of approximately 250 bbl/d, equivalent to a 25% increase in production. For the 4-5/8” gun system considering only the productive length of the perforation would give a production of approximately 220 bbl/d.

4.3 Uncertainties

There are important uncertainties related to both the simulations and the experimental tests. The natural variance in core properties and charge performance will obviously affect the results for each test. Every charge does not have the same performance, and the core strength will also vary from core to core, even if it is drilled from the same block. Uncertainty in field parameters will also affect the simulations and the accuracy of the final result. Cores specifications are close to Oseberg South field data, but to perfectly fit compressive strength, permeability, density and so forth is difficult. These deviations can affect the result but it is believed that a fair comparison of the two perforation techniques still can be performed.

5 CONCLUSION

The main research task was to propose the best perforation techniques for the depleted Oseberg South field with regards to perforation clean-up and cost. Therefore, in this thesis work, perforation efficiencies for the two techniques have been investigated through several simulations and experimental work at JRC. HPTK was used to find the estimated penetration and perforation diameter. These outputs were used in SurgePro to find expected transient dynamic underbalance during perforation. Section IV tests were then conducted to quantify perforator performance and dynamic underbalance clean-up under downhole conditions. The well productivity was then simulated in WEM to quantify well performance for both cases.

HPTK simulations showed as expected a significantly higher perforator performance for the 4-5/8" gun system compared to the 3-1/8" gun system. Effective perforation tunnel was simulated to be 9.49 in versus 6.42 in. Perforation diameter was estimated to be 0.36 in for the 4-5/8" gun system and 0.34 in for the 3-1/8" gun system.

Simulations in SurgePro showed a peak dynamic underbalance of 696 psi for the 4-5/8" gun system perforated in high overbalance and 636 psi for the 3-1/8" gun system perforated in balance. Due to large displacement of wellbore fluid (large OD of the tool string), a long duration of the DUB was seen for the 4-5/8" gun system compared to the 3-1/8" gun system.

Section IV tests showed effective perforation tunnel length of 11.37" and diameter of 1.376" for the 4-5/8" gun system. Test for the 3-1/8" gun system showed 4.297" effective perforation length and 0.79" perforation diameter. Based on this we can conclude that the geometry of the perforation tunnel from the 4-5/8" gun system is significantly more favorable compared to the 3-1/8" gun system. However, investigation of the perforation damage due to crushed zone and possibly an invasion of kill pill fluid showed that the 3-1/8" gun system in a balanced well can be beneficial.

Evaluation of the two perforation techniques in Oseberg South F-17 well was conducted using WEM. The well (with the 100 meters perforated interval) perforated with the 3-1/8" gun system in balance was simulated to have 250 bbl/d. The same well perforated with the 4-5/8" gun system in high overbalance with a kill pill along the reservoir was estimated to produce

between 200-220 bbl/d. The 4-5/8” gun system did create significantly longer and thicker perforation tunnels. However, the lower crushed zone thickness and permeability from the 3-1/8” gun system were shown to be dominant. Reducing cost and possibly increasing production should favor the 3-1/8” gun system for future wells to be perforated at Oseberg South.

References

(n.d.).

(2019, 5 6). Retrieved from Norskpetroleum.no: https://www.norskpetroleum.no/en/facts/field/oseberg-sor/

Aadnøy, B. and R. Looyeh. (2011). *Petroleum Rock Mechanics, ISBN: 9780123855466.*

Al-Tahou, Y., Elsayed, A., Eldaoushy, A., Al-Jasmi, A.K., El-Anany, S., and Alsabee, A. (2017). //Controlling the Period of Underbalanced Perforating, Delivers Increased Productivity in North Kuwait Well//, SPE 184024. *Presented at the SPE Middle East Oil & Gas Show and Conference, 6-9 March, Manama, Kingdom of Bahrain*.

API 19B- Recommended Practices for Evaluation of Well Perforators. (n.d.).

Asadi, M., and Floyd W.P. (1994). //Characterization of the Jet Perforation Crushed Zone by SEM and Image Analysis//. Paper SPE 22812, SPEFE.

Baumann, C., Gultom, D., Williams, H., Yudhatama. A., and Rahman, R. (2014). //Wireline Perforating Technology Maximizes Well Productivity and Minimizes Operational Risks//, SPE 169322. *Presented at the SPE Latin America and Caribbean Petroleum Engineering Conference, 21-23 May, Maracaibo, Venezuela*.

Behrmann, L. A., and Halleck, P.M. (1988). //Effect of Wellbore Pressure on Perforator Penetration Depth//, SPE 18243. *Presented at the SPE Annual Technical Conference and Exhibition, 2-5 October, Houston, Texas*.

Behrmann, L.A. and McDonald, B. (1996). //Underbalance or Extreme Overbalance//, SPE 31083. *Presented at the SPE Formation Damage Control Symposium, 14-15 February, Lafayette, Louisiana*.

Behrmann, L.A., Pucknell, J.K., Hsia, T.Y. (1991). //Measurement of Additional Skin Resulting From Perforation Damage//, SPE 22809. *Presented at the SPE Annual Technical Conference and Exhibition in Dallas, Texas, 6-9 October*.

Blick, E. F. and Civan, F. (1987). //Porous Media Momentum Equation for Highly Accelerated Flow//, SPE 16202. *Presented at the SPE Production Operations Symposium, 8-10 March, Oklahoma City, Oklahoma*.

Bolchover, P. and Walton, I.C. (2006). //Perforation Damage Removal by Underbalance Surge Flow//, SPE paper 98220. *Presented at the SPE International Symposium and Exhibition on Formation Damage Control, 15-17 February, Lafayette, Louisiana, USA*.

Bundy, T. E. and Matthew, E. J. (1990). //Perforating a High-Pressure Gas Well Overbalanced in Mud: Is It Really That Bad?//, SPE 16894.

Byrne, M.T. and McPhee, C.A. (2012). //The Extinction of Skin//, SPE 151807. *Presented at the SPE International Symposium and Exhibition on Formation Damage Control, 15-17 February, Lafayette, Louisiana, USA*.

Casas, S., Mattey, A., Molina, O., Larez, A., Mata, J., Fam, M., and Fernandez, R. (2009). //Application of an Advanced Dynamic-Underbalance Perforating System for Improved Oil Production in

Development Wells: Case Histories from Eastern Venezuela//, SPE paper 122199. *Presented at the Latin American and Caribbean Petroleum Engineering Conference, 31 May-3 June, Cartagena de Indias, Colombia*.

Devinder, S.A. and Mukul, M.S. (2000). //The Nature of the Compacted Zone Around Perforation Tunnels//, SPE 58720. *Presented at the SPE International Symposium on Formation Damage Control, 23-24 February, Lafayette, Louisiana*.

Divyankar, S. (2015). //Horizontal well oriented perforation skin factor: A numerical analysis of skin factor reduction by off-setting perforation phasing from 360 degree to 350/10 degree//, MSc.

(2019). *Equinor internal document.*

Gasmi, K., Alarcon, B., Guerrero, M. and Daoud, M. (2015). //Restored Productivity Using Dynamic Underbalance//, SPE paper 174172. *Presented at the SPE European Formation Damage Conference and Exhibition, 3-5 June, Budapest, Hungary*.

Grove, B., Harvey, J., Zhan, L. and Atwood, D. (2012). //An Improved Technique for Interpreting Perforating-Flow-Laboratory Results: Honoring Observed Cleanup Mechanisms//, SPE 143998.

Grove, B.M., Harvey, J.P. and Zhan, L. (2011). //Perforation Cleanup via Dynamic Underbalance: New Understandings//, SPE paper 143997. *Presented at the SPE European Formation Damage Conference, 7-10 June, Noordwijk, The Netherlands*.

Haggerty, D., Graddock, G.G. and Quattlebaum, C.C. (2012). Evaluation of Established Perforation Cleanup Models on Dynamic Underbalanced Perforating, SPE paper 159413. *Presented at the SPE Annual Technical Conference and Exhibition, 8-10 October, San Antonio, Texas, USA*.

Haggerty, D., McGregor, J. and Akhmadikin, V. (2017). //Configuring Dynamic Underbalance to Achieve Perforation Tunnel Cleanup in a Gas Well at High Static Overbalance//, SPE paper 188769. *Presented at the Abu Dhabi International Petroleum Exhibition & Conference, 13-16 November , Abu Dhabi, UAE*.

Hagoort, J. (2007). //An Improved Model for Estimating Flow Impairment by Perforation Damage//, SPE paper 98137.

Halleck P.M., and Behrmann L.A. (1990). //Penetration of shaped charges in stressed rock//, Paper ARMA-90-0629. *Presented at the 31th U.S. Symposium on Rock Mechanics (USRMS), 18-20 June, Golden, Colorado*.

Halleck, P.M. and Deo, M. (1989). //Effects of Underbalance on Perforation Flow//, SPE paper 16895.

(2019). *Halliburton internal document.*

Halliburton Wireline and Perforating. (n.d.). *Perforating Solutions.*

Han, L., Pedeb, J.M. and Ford, J. (1996). //Effects of Various Parameters on Perforation Plugging and Perforation Cleanup//, SPE paper 31090. *Presented at the SPE Formation Damage Control Symposium, 14-15 February, Lafayette, Louisiana*.

Hsia, T.A. and Behrmann, L.A. (1991). //Perforating Skin as a Function of Rock Permeability and Underbalance//, SPE paper 22810. *Presented at the SPE Annual Technical Conference and Exhibition, 6-9 October, Dallas, Texas*.

Huang, H., and Ayoub, J. (2006). //Applicability of the Forchheimer Equation for Non-Darcy Flow in Porous Media//, SPE paper 102715, presented at the SPE Annual Technical Conference and Exhibition, 24-27 September, San Antonio, Texas, USA.

(2019). *Jet Research Center internal document.*

Jumaat, M.S. (2013). //Repeat Dynamic Underbalance Perforating in Oman//, SPE paper 165920. *Presented at the SPE Asia Pacific Oil and Gas Conference and Exhibition, 22-24 October, Jakarta, Indonesia*.

Karakas, M. and Tariq, S.M. (1991). //Semianalytical Productivity Models for Perforated Completions//, SPE paper 18247.

McGregor, J. (2018). 181001 Premier Oil Report.

McLeod, H.O. (1983). //The Effect of Perforating Conditions on Well Performance//, SPE 10649.

Oljedirektoratet. (2019, 2 12). Retrieved from NPD: http://factpages.npd.no/factpages/Default.aspx?culture=no

Pearson, J.R.A. and Zazovsky, A.F. (1997). //A Model for the Transport of Sand Grains From a Perforation During Underbalance Surge//, SPE paper 38634. *Presented at the SPE Annual Technical Conference and Exhibition, 5-8 October, San Antonio, Texas*.

Perrier, S. and Sugiarto, T. (2012). //Dynamic UnderBalance perforations bring higher productivities than Conventional perforations: a large scale comparative review from the Tunu Gas Field (Indonesia)//, SPE paper 158083. *Presented at the SPE Annual Technical Conference and Exhibition, 8-10 October, San Antonio, Texas, USA*.

Pucknell, J.K. and Behrmann, L.A. (1991). //An Investigation of the Damaged Zone Created by Perforating//, SPE paper 22811. *Presented at the SPE Annual Technical Conference and Exhibition, 6-9 October, Dallas, Texas*.

Sahimi, M. (1994). *//Applications of Percolation Theory//, ISBN-13: 978-0748400768.*

Satti, R., Bale, D., Gilliat, J. and Hillis, P. (2018). //Dynamic Flow Modeling and Risk Mitigation Enables Optimized Perforation Design in Complex Well Completions//, SPE paper 189466. *Presented at the SPE International Conference and Exhibition on Formation Damage Control, 7-9 February, Lafayette, Louisiana, USA*.

Saucier R.J., Lands J.F. (1978). //A Laboratory Study of Perforations in Stressed Formation Rocks//. Paper SPE 6758.

Schatz, J.F., Haney, B.L. and Ager, S.A. (1999). //High-Speed Downhole Memory Recorder and Software Used to Design and Confirm Perforating/Propellant Behavior and Formation Fracturing//, SPE paper 56434. *Presented at the SPE Annual Technical Conference and Exhibition, 3-6 October, Houston, Texas*.

Smith, P.S., Behrmann, L.A. and Yang, W. (1997). //Improvements in Perforating Performance in High Compressive Strength Rocks//, SPE paper 38141. *Presented at the SPE European Formation Damage Conference, 2-3 June, The Hague, Netherlands*.

Stutz, H.L. and Behrmann, L.A. (2004). //Dynamic Under Balanced Perforating Eliminates Near Wellbore Acid Stimulation in Low-Pressure Weber Formation//, SPE paper 86543. *Presented at the SPE International Symposium and Exhibition on Formation Damage Control, 18-20 February, Lafayette, Louisiana*.

Subiaur, S.T., Graham, C.A., Walton, I.C. and Atwood, D.C. (2004). Underbalance Pressure Criteria For Perforating Carbonates, SPE paper 86542. *SPE International Symposium and Exhibition on Formation Damage Control, 18-20 February, Lafayette, Louisiana*.

Tariq, S.M. (1990). //New, Generalized Criteria for Determining the Level of Underbalance for Obtaining Clean Perforations//, SPE paper 20636. *Presented at the SPE Annual Technical Conference and Exhibition, 23-26 September, New Orleans, Louisiana*.

Tariq, S.M., Bell, W.T. and Sukup, R.A. (1995). *Perforating, ISBN: 1-55563-059-6.* SPE.

Thompson, G.D. (1962). //Effects of Formation Compressive Strength on Perforator Performance//, API-62-191. *Presented at the Drilling and Production Practice, 1 January, New York*.

Torvund, T. (1989). //The Oseberg Reservoir Management Planning: A Case History From the Oseberg Field//, OTC 6140. *Presented at the Offshore Technology Conference, 1-4 May, Houston, Texas*.

Tovar, J.J., Appleby, R.R., Cooper, G. and Hamilton, B.J. (2010). //Design and Evaluation of Perforation Performance Using Dynamic Under Balance: North Sea Case Histories//, SPE paper 135712. *Presented at the SPE Annual Technical Conference and Exhibition, 19-22 September, Florence, Italy*.

Wight, J., Graddock, G.G, Haggerty, D., Rojas, F., Montiverdi, J., Yadav, A., Magdaniel, M., Rios, F., and Harive, K. (2016). //A Perforating Tool Kit as a Computational Paradigm//, SPE paper 180302, presented at the SPE Deepwater Drilling and Completions Conference, 14-15 September, Galveston, Texas, USA.

Zeng, F. and Zhao, G. (2008). //Semianalytical Model for Reservoirs With Forchheimer's Non-Darcy Flow//, SPE 100540. *Presented at the SPE Gas Technology Symposium, 15-17 May, Calgary, Alberta, Canada*.

Appendix

Appendix A.1 Axial permeability flow test

Table 1. Pre-shot axial absolute permeability flow data.

Core	q and Axial Δp vs. time	$T_i, T_o, p_i, p_o, \mu(\bar{p},\bar{T})$, & $\rho(\bar{p},\bar{T})$ vs. time
1	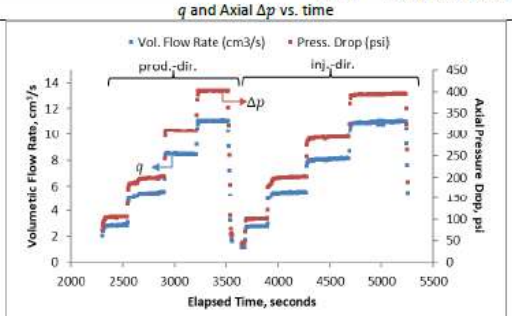	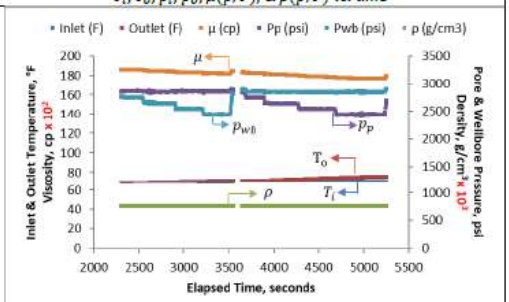
2	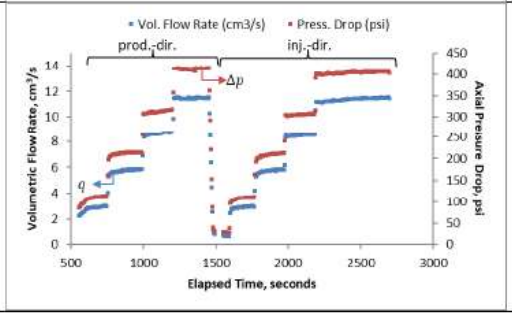	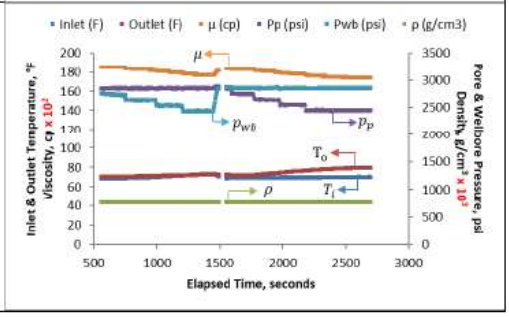

Table 1 continued.

Core	q and Axial Δp vs. time	$T_i, T_o, p_i, p_o, \mu(\bar{p},\bar{T})$, & $\rho(\bar{p},\bar{T})$ vs. time
4	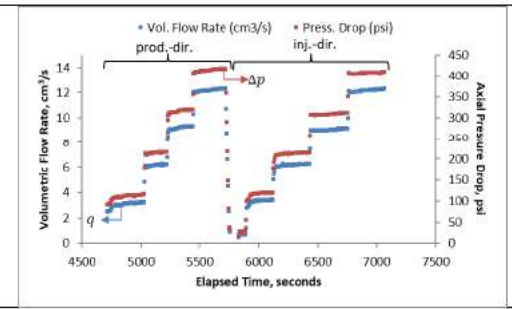	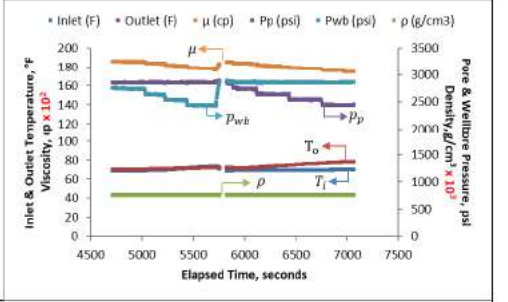
6	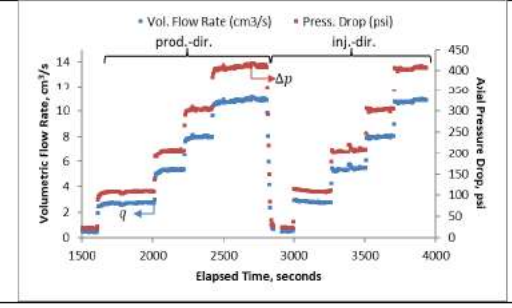	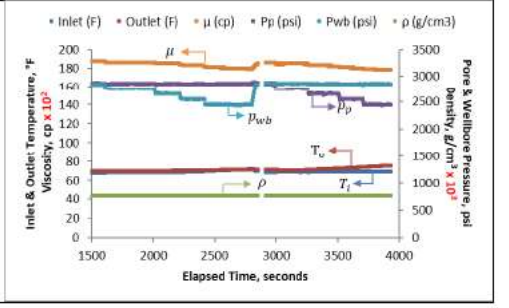

Apendix A2: Input parameters SurgePro:

Well General	Unit	Imp	Value
Meas Depth or PBTD	m	Y	6720.00
Deviation Type			From File
-TVD at Meas Depth	m		(2979.32)
-Azimuth	degrees		0
Interior Open to Atmos?		Y	No
-Well Interior Orifice	in		
-Well Interior Pressure	psi	Y	15
Annulus 1 Open to Atmos?		Y	No
-Annulus 1 Orifice	in		
-Annulus 1 Pressure	psi	Y	15
Annulus 2 Open to Atmos?		Y	
-Annulus 2 Orifice	in		
-Annulus 2 Pressure	psi	Y	
Use Surface Pump?			No
-Pump Type			
-Pump To			
-Pump Flow Capacity	scf/min		
-Maximum Pump Pressure	psi		
Use Default Roughnesses?		Y	Yes

As Drilled	Unit	Imp	Value 1	Value 2
Use?			Yes	Yes
Top	m	Y	0.00	4751.00
Diameter	in	Y	12.750	8.500

Formations	Unit	Imp	Value 1	Value 2
Use?			Yes	No
Top	m	Y	0.00	
Rock Type			Sandstone	
Porosity			0.21	
Permeability	md	Y	263.000	
Formation Skin Thickness	in	Y	5	
Formation Skin Permeabili	md	Y	30.000	
Equivalent Skin			(4.5)	
Use Rock Defaults?			No	
-Density	kg/m^3		2650	
-Young's Modulus	10^6 psi	Y	3.64	
-Poissons Ratio			0.25	
-Compressive Strength	psi		5800	
-Tensile Strength	psi		250.0	
-Grain Size	in		0.020	
-Crushed Grain Size	in		(0.010)	
-Crushed Gr Cohesion	psi	Y	10.0	
Formation Fluid Type		Y	Medium Oil	
Use Fluid Defaults?			No	
-Density at STP	lb/gal		7.093	
-Use Speed?			Yes	
-Sound Speed	ft/s	Y	3500	
-Compressibility	1/10^6 psi	Y	(7.13)	
-Compressibility at Res C	1/10^6 psi		(5.85)	
-Viscosity at STP	cp		1.17	
-Viscosity at Res Conds	cp		(0.40)	
Formation Pressure	psi	Y	2850	
Temperature	C		110	
Depth for Pres/Temp	m	Y	6390.00	
Use Default Stresses?			No	
-Stress Magnitude		Y		
-Vertical Gradient	psi/ft		0.91	

Wireline 3-1/8":

Well Fluids	Unit	Imp	Value 1	Value 2	Value 3
Use?			Yes	Yes	Yes
Type		Y	Nitrogen	Sea Water	Sea Water
Top	m	Y	0.00	0.00	1100.00
Position		Y	Interior	Annulus 1	Interior
Use Defaults?			Yes	Yes	Yes
-Density at STP	g/cm^3	Y	(0.00)	(1.03)	(1.03)
-Use Sound Speed?			(Yes)	(Yes)	(Yes)
-Sound Speed	ft/s	Y	(1135)	(5000)	(5000)
-Compressibility	1/10^6 psi	Y	(49224.45)	(2.88)	(2.88)
-Compressibility at D	1/10^6 psi		(4922.45)	(2.74)	(2.65)
-Viscosity at STP	cp	Y	(0.02)	(1.50)	(1.50)
-Viscosity at Depth	cp		(0.02)	(0.55)	(0.66)
Add Solids?			No	No	No
-Density	g/cm^3				
-Solids Gr Size	in				
-Volume Fraction					
Total Mass in Well	lb		(34.6)	(238253.0)	(182011.9)

Tubes	Unit	Imp	Value 1	Value 2	Value 3	Value 4	Value 5	Value 6
Use?			Yes	Yes	Yes	Yes	Yes	No
Type		Y	Casing-Ceme	Std Tubing	Packer	Std Tubing	Casing-Ceme	
Top	m	Y	0.00	0.00	4660.00	4670.00	4751.00	
Bottom	m	Y	4751.00	4660.00	4670.00	4820.00	6720.00	
Outside Diam	in	Y	9.625	5.500	(8.541)	3.500	7.000	
OD 2 (for Adapter Sub)	in	Y						
Use Default ID?			Yes	Yes		Yes	Yes	
-Inside Diameter	in	Y	(8.541)	(4.900)	2.500	(2.798)	(6.191)	
Inner Cyl OD	in	Y						
-inner Cyl Fires Tool 1?								
Grade		Y	N-80	N-80		N-80	N-80	
Weight per Length	lb/ft	Y	53.50	17.00		12.00	29.00	
Use Default Burst/Collapse?			Yes	Yes		Yes	Yes	
-Burst Pressure	psi	Y	(7881)	(7641)		(14041)	(8086)	
-Collapse Pressure	psi	Y		(8256)		(14438)		
* -B/C Multiplier		Y	1.00	1.00		1.00	1.00	
Packer Set?					Yes			
-Pressure Rating	psi				10000			
Cement Youngs Modulus	10^6 psi		2.00				2.00	
Cement Comp Strength	psi		8000				8000	

Cylinders	Unit	Imp	Value 1	Value 2	Value 3	Value 4	Value 5
Use?			Yes	Yes	Yes	Yes	Yes
Type		Y	Std Wireline	Cap	Firing head	Cap	Bridge Plug
Top	m	Y	0.00	5855.00	5869.00	5971.00	6600.00
Bottom	m	Y	5855.00	5858.00	5870.00	5971.50	6605.00
Cable Type		Y					
Diameter	in	Y	0.400	3.125	3.125	3.125	6.191
Active?					Yes		
-Tool To Fire					1		
Pressure-Actuated?					No		
-Firing Pressure	psi						
Pressure Rating	psi	Y					20000
Pressure Underneath	psi	Y					7000

Existing Perfs	Unit	Imp	Value 1	Value 2	Value 3	Value 4	Value 5
Use?			Yes	Yes	Yes	Yes	Yes
Top	m	Y	6125.00	6164.00	6237.00	6294.00	6459.00
Bottom	m	Y	6137.00	6198.00	6275.00	6316.00	6555.00
Hole Density	#/ft	Y	3.6	3.6	3.6	3.6	3.6
Phasing	degrees	Y	0	0	0	0	0
-Planes							
Casing Hole Diam	in	Y	0.29	0.29	0.29	0.29	0.29
Formation Hole Diam	in	Y	0.34	0.34	0.34	0.34	0.34
*Penetration	in	Y	6.42	6.42	6.42	6.42	6.42
Max Damage Thickness	in	Y	0.500	0.500	0.500	0.500	0.500
Perm Damage Factor			0.50	0.50	0.50	0.50	0.50

Tools	Unit	Imp	Value 1	Value 2	Value 3	Value 4	Value 5
Use?			Yes	Yes	Yes	Yes	Yes
Tool Type			Punch Chan	Punch Chan	Perf Gun	Punch Chan	Punch Chan
Ignition Point		Y	Top	Top	Top	Top	Top
Ignition Delay	s		0.0000	0.0000	0.0000	0.0000	0.0000
* CARRIER			<<<<<<<<<<	<<<<<<<<<<	<<<<<<<<<<	<<<<<<<<<<	<<<<<<<<<<
Use Carrier?		Y					
Tool Fluid		Y	Air	Air	Air	Air	Air
Carrier Size		Y	3-1/8 (79)	3-1/8 (79)	3-1/8 (79)	3-1/8 (79)	3-1/8 (79)
Carrier OD	in	Y	(3.125)	(3.125)	(3.125)	(3.125)	(3.125)
Use Default ID?			Yes	Yes	Yes	Yes	Yes
-Carrier ID	in	Y	(2.468)	(2.468)	(2.468)	(2.468)	(2.468)
Carrier Grade			C-75	C-75	C-75	C-75	C-75
-Burst Pres	psi		(13787)	(13787)	(13787)	(13787)	(13787)
-Collapse Pres	psi		(14101)	(14101)	(14101)	(14101)	(14101)
* -B/C Multiplier		Y	1.00	1.00	1.00	1.00	1.00
*Gun Vol Factor		Y	0.95	0.95	0.74	0.95	0.95
Carrier Top	m	Y	5858.00	5863.50	5870.00	5960.00	5965.50
Carrier Bottom	m	Y	5863.50	5869.00	5960.00	5965.50	5971.00
Transfer Hole Diam	in			0.00		0.10	0.10
* CHARGE/HOLES	m	Y	<<<<<<<<<<	<<<<<<<<<<	<<<<<<<<<<	<<<<<<<<<<	<<<<<<<<<<
Charge/Hole Top	m	Y	5858.00	5863.50	5870.00	5960.00	5969.78
Charge/Hole Bot	m	Y	5859.22	5864.72	5960.00	5961.22	5971.00
-Hole Density	#/ft	Y	0.3	0.3	3.6	0.3	0.3
-Hole Phasing	degree	Y	60	60	0	60	60
-Planes	#/ft						
Charge Type		Y			HMX		
-Zinc Case?		Y			No		
-Weight	g	Y	1.0	1.0	17.5	1.0	1.0
Igniter Strength	gr/ft	Y	80.0	80.0	80.0	80.0	80.0
Total Explosive Mass	kg		(0.12)	(0.12)	(20.52)	(0.12)	(0.12)
*Gun Internal Rem		Y	(0.90)	(0.90)	0.45	(0.90)	(0.90)
*Gun External Rem		Y	(0.020)	(0.020)	0.025	(0.020)	(0.020)

Carrier Hole Diam	in	Y	1.75	1.75	0.35	1.75	1.75
Hole Opening Period	s		0.010	0.010	0.010	0.010	0.010
Hole Opening Delay	s		0.001	0.001	0.001	0.001	0.001
Well Casing Hole Diam	in	Y			0.29		
Formation Hole Diam	in	Y			0.34		
* -Penetration	in	Y			6.42		
-Max Damage Thickness	in	Y			0.500		
-Perm Damage Factor					0.50		

Pipe 4-5/8":

Well Fluids	Unit	Imp	Value 2
Use?			Yes
Type		Y	(Oil-Based Mu
Top	m	Y	0.00
Position		Y	Annulus 1
Use Defaults?			No
-Density at STP	g/cm^3	Y	1.18
-Use Sound Speed?			Yes
-Sound Speed	ft/s	Y	4000
-Compressibility	1/10^6 psi	Y	(3.93)
-Compressibility at D	1/10^6 psi		(2.86)
-Viscosity at STP	cp	Y	30.00
-Viscosity at Depth	cp		(1.74)
Add Solids?			No
-Density	g/cm^3		
-Solids Gr Size	in		
-Volume Fraction			
Total Mass in Well	lb		(274326.4)

Tubes	Unit	Imp	Value 2	Value 3	Value 4	Value 5	Value 6
Use?			Yes	Yes	Yes	Yes	Yes
Type		Y	Std Tubing	Std Tubing	Std Tubing	Casing-Ceme	Ported Sub
Top	m	Y	0.00	4710.00	4735.00	4751.00	4920.00
Bottom	m	Y	4710.00	4735.00	4920.00	6720.00	4927.00
Outside Diam	in	Y	5.500	7.000	4.000	7.000	4.625
OD 2 (for Adapter Sub)	in	Y					
Use Default ID?			Yes	Yes	No	Yes	
-Inside Diameter	in	Y	(4.545)	(2.522)	2.500	(6.191)	3.000
Inner Cyl OD	in	Y					
-inner Cyl Fires Tool 1?							
Grade		Y	N-80	N-80	N-80	N-80	N-80
Weight per Length	lb/ft	Y	26.00	115.00	12.70	29.00	
Use Default Burst/Collapse?			Yes	Yes	Yes	Yes	
-Burst Pressure	psi	Y	(12150)	(44776)	(26250)	(8086)	
-Collapse Pressure	psi	Y	(12681)	(34806)	(24375)		
* -B/C Multiplier		Y	1.00	1.00	1.00	1.00	
Packer Set?							
-Pressure Rating	psi						
Cement Youngs Modulus	10^6 psi					2.00	
Cement Comp Strength	psi					8000	

Cylinders	Unit	Imp	Value 1	Value 2	Value 3
Use?			Yes	Yes	Yes
Type		Y	Firing head	Cap	Bridge Plug
Top	m	Y	4927.00	6564.00	6600.00
Bottom	m	Y	4928.00	6565.00	6605.00
Cable Type		Y			
Diameter	in	Y	4.625	4.625	6.191
Active?			Yes		
-Tool To Fire			1		
Pressure-Actuated?			No		
-Firing Pressure	psi				
Pressure Rating	psi	Y			20000
Pressure Underneath	psi	Y			7000

Tools	Unit	Imp	Value 1	Value 2	Value 3	Value 4	Value 5	Value 6
Use?			Yes	Yes	Yes	Yes	Yes	Yes
Tool Type			Punch Chan	Perf Gun	Punch Chan	Blank Gun	Punch Chan	Perf Gun
Ignition Point		Y	Top	Top	Top	Top	Top	Top
Ignition Delay	s		0.0000	0.0000	0.0000	0.0000	0.0000	0.0000
* CARRIER			<<<<<<<<<<	<<<<<<<<<<	<<<<<<<<<<	<<<<<<<<<<	<<<<<<<<<<	<<<<<<<<<<
Use Carrier?		Y						
Tool Fluid		Y	Air	Air	Air	Air	Air	Air
Carrier Size		Y	4-5/8 (117)	4-5/8 (117)	4-5/8 (117)	4-5/8 (117)	4-5/8 (117)	4-5/8 (117)
Carrier OD	in	Y	(4.625)	(4.625)	(4.625)	(4.625)	(4.625)	(4.625)
Use Default ID?			Yes	Yes	Yes	Yes	Yes	Yes
-Carrier ID	in	Y	(3.757)	(3.757)	(3.757)	(3.757)	(3.757)	(3.757)
Carrier Grade			C-75	C-75	C-75	C-75	C-75	C-75
-Burst Pres	psi		(12315)	(12315)	(12315)	(12315)	(12315)	(12315)
-Collapse Pres	psi		(12754)	(12754)	(12754)	(12754)	(12754)	(12754)
* -B/C Multiplier		Y	1.00	1.00	1.00	1.00	1.00	1.00
*Gun Vol Factor		Y	0.95	0.79	0.95	0.95	0.95	0.79
Carrier Top	m	Y	4928.00	4943.00	5045.00	5085.00	5096.00	5123.00
Carrier Bottom	m	Y	4943.00	5045.00	5085.00	5096.00	5123.00	5188.00
Transfer Hole Diam	in			0.10	0.10	0.10	0.10	0.10
* CHARGE/HOLES	m	Y	<<<<<<<<<<	<<<<<<<<<<	<<<<<<<<<<	<<<<<<<<<<	<<<<<<<<<<	<<<<<<<<<<
Charge/Hole Top	m	Y	4928.00	4943.00	5045.00		5096.00	5123.00
Charge/Hole Bot	m	Y	4943.00	5045.00	5085.00		5123.00	5188.00
-Hole Density	#/ft	Y	0.2	3.6	0.2		0.2	3.6
-Hole Phasing	degree	Y	60	0	60		60	0
-Planes	#/ft							
Charge Type		Y		HMX				HMX
-Zinc Case?		Y		No				No
-Weight	g	Y	1.0	39.0	1.0		1.0	39.0
Igniter Strength	gr/ft	Y	80.0	80.0	80.0	80.0	80.0	80.0
Total Explosive Mass	kg		(0.33)	(49.15)	(0.88)	(0.19)	(0.59)	(31.32)
*Gun Internal Rem		Y	(0.90)	0.45	(0.90)	(1.00)	(0.90)	0.45
*Gun External Rem		Y	(0.020)	0.025	(0.020)	(0.000)	(0.020)	0.025

Carrier Hole Diam	in	Y	0.30	0.35	0.30		0.30	0.35
Hole Opening Period	s		0.010	0.010	0.010		0.010	0.010
Hole Opening Delay	s		0.001	0.001	0.001		0.001	0.001
Well Casing Hole Diam	in	Y		0.31				0.31
Formation Hole Diam	in	Y		0.36				0.36
* -Penetration	in	Y		9.49				9.49
-Max Damage Thickness	in	Y		0.500				0.500
-Perm Damage Factor				0.50				0.50

Appendix A3: Sensitivity study on effect of reservoir pressure and permeability, SurgePro

This section contains sensitivity study from simulations performed in SurgePro. Base case will be consisting of Oseberg South F-17 similar parameters. Table 11 shows how permeability and reservoir pressure affects the dynamic underbalance and influx during dynamic underbalance.

Table 11- Sensitivity study

Parameter		**Min Well Pressure Drawdown (psi)**	**Max Dynamic Surge in WR ($P_{res} - P_{peakDrawdown}$) (psi)**	**Max Flow Rate Through One Perforation (cm^3/s)***
Permeability (mD)	**10**	2060	790	45
	12	2070	780	66
	15	2080	770	155
	30	2080	770	292
	50	2080	770	400
	100	2060	790	688
	200	2060	790	1112
Reservoir Pressure (psi)	**2000**	1760	240	386
	2200	1850	350	494
	2400	1930	470	647
	2600	2000	600	832
	2850	2060	790	1112